MYOELECTRIC CONTROL OF EXOSKELETON KNEE

Thesis
Submitted for the award of
Doctor of Philosophy

by

Inderjeet Singh Dhindsa
(Regd. No.: 951204001)

Under the supervision of

Dr. Ravinder Agarwal
Professor, EIED
TIET, Patiala

Department of Electrical and Instrumentation Engineering
THAPAR INSTITUTE OF ENGINEERING AND TECHNOLOGY,PATIALA
(Declared as Deemed-to-be-University u/s 3 of the UGC Act., 1956)
Punjab (India)-147004
August, 2020

Declaration

I hereby declare that the work presented in this thesis titled, '**Myoelectric Control of Exoskeleton Knee**' in partial fulfillment of the requirements for the award of the degree of Doctor of Philosophy in Electrical and Instrumentation Engineering Department (EIED), Thapar Institute of Engineering & Technology, Patiala, Punjab, is an authentic record of my own work carried out under the supervision of Dr. Ravinder Agarwal, Professor. EIED, TIET Patiala.

The matter presented in this thesis has not been submitted elsewhere for the award of any other degree in India or Abroad.

(Inderjeet Singh Dhindsa)

This is to certify that the above statement made by the candidate is correct to the best of my knowledge.

(Dr. Ravinder Agarwal)
Prof. EIED, TIET
Patiala, India

Abstract

Exoskeleton is primarily designed to increase the physical performance of the wearer. Exoskeleton system are utilized for power-assist device, human-amplifier and rehabilitative device *etc*. Last three decades have witnessed significant development in the field of myoelectric control of rehabilitative and assistive devices. The major focus of the myoelectric prediction has been on predicting the motion modes for different locomotion terrain, gesture control and prediction of kinetic parameters like joint torque/force.

The present research work is focused in the direction of myoelectric control of exoskeleton knee. The research work is divided in four parts namely,development of multichannel SEMG acquisition system to acquire SEMG signal from lower limb muscle while carrying out daily life activities, selection of optimal group of muscles to control the exoskeleton, predicting the knee angle information from SEMG signal of selected muscles and development of a simple prototype of knee exoskeleton. An eight-channel bioinstrumentation system based on ADS1298 was developed to record the SEMG signals from the selected lower limb muscles.

Human lower limb consist of numerous muscles. One of the main considerations of the myoelectric controlled exoskeleton is the selection of muscles, which can control the exoskeleton system. Biological musculoskeletal model of human is highly redundant in nature. Apart from few exceptions, there exits more muscles than necessary to produce desired joint movement. The human lower limb has more than fifty muscles, but the human motion intent can be predicted by considering only some of these muscles.

The research work proposes a principal variable based method for muscle selection. The selected group of muscles are sufficient to describe the knee movements. The force developed in the eighteen lower limb muscles while performing a sit to stand movement was considered as a base for muscle selection. The principal variable method is based on the criterion of minimum conditional covariance of the rejected variables. For a two-channel system Vastus lateralis and Rectus femoris are sufficient in describing knee flexion/extension. For a three-channel system Gluteus medius and for a four-channel system Semitendinosus joined the set of optimum muscles. The results were further substantiated statistically by performing a t-test on the muscle force obtained from SEMG signal of the selected muscles and that obtained from Inverse dynamic analysis of the MMHB.

A new approach of predicting the joint angles discretely is developed. The complete range of motion of the knee joint was quantized into levels or classes. The instantaneous

level/class of the knee angle was predicted using a classifier with features of the SEMG signals as predictor variables. The parameters of the classifiers were evaluated for different activities: Sitting down on and standing up from chair, stair assent, stair descent and level plain walking was carried out.

The SEMG signal from the lower limb muscles were acquired using the developed bioinstrumentation system while performing daily life activities. The complete range of motion of the knee angle was divided into different levels. The performance of LDA, k-NN, Naive bayes and SVM classifiers for predicting the instantaneous knee angle level were evaluated. SVM with a quadratic kernel outshined others with the average classification accuracy of 92.25 $\pm$ 2.24 % for sitting down/standing up from a chair, 87.58 $\pm$ 2.30 % for walking on plain ground, 89.25 $\pm$ 2.32 % for ascending stairs and 89.91 $\pm$ 2.37 % for descending stairs.

A prototype of the knee exoskeleton was designed in SolidWorks. It has a shank support segment, a thigh support segment and an actuator. The predicted knee angle was used to control the prototype offline. This work presents a successful development of a myoelectric knee angle prediction capable of controlling exoskeleton.

Acknowledgments

The quest for knowledge is a journey that is long and difficult but equally rewarding. That is why it is a necessity to have strong support from the people around you to make this journey a success. Without the support from many people, I would not have completed my work. It is pleasant aspect that I have now the opportunity to express my gratitude for all of them.

First of all, I would like to express my gratitude to my thesis advisors, **Prof.(Dr.) Ravinder Agarwal** for motivation, patient guidance and every-time support. Success can never be attained without proper guidance. I am truly very fortunate to have the opportunity to work with him.

I am also thankful to **Prof.(Dr.)R.S.Kaler**, Head Electrical and Instrumentation Engineering Department for extending administrative support. I specially thank members of my Doctoral Advisory Committee consisting of **Dr. Deepti Mittal, Dr. Jainy Sachdeva** and **Dr. Sanjay Sharma** for their several insightful discussions and advise.

I would like to express my gratitude to **Dr. Hardeep Singh Ryait**, without him I would never have thought of pursuing Doctorate. I found his guidance to be extremely valuable.

I would like to thank my family for standing by me through all the joys and sorrows that life had to offer. My heartfelt thanks and life-long gratitude go to my mother **Smt. Paramjeet Kaur** and Father **Sh. Gurucharan Singh Dhindsa** for all their love, constant support, encouragement and sacrifices and affection that they have showered upon me.

I would like to place on record that **Mrs. Pushpinder Kaur Dhindsa**, my beloved wife, who has always been my constant source of inspiration and encouragement in enriching my wisdom in the world of fast expanding science and technology.

My heart felt affections are due for my daughters **Kulnoor Kaur Dhindsa** and **Divyanoor Kaur Dhindsa** who mostly have suffered during my absence and they never brought up such issues to me.

I am also heartily grateful to my sister **Bhupinder Kaur Dhillon** and brother in law **Parminder Singh Dhillon** for their valuable cooperation and motivation while I was getting frustrated with the confusions during the work.

I have no words to acknowledge the contributions and support received from my colleagues, friends and well wishers namely **Dr. Surinder Malan, Mr. Ajay Malik, Mr. Krishan Dehiya, Mr. Ravinder Punia, Mr Deepender Gill** and **Mr. Ravinder Kumar** for their unparalleled help, support and suggestions.

I would also like to thank **Mr. Balwinder Saini** for his help in PCB designing and my fellow research scholar **Mr. Rohit Gupta** for having detail discussions on my research work and helping me with the proof reading of this thesis.

I would also like to thank all of them, whose names remain unmentioned but who have never retraced back from helping me whenever the need arose.

Finally, my acknowledgments would not be complete without expressing my gratitude towards Almighty God. I feel very fortunate to come to know Him during all these years of my life and have continually been blessed by His endless love ever since. He is the true shepherd of my life.

(Inderjeet Singh Dhindsa)

Contents

List of Figures

List of Tables

Glossary

Notation	Description
AMS	Anybody Modelling System
ANOVA	Analysis of Variance
AP	Action Potential
AR	Autoregressive
BIFE	Biceps Femoris
CMRR	Common Mode Rejection Ratio
CNS	Central Nervous System
DOF	Degree of Freedom
DT	Decision Tree
EEG	Electroencephalogram
EMG	Electromyographic
FD	Frequency Domain
GLME	Gluteus Medius
GUI	Graphical User Interface
HMM	Hill based muscle model
IeMG	Integrated EMG

Notation	Description
KA	Knee Angle
k-NN	k Nearest Neighbor
LDA	Linear Differential Analysis
MAV	MEAN Absolute Value
MMHB	Musculoskeletal model of human body
MNF	MEAN Frequency
MUAP	Motor unit action potential
NB	Naive Bayes
PCA	Principal Component Analysis
PGA	Programmable Gain Amplifier
REFE	Rectus Femoris
RLD	Right Leg Drive
RMS	Root Mean Square
ROM	Range of Motion
SEMG	Surface Electromyographic
SENIAM	Surface ElectroMyoGraphy for the Non-Invasive Assessment of Muscles
SETE	Semitendinosus
SQ	Squat
SSC	Signal Sign Change
ST	Stand
ST2SQ	Stand to Squat
STFT	Short Term Fourier Transform
SVM	Support Vector Machine
SVMQ	SVM with a quadratic kernel

Notation	**Description**
TD	Time Domain
VALA	Vastus Lateralis
VAR	Variance
WAMP	Willison Amplitude
WL	Waveform Length
WPT	Wavelet Packet Transform
WT	Wavelet Transform
ZC	Number of Zero Crossing

Chapter 1

Introduction

The ability of a human being to carry out a physical task depends on human muscle strength, so it is a natural human intent to increase his/her muscle strength. Further, human muscle strength decreases substantially with ageing or due to particular neuromuscular disorder. A device which could increase the human strength describes the human civilization. Robotic manipulators like electric motors or hydraulic actuators can be used to increase the strength. However, the control algorithm governing these robotic manipulators lacks the flexibility to perform smooth movements as humans. It appears that by bringing the human and the robotic manipulators together under the human control, may prompt an answer which will profit by the points of interest offered by both individually. The machines mechanical power integrated with the natural human control system could accomplish tasks/activities requiring high forces in a very efficient manner [1]. This is the fundamental principle of robotic exoskeleton systems development.

The word exoskeleton originated from two words: a Greek word "Exos" meaning outer and "Skeltos" meaning skeleton. So, exoskeleton is a hard outer structure of some animals for providing protection from predators. Many animals like tortoise, insects (like grasshoppers & cockroaches) and aquatic animals (like lobsters and crabs) have natural exoskeleton for their safety. Robotic Exoskeleton is an electromechanical suit which is worn by a human operator. The electric and/or mechanical actuators augment the capabilities of the wearer.

1.1 Applications of exoskeleton

Exoskeletons, present a new opportunity in the field of human power augmentation and rehabilitation. The exoskeleton system can be used for variety of basic applications like rehabilitation devices, human-amplifiers and power-assist systems etc. Following are some of the applications of exoskeletons.

a) In military applications, exoskeleton presents a scenario of increased capabilities of soldiers. Ground soldiers have to cover a considerable distance on foot carrying heavy gear, often on difficult terrain. Attwells *et al.* carried out a study on the impact of load on soldiers gait movement and posture [2]. An exoskeleton can increase the weight carrying capacity by passing the weight of the heavy equipment to the ground and the actuators can increase the walking and running capabilities of the soldiers. Berkley lower extremity exoskeleton and Raytheon's XOS (earlier known as Sarcos WEAR) are examples of military exoskeletons [3–5].

b) In manufacturing industries where the workers are involved in heavy lifting, they often suffer from health issues like back problems. An exoskeleton has the potential to significantly reduce the factors associated with the development of work related musculoskeletal injuries. Human-exoskeleton coordination for manual handling works represents an innovative option providing safety to workers [6; 7].

c) Exoskeletons can be of great help in disaster management by allowing the relief workers to carry heavy rescue equipment, first aid and communication equipment.

d) In medical science, exoskeletons are useful for rehabilitation of patients suffering from neuromuscular disorder [8–10]. For gait correction in patients who have cerebral palsy [11; 12]. Wu *et al.* carried out a comparative study of exoskeleton and knee-ankle-foot orthosis on patients with spinal cord injury. They concluded that the patients with eight week gait training with powered exoskeleton could comparatively walk faster and covered a large distance without an incidence of fall than when using a knee–ankle–foot orthosis [13]. Yamamoto *et al.* proposed an exoskeleton for helping medics during patient transfer [14].

e) The globe is facing many issues related to its ageing population. As per the Sept. 2005 report of the Ministry of Health and family welfare, Govt. of India, the number of people aged over 60 will grow from 8% of INDIA's population in 2010 to 19% by 2050. This increase in elderly population presents some serious challenges.

Exoskeleton developed at Sogang University helps the elderly to maintain balance while walking [15]. Galle *et al.* showed that an ankle foot exoskeleton for plantar flexion assistance for elderly resulted in lower metabolic cost as compared to normal walking [16]. Cyberdyne Inc. Japan has developed an exoskeleton named Hybrid assistive limb for improving the mobility of the elderly [17]. Majority of the elderly population is suffering from joint pains. Osteoarthritis is a major cause of disability in the elderly population. The present treatment of Osteoarthritis is to alleviate pain [18]. Some treatments attempts are used to slower the disease progression. A portable exoskeleton device presents a solution to Osteoarthritis and may delay joint replacement surgery.

f) Persons living in a hilly area are required to move around the steep terrain for their daily activities. They have to carry the heavy load by themselves or are dependent on horses and mules, as vehicles cannot be used due to lack of motor able roads. Exoskeleton by augmenting the physical powers of the wearer offers a better alternative.

1.2 Myoelectric control

lack of understanding of mechanisms responsible for human control movement is one of the significant challenge in design of exoskeletons. Research has been going on, in the field of controlling exoskeleton and many different approaches have been proposed [19–23]. This study intends to propose an algorithm to control the exoskeleton myoelectrically i.e. by using Electromyographic (EMG) signals from human lower limb muscles.

The EMG signals represents the amount of electrical potential that muscle cells generate when they contract or are at rest. EMG signals of skeletal muscles (set of muscles attached to bones) are important biological signals containing information about human motion intent. An exoskeleton system can be controlled by means of skeletal muscles's EMG signals. With respect to the place of signal acquisition, the EMG signals are grouped into two categories. The EMG signals detected from inside the muscles using needle electrodes are called intramuscular EMG (IEMG) whereas the EMG signals detected from skin surface of the muscles using surface electrodes are called Surface Electromyographic (SEMG). Giroux and Lamontagne revealed that there is no significant differences in isometric and dynamic muscle contraction detection using either IEMG or SEMG [24]. Both IEMG and SEMG are suitable for different types of applications and have their

advantages and disadvantages. The extraction procedure of IEMG signals being invasive requires continuous medical supervision making it practically unsuitable to control the exoskeleton. The SEMG signal on the other hand requires non-invasive surface electrode method and is suitable for controlling the exoskeleton.

In control systems for the exoskeleton, the use of SEMG offers numerous advantages. The SEMG signals can be measured and evaluated prior to the development of muscle force. Although, great progress has been made in the field of robotic manipulators and exoskeletons, many design challenges are still there. A portable lower limb exoskeleton demonstrating a significant reduction in the metabolic cost of daily life activities like walking or running is yet to be developed.

1.3 Objectives of thesis

The present research aims is to contribute a small degree towards the myoelectric control of exoskeleton system. This research work intends to achieve the following technical goals:

- To study the anatomic structure of human knee to identify the muscles responsible for different knee movements while carrying out daily life activities like walking, running, sitting down and standing up.
- To develop the data acquisition system employing A/D conversion and Signal Conditioning for the recording of multi-channel SEMG signals from different leg muscles.
- To develop a relationship between the joint torque and kinematics measurement of exoskeleton and propose a control algorithm to operate exoskeleton knee using appropriate number of leg muscles.
- To develop a low cost prototype of a myoelectric exoskeleton knee device-covering span between 40-180 degree. Further, the span will be confirmed based on the above research outcomes

1.4 Proposed design

A knee angle prediction from the SEMG signal of lower limb muscles is proposed in the present thesis. The proposed design shown in Fig 1.1 was used to control exoskeleton

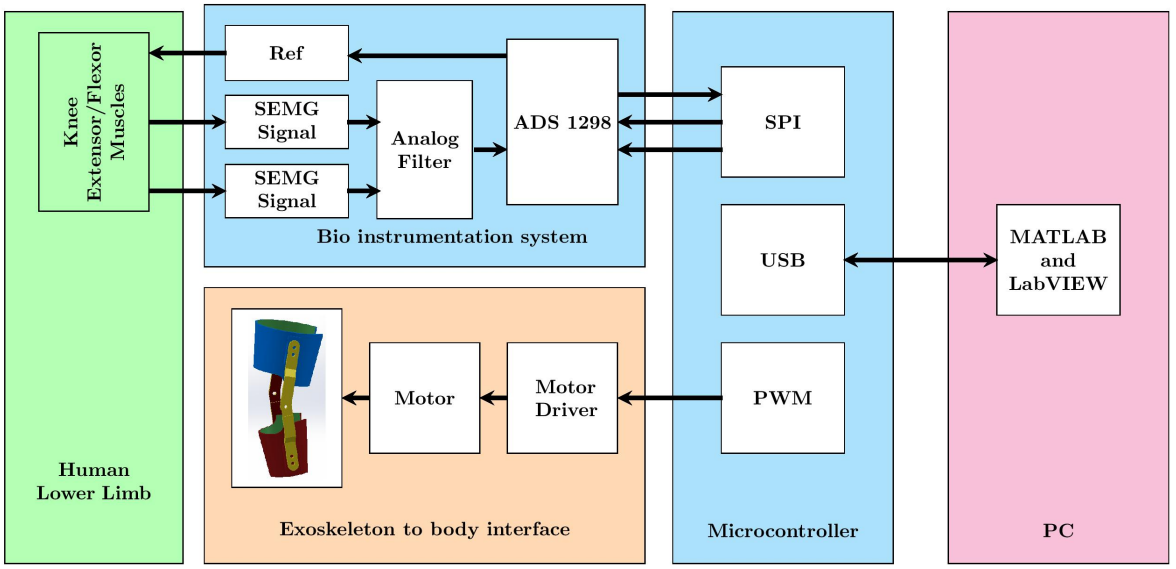

FIGURE 1.1: Block diagram of the proposed design for exoskeleton knee control

knee myoelectrically. An eight-channel bioinstrumentation system based on ADS1298 was developed to record the SEMG signals from the selected lower limb muscles. The detailed description of the bioinstrumentation system is presented in Chapter 3. The complete range of motion of the knee angle is divided into levels or classes and a MATLAB program processes the recorded SEMG signals and predicts the current level/class of the knee angle. Another program compares the predicted level/class of the knee angle with the current level/class and controls a DC motor. The DC motor, in turn, controls the exoskeleton prototype.

1.5 Outline of the thesis

Chapter 2: Literature Review Prior to presenting the myoelectric control of exoskeleton knee, it is useful to have a historical perspective. This chapter presents a thorough literature review of exoskeletons. Depending upon the sensory and actuation systems exoskeletons can be grouped into three generations: Primitive exoskeletons, Mechanical sensor based exoskeletons and Biosensor based exoskeletons. Prominent exoskeletons of all three groups have been reviewed in this chapter. The later part of the chapter reviews the development in the field of myoelectric pattern recognition systems. The chapter concludes with a brief description of common classifiers used in pattern recognition.

Chapter 3: Development of system for SEMG recording This chapter begins with a discussion on SEMG signal generation. The factors affecting the EMG signals are discussed. This chapter presents the design of an eight-channel EMG acquisition system.

Chapter 4: Muscle Selection The chapter begins with an anatomical description of the knee joint. Biological musculoskeletal model of human is highly redundant in nature. Apart from few exceptions, there exits more muscles than necessary to produce desired joint movement. The human lower limb has more than fifty muscles. However, it is possible to predict the intent of human motion by only considering some of these muscles. This chapter presents a method of selecting the set of muscles suitable for controlling a lower limb exoskeleton.

Chapter 5: Knee angle prediction from SEMG signal The control algorithm for controlling an exoskeleton myoelectrically is presented. The output of the classifier was validated using a prototype exoskeleton

Chapter 6: Conclusions and Future work It summarizes the work presented in chapter 2 to chapter 5 with the concluding remarks. The issues to be encountered for further development in myoelectric control of exoskeleton systems are mentioned leading to the future orientation of this research.

Chapter 2

Literature review

This chapter explores the comprehensive literature review of the studies made in this field. The chapter starts with a review of developments in the field of exoskeletons followed by a review of progress in the field of myoelectric pattern reorganization and a brief discussion on the classifiers used in myoelectric pattern recognition.

2.1 Exoskeleton developments

In the field of exoskeleton, one of the initial recorded work is that of Nicholas Yagn, a Russian army engineer. He was granted US Patents 420179 and 440684 in the year 1890 for his work on "Apparatus for facilitating walking, running, and jumping" [25; 26]. Yagn's first design is shown in Fig 2.1(a). The main parts of the design are the two bow-springs connected between the foot and mid-way to the waist. The mechanism allows the free vertical movements of the spring ends when the legs bend while performing daily life activities. The wearer's body weight compresses the spring during bending. This results in the accumulation of energy in the spring. The stored energy is released later on and increases the walking, running, and jumping capabilities of the wearer.

In the Yagn's second design shown in Fig 2.1(b) the bow-spring accumulators were replaced by a compressed fluid accumulator. The fluid accumulator is bellow shaped stockings placed at the sole of the design. It is connected to a fluid reservoir containing fluid under pressure through a flexible gas tight tube. It expands or collapses based on internal or external pressure. When the accumulator is fully expanded, it acts as an elastic bearing for the body. The compressed gas aids the wearer during lifting of feet and provides

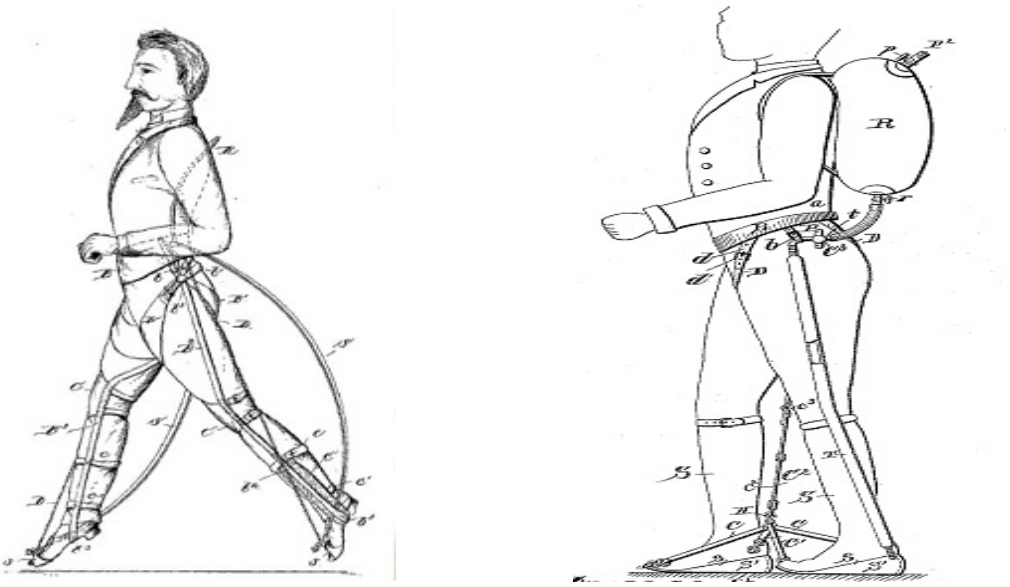

(a) Patent No 420179 (b) Patent No 440684

FIGURE 2.1: Yagns exoskeleton designs

a cushion (shock absorber) as the feet come down. Although, Yagns proposals were for augmenting, the wearer's running, walking and jumping capabilities. However, there is no information that such devices were ever built and functioned successfully [27].

2.1.1 Primitive exoskeleton's

2.1.1.1 HARDIman

General Electric Research in the year 1960, developed a whole-body exoskeleton named "Human Augmentation Research and Development Investigation" (HARDIman) shown in Fig 2.2(a). The design was a huge hydraulically powered machine weighing around 680 kg and exhibiting 30 Degree of Freedom (DOF). It was designed to amplifying the strength of the wearer by more than 25 times [28]. The exoskeletons design was simply too large and bulky to move and operate [27].

2.1.1.2 PITMAN

In 1985, Jeffrey Moore proposed a powered armor suit for infantrymen called PITMAN as shown in Fig 2.2(b). The PITMAN concept relied on brainwave-induced commands. A 200 lb. robotic suit equipped with a mechanical actuator in the legs enables the wearer to jump and sprint at levels far exceeding the greatest Olympians. To control the mechanism

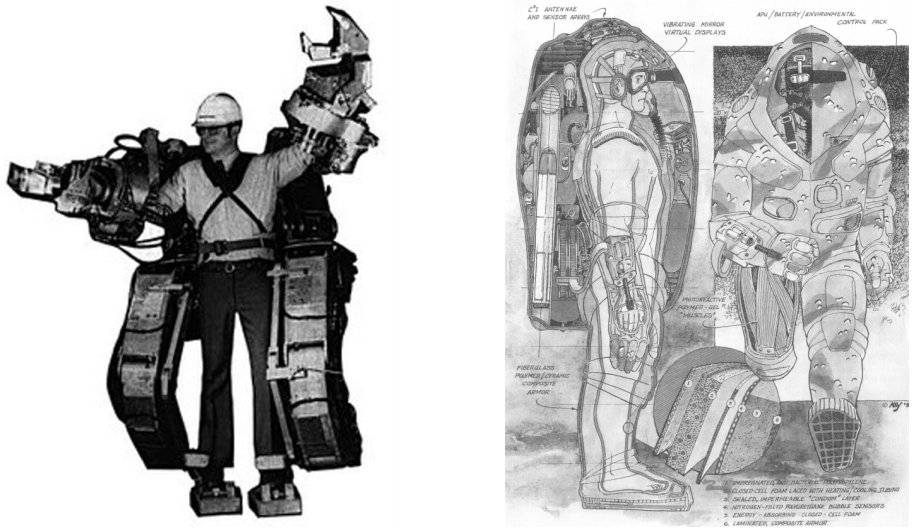

(a) HARDIman (b) PITMAN

FIGURE 2.2: Primitive exoskeletons

of the exoskeleton was proposed around a network of brain scanning sensors proposed in the helmet. These sensors would measure the shift in the magnetic fields as a result of the limb movement decisions taken by the brain [29]. The PITMAN was far ahead of its time and could not see the light of the day for the lack of funding.

2.1.2 Mechanical sensor based exoskeleton

H. Kazerooni in 1990 proposed a concept, which combined the mechanical strength of the hydraulic actuator with the human intellect in the form of a human extender, a robotic manipulator that could be worn by a wearer. The physical contact between the wearer and extender allowed for the exchange of mechanical power and information signal. The extenders actuator provided the required strength under the control of the wearer. Extender substantially attenuated the load experienced by the wearer [30; 31].

The development in the field of exoskeleton gained momentum after 2001. A project named Exoskeletons for Human Performance Augmentation (EHPA)was initiated by U.S. Defense Advanced Research Projects Agency (DARPA) in 2001 with an aim to enhance the physical strength of soldiers.

A number of institutes made progress in research on technologies related to exoskeleton through the EHPA program. Exoskeleton of Massachusetts Institute of Technology (MIT) [32; 33], Berkley University's BLEEX [3] and Sarcos Research Corporation's "Wearable

(a) MIT (b)BLEEX (c) Raytheon Sarcos XOS

FIGURE 2.3: DARPA exoskeletons

Energetically Autonomous Robot" (WEAR) [34] are some of the prominent exoskeletons developed under the DARPAs EHPA program.

2.1.2.1 MIT exoskeleton

The MIT exoskeleton is based on a quasi-passive design. The exoskeleton stores the energy in the negative energy phase of the gait and utilize the same during the positive energy phase of the walking gait [32]. The MIT exoskeleton depicted in Fig 2.3(a) is interfaced to the wearer using shoulder straps and thigh cuffs. The exoskeleton employs a 3 DOF at hip joint. A spring mechanism designed at the hip joint stores the energy during extension and releases it during flexion. The spring allowed the user to swing his/her hip freely in the direction of flexion. The direction of the hip abduction/adduction was also loaded with spring to overcome the moment induced by the load of the backpack. The MIT exoskeleton uses the sensory information from a potentiometer on the knee joint and full-bridge strain gauges on the exoskeleton shin. The exoskeleton requires 2W of electrical power during loaded walking and weighs around 12Kg[27; 32].

2.1.2.2 BLEEX

A team of researchers led by Prof. Homayoon Kazerooni at University of California, Berkeley, developed a lower limb exoskeleton for enhance the abilities and strength of soldiers, firefighters, and rescue workers named BLEEX. BLEEX is shown in Fig 2.3(b).

The BLEEX had a total of eleven DOFs [35; 36]. Out of the eleven DOFs, eight are actuated (hip flexion/extension, hip abduction/adduction, knee flexion/extension and ankle plantar-flexion/dorsi-flexion). The remaining three DOFs are equipped with passive impedance's using springs [4]. The BLEEX control mechanism uses the sensory information from 16 accelerometers and 8 encoders. An inclinometer is used to measure the orientation of the backpack. Force distributions at feet are determined by a load cell and foot switch. 8 single-axis force sensors are utilized for controlling each of the actuators [3].

2.1.2.3 Sarcos WEAR/ Raytheon's XOS

The Sarcos Research Corporation, under the DARPA EHPA program proposed Wearable Energetically Autonomous Robot (WEAR), a whole-body exoskeleton. The exoskeleton depicted in Fig 2.3(c) carried its own power supply and employed rotary hydraulic actuators at the joints. Defense contractor Raytheon acquired The Sarcos Research Corporation in November 2007 and upgraded WEAR to a new brand XOS (XOS-1 was unveiled in 2008).

The mechanical sensor based exoskeletons had a common feature that sensors placed on/between the human operator and exoskeletons predict the human motion intent. The exoskeletons actuators were then triggered either by the kinematic position command or by the dynamic contact force command. In both the cases, the motion intent information is generated after the actual motion has been started. This resulted in a delay in the relative movement of the human and exoskeleton system. This lag in relative motion was the primary disadvantage of these exoskeletons and an appropriate mechanism to predict the human motion intent in advance is required.

2.1.3 Biosensors based exoskeleton

The next generation of exoskeleton were controlled through biosignals (Electroencephalogram (EEG), EMG). The motion intent is predicted by the biosensors placed on the human body. Biosensors offers the advantage of advance prediction of the motion intent before the actual movements of joint. The exoskeleton uses this information and amplifies the joint moment by a preselected gain factor, resulting in a decrease in the reaction time of the human/machine system. Only SEMG based exoskeletons are reviewed in the present section.

(a) PAS (b) UCLA Exoskeleton (c) HAL

FIGURE 2.4: Biosensor based exoskeletons

2.1.3.1 Power assist suit (PAS)

Yamamoto *et al.* proposed an exoskeleton named Power Assist Suit (PAS), for assisting medics during patient transfer. The PAS shown in Fig 2.4(a), utilized a force sensing resistor attached to the skin surface above the muscle in determining the wearer intent [14]. Rubber cuff based pneumatic rotatory actuators were used to make the joints flexible. Muscle force was detected using muscle hardness sensor.

2.1.3.2 UCLA shoulder exoskeleton

Rosen *et al.* proposed a myoelectric controlled exoskeleton system for human elbow joint. UCLA shoulder exoskeleton is shown in Fig 2.4(b). The SEMG signals from two muscles of upper limb were used to predict the elbow joint torque for controlling an an upper limb exoskeleton capable of lifting heavy load.

2.1.3.3 Hybrid assistive limb (HAL)

Lee and Sankai developed an exoskeleton named Hybrid Assistive Limb (HAL). HAL is suitable for performance augmenting as well as rehabilitative purposes [17]. The HAL consisted of an aluminum and nicklemolyddenum alloy frame enclosed in a plastic casing. The exoskeleton is attached to the wearer's body using hooks and velcro straps. The exoskeleton weighs approximately 23kg.The exoskeleton's weight is transferred to the

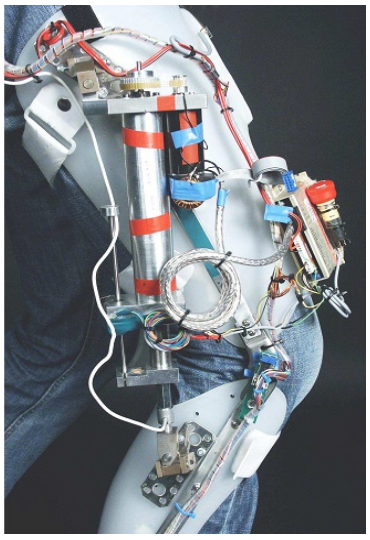

(a) BU exoskeleton

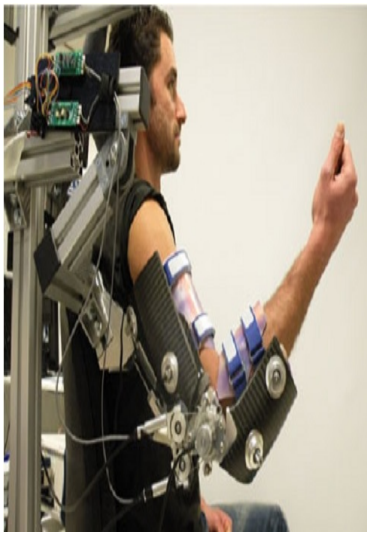

(b) Neuroexos ELbow

(c) PAM

FIGURE 2.5: Biosensor based Exoskeletons cotd...

ground through the footplate and the wearer doesn't bear any burden. Presently HAL exoskeletons is produced and marketed in japan by Cyberdyne Inc. as a rehab device. The most recent device was the HAL-5, which included both an upper and lower limb exoskeleton. HAL-5 depicted in Fig 2.4(c) is the latest model in HAL series.

2.1.3.4 Berlin university lower limb extremity exoskeleton

Fleischer *et al.* at Berlin University doweleped an exoskeleton utilizing SEMG signals. The exoskeleton is depicted in Fig 2.5(a). The SEMG signals are obtained from three extensor and three flexor muscles. The EMG signals are fed into a muscle model, which estimates the knee torque. The estimated torque is fed as input to a torque controller, which amplifies it with the desired support ration to obtain the desired target torque [19; 37; 38]. The torque produced by the DC motor (Maxon RE35 DC motor) was measured using force sensors and knee angle data. the torque controller generates the required control signal to achieve the desired torque[37].

2.1.3.5 Neuroexos elbow

A dual shell exoskeleton for the upper limb NEUROExo was proposed by Lenzi *et al.* Fig 2.5(b) shows the NEUROExo elbow. The proposed exoskeleton consisted of two shells: The inner shellsare tailor-made to match the subject's limb dimensions. The inner shells are made of two layers: the inner layer made of ethylene vinyl acetate and the

outer layer made of polypropylene. The outer shells are made of double wall carbon fiber structure [39–41].

The elbow exoskeleton is powered by an antagonist driven complaint joint [41]. The mechanism consisted of two hydraulic actuators for generating antagonistic displacements, a stroke amplifier for converting the piston displacement to transmission elongation and steel wire for transmitting the force to the exoskeleton through bowden cables. Linear envelops of the SEMG signals from two upper limb muscles were used to obtain the flexor and extensor forces. A closed loop controller is used to control the cable forces according to the flexor and extensor forces obtained from SEMG signals [39].

2.1.3.6 Pneumatic artificial muscle based exoskeleton

Chandrapal *et al.* developed a pneumatic artificial muscle (PAM) based knee exoskeleton. The exoskeleton is shown in Fig 2.5(c). PAM consists of an inflatable membrane with an outer high strength braided shell [42; 43]. Four PAM (two knee flexors and two knee extensors) were used in the exoskeleton design. The exoskeleton was controlled myoelectrically through EMG signal of five lower limb muscles [21]. The control algorithm predicts the knee joint torque from the muscle activation signal of the five muscles and knee angle[44]. The predicted torque is compared with the torque information obtained from the load cells. The controller varies the pressure within the PAM corresponding to the error signal by means of proportional pressure regulator and high speed valves[21].

2.2 Myoelectric pattern recognition

The complexity of EMG signal is the greatest challenge in the field of myoelectric controlled exoskeletons and prostheses[45]. The response time of the prostheses/orthotic device is to be maintained below 300 ms for the smooth operation of the device [46]. Although a prosthetic device with myoelectric control was first proposed in 1973 [47]. However, the limited computing ability of that time restricted the design to laboratory.

Three different approaches of myoelectric controls are available in the literature. In the first approach, muscle force or torque is predicted from SEMG signals of selected muscles [20; 38; 48; 49]. The muscle activation signals obtain from the SEMG signal of the recruited muscle is fed to a muscle model that estimates the joint forces and/or joint

moments. The commonly used muscle models are Hill muscle model [50] and Hammerstains muscle model [51].The second approach deals with estimating modes of motion like hand opening, hand closing,forearm pronation, forearm supination, finger movements, wrist flexion and wrist extension for upper limb [52–54] and predicting locomotion modes (walking on different terrains) [55–60].

The third approach deals with determining the exact body postures by predicting the joint positions from the SEMG signals [61–65].

2.2.1 Myoelectric control of upper limb

Chang *et al.* predicted four hand movements with an accuracy of 90 % using features of SEMG signals and mahalonobius distance [53].

Zardoshti *et al.* used k Nearest Neighbor (k-NN) classifier to predict hand gestures from Time Domain (TD) features of SEMG signals of upper limb muscles. They concluded that the SEMG histogram has high tolerance towards noise and is suitable for speed estimation [54].

Englehart *et al.* compared the performance of feature selection and feature projection (using Principal Component Analysis (PCA)) for different features mainly: TD, Short Term Fourier Transform (STFT), Wavelet Transform (WT) and Wavelet Packet Transform (WPT) in classification of movements of upper limb using a Linear Differential Analysis (LDA) classifier and a multi layer perceptron (MLP) classifier. They concluded that feature projection is comparatively better option to feature selection.Overall the performance of a PCA reduced WPT feature set with a LDA classifier was reported as best with an error of 6.25% [45].

Englehart *et al.* compared the performance of four channel system to that of a two channel system for classifying six hand movements (hand open/close, wrist extension/flexion and radial/ulnar deviation of wrist) using a wavelet based continuous myoelectric control. Features (TD, STFT, WT and WPT) were evaluate and further subjected to dimensional reduction using PCA and classified using a LDA classifier. They observed that the four channel system perform superior as compared to two channel system [66]. Further, the classification accuracy achieved with WT and WPT feature set was better than that obtained with TD and STFT feature set. They also proposed a new technique of continuous classification based on the concept of sliding window. The size of the sliding window and the window increment size affect the classification accuracy of the system [66].

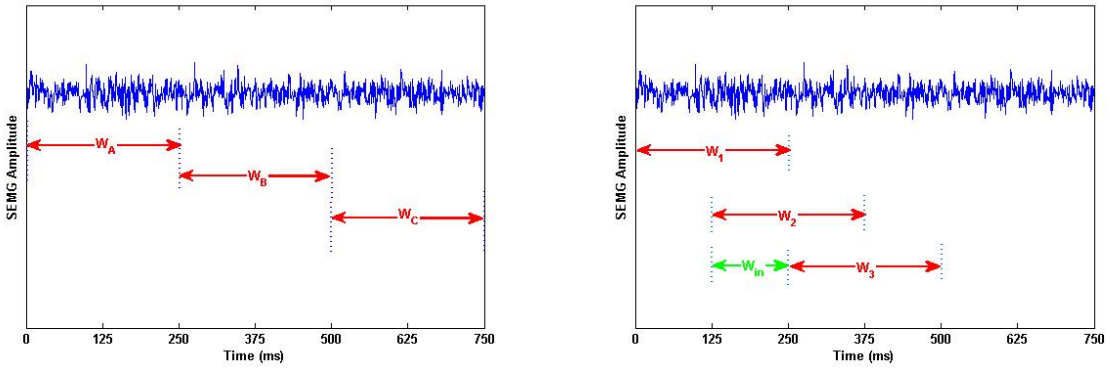

(a) Disjoint Windowing (b) Overlapped Windowing

FIGURE 2.6: Windowing of EMG signal

Englehart and Hudgins proposed a pattern recognition based system for controlling an upper extremity prostheses. SEMG signals from four channels were segmented into windows and a feature vector consisting of Four features: number of slope sign changes, number of zero crossings, waveform length and mean absolute value was obtained for each window. A 16-dimensional feature vector (four features per channel for a four-channel system) was fed to a LDA classifier [46]. They proposed two different windowing schemes. An adjacent disjoint windowing scheme and overlapped windowing scheme. Fig 2.6 shows both the windowing schemes. The results indicated that overlapped windowing scheme with suitable increment size resulted in dense decision streams and increase the classification accuracy of the system [46].

Boostani *et al.* evaluated nineteen features obtained from the SEMG signals recorded from the eight upper limb muscles. They used Davies-Bouldin criteria and scattering criteria to increase the estimation of feature space. According to them energy of the wavelet coefficients of ninth scale and cepstrum coefficients are the best features for controlling a prosthetic hand [67].

Hargrove *et al.* classified eleven motion classes of upper limb corresponding to hand, wrist and forearm. SEMG signal were recorded from 50 mono polar electrodes placed around the forearm in five eqi-placed constellations of ten electrodes each. TDfeatures, Autoregressive (AR) coefficients and combination of AR and TD features (TDAR) were extracted from the SEMG signals and supplied as input to a LDA classifier. TDAR features yielded the best classification accuracy and were least affected by the electrode displacements [68].

Du *et al.* compared the performance of grey relational analysis (GRA) classifier and Multi layer neural network (MLNN) in predicting eleven different hand motions from SEMG

signal recorded from seven muscles of upper limb. Six features including Integrated EMG (IeMG), Number of Zero Crossing (ZC), Waveform Length (WL), Variance (VAR), Signal Sign Change (SSC), and Willison Amplitude (WAMP) were calculated and fed as input to the classifier. GRA Classifier achieved high average accuracy and took less processing time as compared to MLNN [69].

Phinyomark evaluated thirty seven features (twenty four time domain and thirteen frequency domain)to obtain a redundant feature set capable of classifying six different hand movements using LDA classifier [70]. They further grouped the TDF on the basis of energy information, complexity information, frequency information, and time dependency information. They concluded that the performance of frequency domain features was not suitable for EMG recognition systems as compared to time domain features.MEAN Absolute Value (MAV), WAMP, WL, and MEAN Frequency (MNF) were proposed as optimal features for controlling prosthesis.

Chu *et al.* proposed a system to recognize nine different types of hand motions from SEMG signals acquired from fore upper limb muscles [71; 72].

Ryait *et al.* proposed a strategy of using the acupressure points as sensor location for acquiring the SEMG signals [73; 74]. They developed a system to identify four different activities of wrist/hand including: wrist opening, wrist close, wrist up and wrist down from SEMG signals acquired from six acupressure points on the arm namely, CW, CWB, CBEB, CBET, CAM and, CAMB. They evaluated six parameters from the recorded SEMG signals including Root Mean Square (RMS), Total Energy, slope, median frequency, and peak frequency. They used PCA to select the appropriate set of acupressure points for controlling the wrist movements. They deduced that CBET and CBEB are suitable sensor locations for controlling the wrist movements for a two channel system, and for a three channel system the best combination is of CAM, CAMB and CBET. Among the EMG parameters slope was considered best for controlling the four wrist movements [74].

Ryait *et al.* proposed a SEMG based multifunction controlled arm capable of performing elbow flexion/extension and wrist pronation/supination from SEMG signals acquired from above elbow locations [75].

Sanjeev *et al.* at CSIO Chandigarh, proposed a below elbow myoelectric arm capable of providing a proportional grip force. RMS of the SEMG signal acquired from three electrode placed transversely on the residual stump of the amputee was used to provide a proportional grip control [76].

Sanjeev *et al.* proposed a design of myoelectric arm capable of performing opening/closing of hand, wrist rotation and lifting of objects with variable grips from EMG signals from the two muscles of an amputees forearm: pronator teris and supination [77]. A single DC motor along with two electromagnetic clutches is controlled depending on the magnitude of EMG signal.

Aung *et al.* predicted joint angles of the upper limb using a back propagation neural network (BPNN) and SEMG signals from four muscles: anterior deltoid, posterior deltoid, bicep brachii and tricep brachii [78].

Han *et al.* presented a state-space model utilizing the WL and ZC of the SEMG signals and Hill based muscle model (HMM) for continuous prediction of the human elbow joint angle [79].

Veer and Vig classified four activities of the upper limb: Elbow flexion, elbow extension, elbow adduction and elbow abduction from the SEMG signals of upper limb muscles using PCA [80; 81].

Leizhang evaluated MAV, standard deviation of EMG, standard deviation of frequency and db3 wavelet coefficients from the SEMG signals of upper limb muscles. A BP neural network used the evaluated features to predict the elbow angle [62].

Xiao *et al.* at Hefei University proposed a joint angle estimation system utilizing MAV, WL, ZC, SSC and DASDV features of SEMG signals of upper limb muscles. The prediction system utilizing EMG features signals along with their time delayed signals and a random forest regressor performed best in predicting elbow flexion and extension angle [61].

2.2.2 Myoelectric control of lower limb

Fleischer *et al.* predicted the knee torque from the SEMG signals recorded from the thigh muscles using a Hill type model. A torque controller determines the amount of support to be provided to the wearer by comparing the predicted and instantaneous torque [38].

Huang *et al.* used features acquired from sixteen muscles of human lower limb and identified seven movement modes (ascending and descending stairs, standing still,level ground walking, ipsi-lateral and contra-lateral turning and stepping over an obstacle) using a phase dependent pattern recognition system [55]. They used force sensing resister

based foot switches placed under the subject's feet to record the gait events. They evaluated the performance of a LDA classifier and an artificial neural network (ANN) classifier. Both the classifiers gave significantly similar performance in predicting the locomotion modes. They recommended LDA classifier for real time prosthetic control because of its ease in designing, fast training time and high computational efficiency.

Delis *et al.* proposed an algorithm to predict knee angle from EMG signal acquired from vastus lateralis, rectus femoris and semitendinosus muscles of human lower limb [63]. They evaluated feature vector consisting of Amplitude histogram bin counts and AR coefficients for each EMG channel. They proposed a two-stage knee angle prediction algorithm consisting of a self-organization map (SOM) based feature projection stage and a MLP neural network based pattern recognition stage. According to them, the proposed algorithm provided lower error to signal percentage and a higher correlation between the actual and predicted knee angle [63].

Young and Hargrove studied an intent recognition system for transfemoral amputees. They used EMG signals from the nine muscles along with thirteen mechanical sensors. The data acquired was segmented and features (Minimum, Maximum, mean and standard deviation for mechanical sensors. Waveform length, mean absolute value, and AR coefficients for EMG signals) were acquired. They predicted the motion intent using Dynamic Bayesian network, LDA and LDA with majority votes. They deduced that EMG information in combination with mechanical sensory information reduced the motion intent recognition errors [57].

Gupta and Agarwal studied the performance of six classifiers (k-nearest neighbor, neural network, LDA, SVM, Naive Bayes (NB) and Decision Tree (DT))and twelve different window sizes for predicting the different locomotion modes among plain walking, stair assent and stair dissent [59]. They reported that the performance of LDA classifier in identifying the correct locomotion mode is superior as compared to the remaining five classifiers. Window W_4 with size of 128ms and window shift of 128ms outperformed the other window sizes with relative standard deviation of 0.63 ± 0.08 [59].

2.3 Conclusion

This chapter starts with a thorough review of exoskeletons. Exoskeletons can be grouped into three generations depending upon the sensory and actuation systems: Primitive exoskeletons, Mechanical sensor based exoskeletons and Biosensor based exoskeletons.

The later part of the chapter reviews the development in the field of myoelectric-based pattern recognition systems. There are three design approaches available in the literature: Force/torque based, Motion mode based and Posture or joint angle based. Force/torque based system utilized the muscle activation signals of appropriate muscles as input to the biomechanical models for obtaining the joint force/torque. Hill muscle model and Hammerstain muscle models have been used predominantly in the literature. However, several parameters of these biomechanical models need to be determined. Further, it is hard to apply a biomechanical model to describe the characteristics of human limbs of a wide population.

In the next approach, features from the SEMG signals of appropriate muscles are used to forecast the locomotion mode like level ground walking, ascending/descending stairs and ascending/ descending ramps for lower limbs and to anticipate the gestures for upper limb like hand opening/ closing, forearm pronation/supination and wrist flexion/extension . But, these pattern recogination system lacks in predicting the joint positions.

The third approach uses a regression based system to forecast the exact body postures by predicting the joint positions from SEMG signals. Present research work introduces a new approach of predicting the joint angles. The complete range of motion of the knee joint was quantized into levels or classes. The instantaneous level/class of the knee angle was predicted using a classifier with features of the SEMG signals as predictor variables. The last section of the chapter discussed the common classifiers (LDA, NB, k-NN and SVM) used in pattern recognition of SEMG signals.

Chapter 3

Development of system for SEMG recording

The chapter begins with a brief discussion of SEMG signal, its origin, factors affecting the EMG recording like noise, electrode placements, skin preparation *etc.* The later part of the chapter presents the design of an eight-channel bio instrument system capable of recording SEMG signal.

3.1 SEMG signal generation

In the human body, Central Nervous System (CNS) supervises the contraction and relaxation of muscles through a multifaceted electro chemical process. The brain transmits a control signal over nervous system towards motor neuron, which innervates various muscle fibers. This signal is called Action Potential (AP). However, in the case of reflexes it is generated by the spinal cord [82]. Fig 3.1 illustrates the sensory-motor control loop of humans.

AP originating in the CNS reaches the alpha motor neuron, which further transfer it towards its own axon and neuromuscular junction. Upon reaching the neuromuscular junction, AP causes the neurotransmitter acetylcholine to fuse with the plasma membrane. This results in calcium and sodium ion exchange across the membrane and development of a potential gradient in the muscle fiber. This results in contraction/activation of the muscle. When the muscle is activated it produces a Motor unit action potential (MUAP). The repeated continuous activation of the muscle produces MUAP trains. The

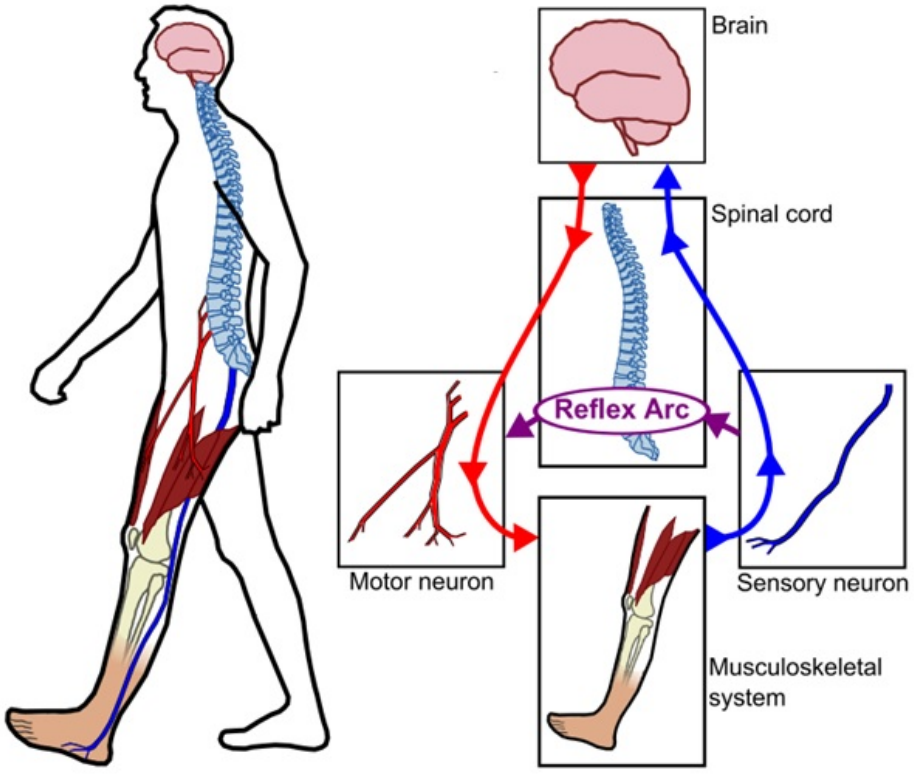

FIGURE 3.1: Sensory motor control loop for humans

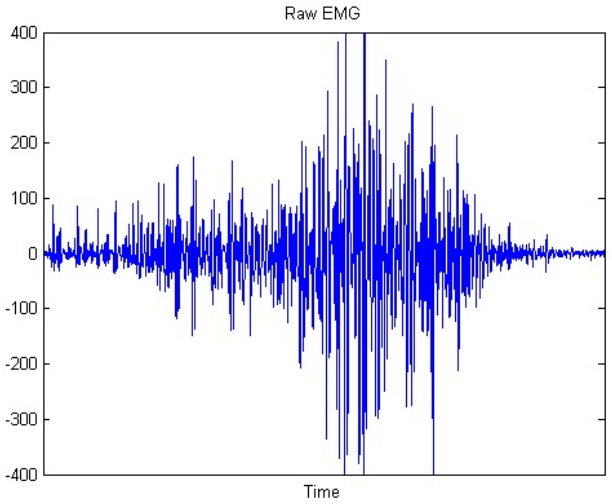

FIGURE 3.2: RAW SEMG signal

trains from concurrently active motor units superimposes to produce EMG signal [83]. The EMG signal lies in the frequency range from 0-500 Hz having dominancy in the range of 50 - 150 Hz. The amplitude of the EMG signal varies from 50 μV to 30 mV [84]. An unfiltered and unprocessed EMG signal is called raw EMG signal. Fig 3.2 depicts a raw EMG signal recorded from Vastus Lateralis (VALA) muscle during knee flexion.

3.2 Noise in EMG recording

EMG signal is stochastic in nature, amplitude of the signal lies in the range of few milli volts. It is highly influence by noise. Mainly four types of noise affect EMG signals:

- **Ambient Noise:** It is the noise generated from the electromagnetic devices like radio and TV transmission, fluorescent lamps and electrical power sources (50/60 Hz). The magnitude of this noise may be of the order of two to three times the EMG signal [85].This noise can be substantially minimized by using high Common Mode Rejection Ratio (CMRR) differential amplifiers, use of shielded leads and employing a Right Leg Drive (RLD) circuitry.

- **Motion Artifact:** Movement of the cables connecting the electrodes to the amplifier and the interface between the skin and the electrodes surface creates motion artifacts. The motion artifacts noise has amplitude comparable to the EMG signal. Recessed electrodes can remove the movement artifact significantly [84]. This noise can also be reduced by proper skin preparation prior to signal recording [86; 87]. Further, the frequency range of motion artifacts noise lies from 0 - 10 Hz [88]. Incorporating a high pass filter in either hardware or software reduces this noise. Wavelet de-noising also reduces motion artifact noise in EMG signals [89; 90].

- **Inherent noise:** All electronics equipment generates electrical noise. This noise has frequency components that range from 0 Hz to several thousand Hz. This noise can only be reduced by using high quality components [84].

- **Inherent instability of signal:** The firing rate of motor units is quasi-random in nature this noise lies in the frequency range of 0 – 20 Hz. Incorporating a high-pass filter of 20 Hz in either hardware or software reduces this noise.

3.3 SEMG electrodes

One of the most important components in SEMG recording is the electrode. Two types of electrodes are used for SEMG recording:

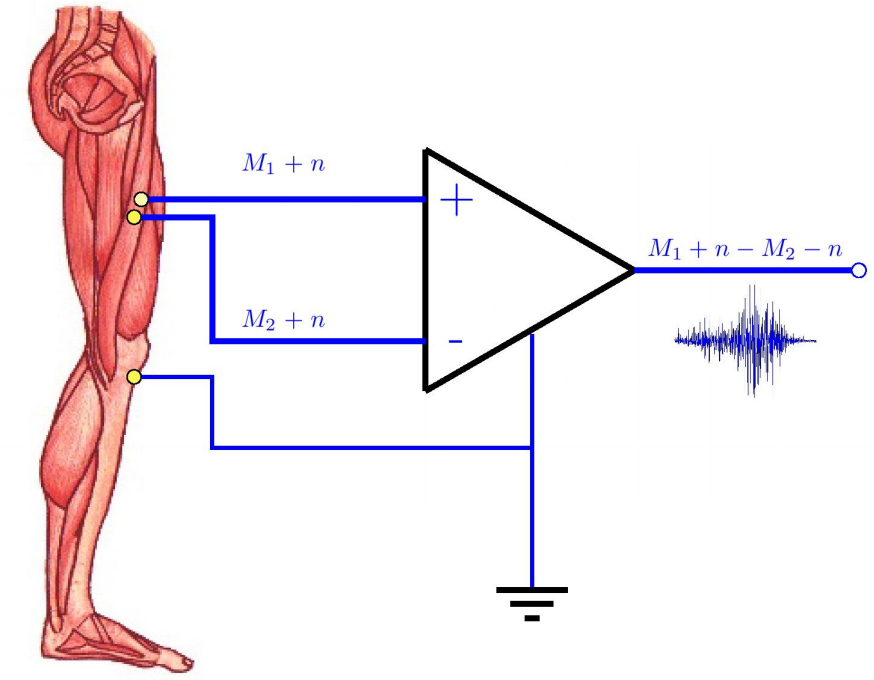

FIGURE 3.3: Bipolar configuration for SEMG recording

Gelled Electrode: These electrodes use a conductive gel or an electrolytic as a chemical interface between the skin and the electrode's metallic part. Usually, Ag-AgCl electrodes are used to provide a better signal to noise ratio [91]. The interface between the electrolyte and electrode reduces the electrode-skin impedance and thereby enhances the signal quality.

Dry Electrode: These electrodes do not require a gel interface between the skin and electrode. These are mainly used in applications where the geometry or size of electrode does not allow the application of electrolytic gel [92].

3.4 Electrode configurations

Commonly used electrodes configurations for SEMG recording are Monopolar and Bipolar configuration:

- **Monopolar Configuration:** In this configuration a single electrode placed on the skin above the muscle and signal is recorded with respect to a reference electrode [92; 93].

- **Bipolar Configuration:** This is the most commonly used configuration for SEMG recording configuration. Fig 3.3 illustrates this configuration. It uses a differential amplifier and a pair of surface electrodes placed 1-2cm apart. The input to the differential amplifier is the potential of each electrode with respect to the reference. The differential amplification suppresses the correlated signal common to both the electrodes. A neutral ground or reference electrode is essential for providing common reference for the differential amplifier. The reference electrode must be placed at an electrically unaffected region such as joints, boney area like frontal head or tibia bone [94]. The positioning of the electrode on the muscle surface influences the quality of the recorded signal. The electrode needs to be placed on the midline of the muscle belly, between the myotendonous junction and the nearest innervations zone [95]. The Surface ElectroMyoGraphy for the Non-Invasive Assessment of Muscles (SENIAM) project gave recommendations for placements of the SEMG electrodes for different muscles [96–99].

3.5 Bio instrumentation system

Fig 3.4 presents the block diagram of the bio instrumentation system. The system has three main parts: An analog to digital converter (ADS1298), a microcontroller for communicating between PC, ADS1298, and a software platform for data acquisition, visualization, post processing and storage of EMG signals (LabVIEW / MATLAB)

3.5.1 ADS1298

ADS1298 has eight low power, multichannel, simultaneously sampling, 24-bit delta sigma analog to digital converters (ADCs) with integrated programmable gain amplifiers (PGAs) [100]. Fig 3.5 shows the functional block diagram of ADS1298. Each channel of ADS1298

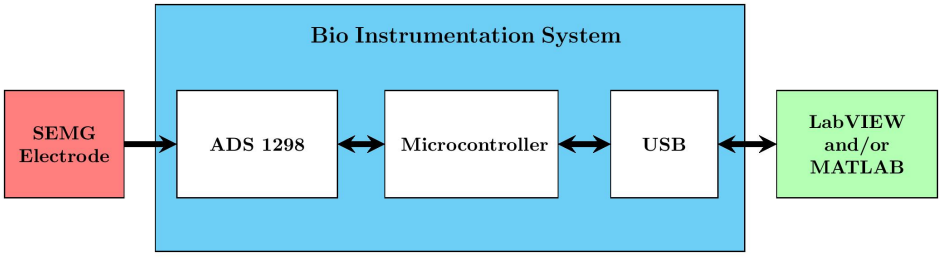

FIGURE 3.4: Block diagram of bio instrumentation system

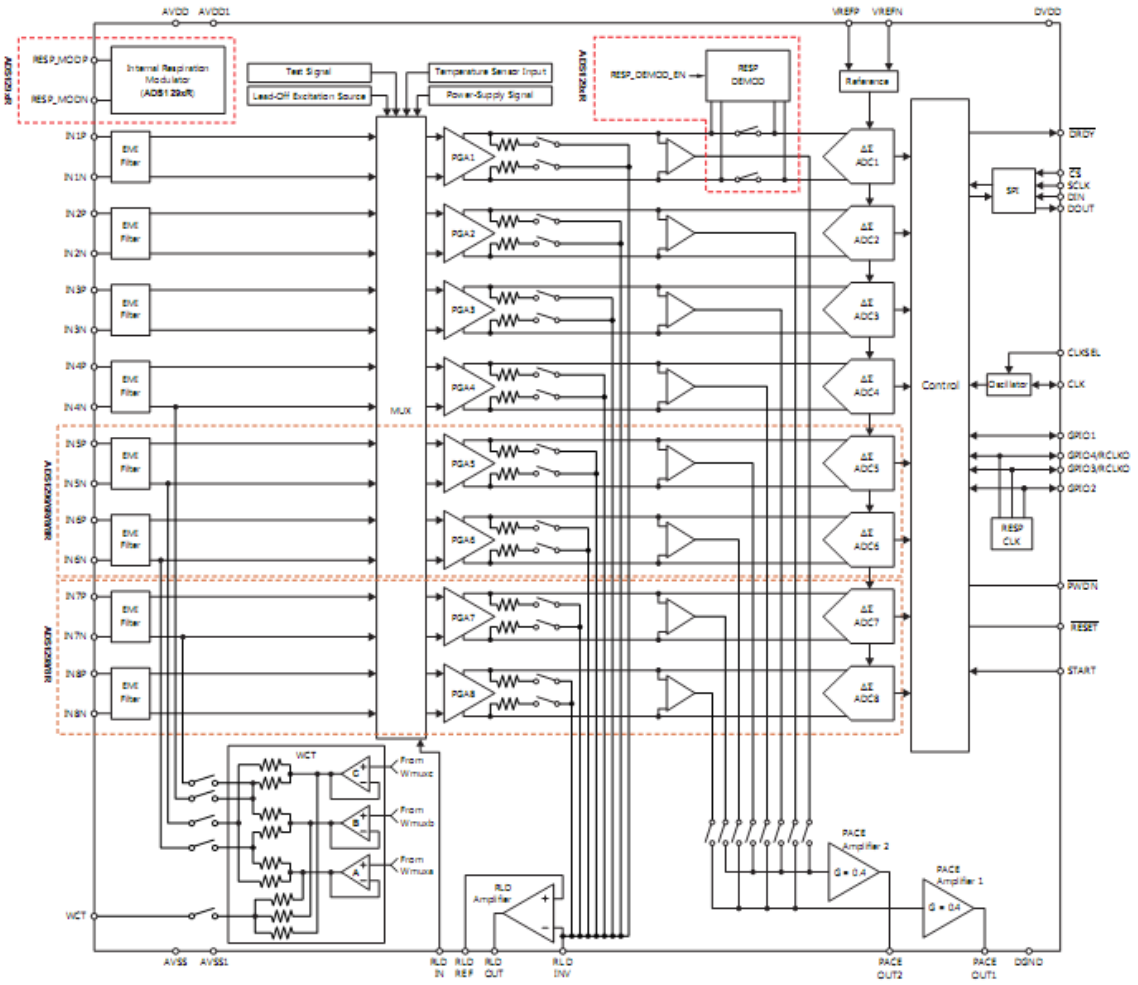

FIGURE 3.5: Functional block diagram of ADS1298

has an associated MUX which can be programmed by setting the bits of respective CHnSET registers. Further, the MUX setting also allows to set the gain among the seven available levels(1, 2, 3, 4, 6, 8, or 12). Fig 3.6 gives the description of the CHnSET register settings.The ADCs can be programmed to work at one of the eight data rates among: 250SPS, 500SPS, 1KSPS, 2KSPS, 4KSPS, 8KSPS, 16 KSPS and 32 KSPSby configuring DR2-DR0 bits of CONFIG1 register. The clock can be generated either by using an internal oscillator (2.048 MHz) or from an external clock generator.

RLD amplifier of ADS1298 was configured by setting the relevant bits of CONFIG3 register. The RLDREF signal can be fed externally or can be set internally to a value (AVDD-AVSS)/2 by setting bit 3 of CONFIG 3 register. The ADS1298 outputs a 24 bit value of data per channel in binary two's complement format (with MSB first). The smallest values which can be measured correctly is $VREF/(2^{23}-1)$. Table 3.1 summarizes the output data for different input signal voltages. The ADS1298 provide a flexible way

BIT7	BIT6	BIT5	BIT4	BIT3	BIT2	BIT1	BIT0
PD	GAIN2	GAIN1	GAIN0	0	MUXn2	MUXn1	MUXn0

Gain settings

Gain is 6	0	0	0
Gain is 1	0	0	1
Gain is 2	0	1	0
Gain is 3	0	1	1
Gain is 4	1	0	0
Gain is 8	1	0	1
Gain is 12	1	1	0

MUX settings

Normal Electrode	0	0	0
Input Short	0	0	1
Used for RLD ckt	0	1	0
Supply measurement	0	1	1
Temp Sensor	1	0	0
Test signal	1	0	1
Positive electrode of RLD driver	1	1	0
Negative electrode of RLD driver	1	1	1

FIGURE 3.6: CHnSET register of ADS1298

TABLE 3.1: Output of ADS1298

Input Signal	**Output Data**
$\leq$ -2.4 V	800000H
-0.286 μV	FFFFFFH
0 V	000000H
0.286 μV	000001H
$\geq$ 2.4 V	7FFFFFH

of programming and configuring the device by writing values into its registers. An opcode needs to be send through SPI communication to control and configure the operation of the device. There are ten different commands for programming ADS1298. Table 3.2 summarizes the commands of ADS1298. Fig 3.7 shows the board file and PCB board with soldered components. Schematic of the design is peicted in Fig 3.8.

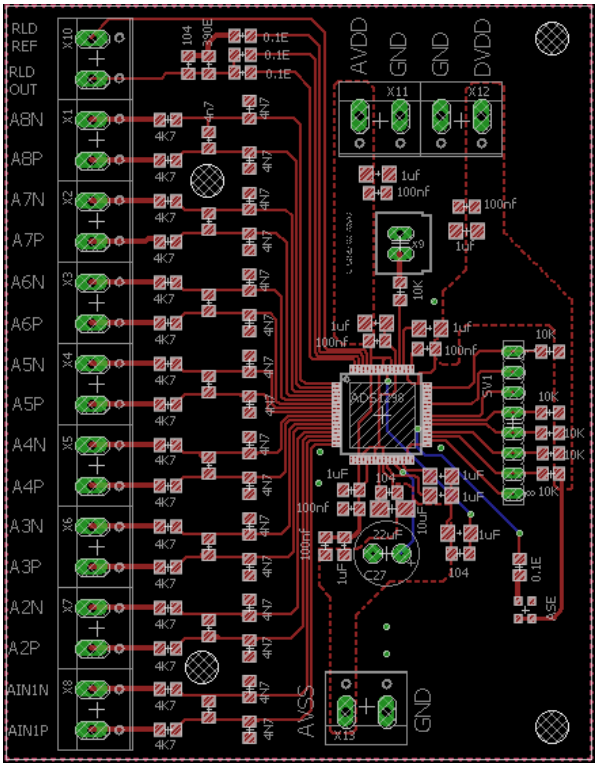

(a) board file

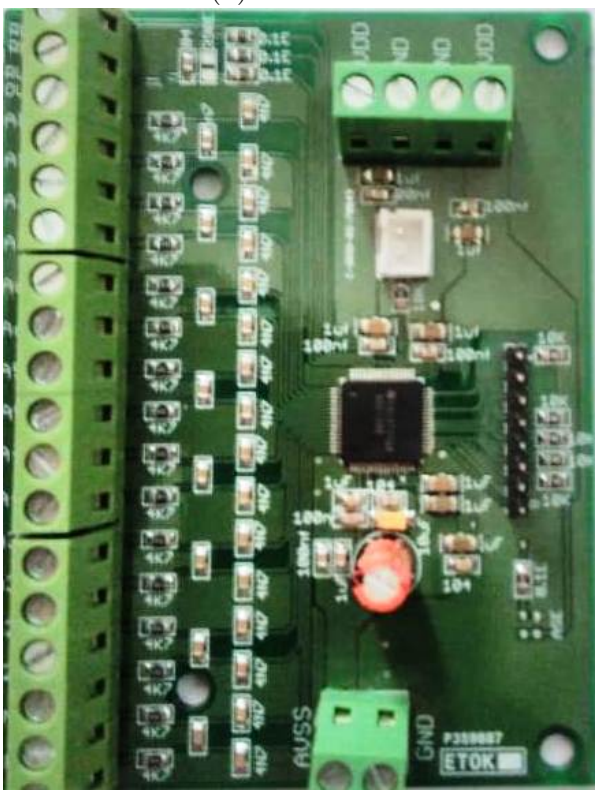

(b) PCB with components

FIGURE 3.7: PCB board file and final assembly of design

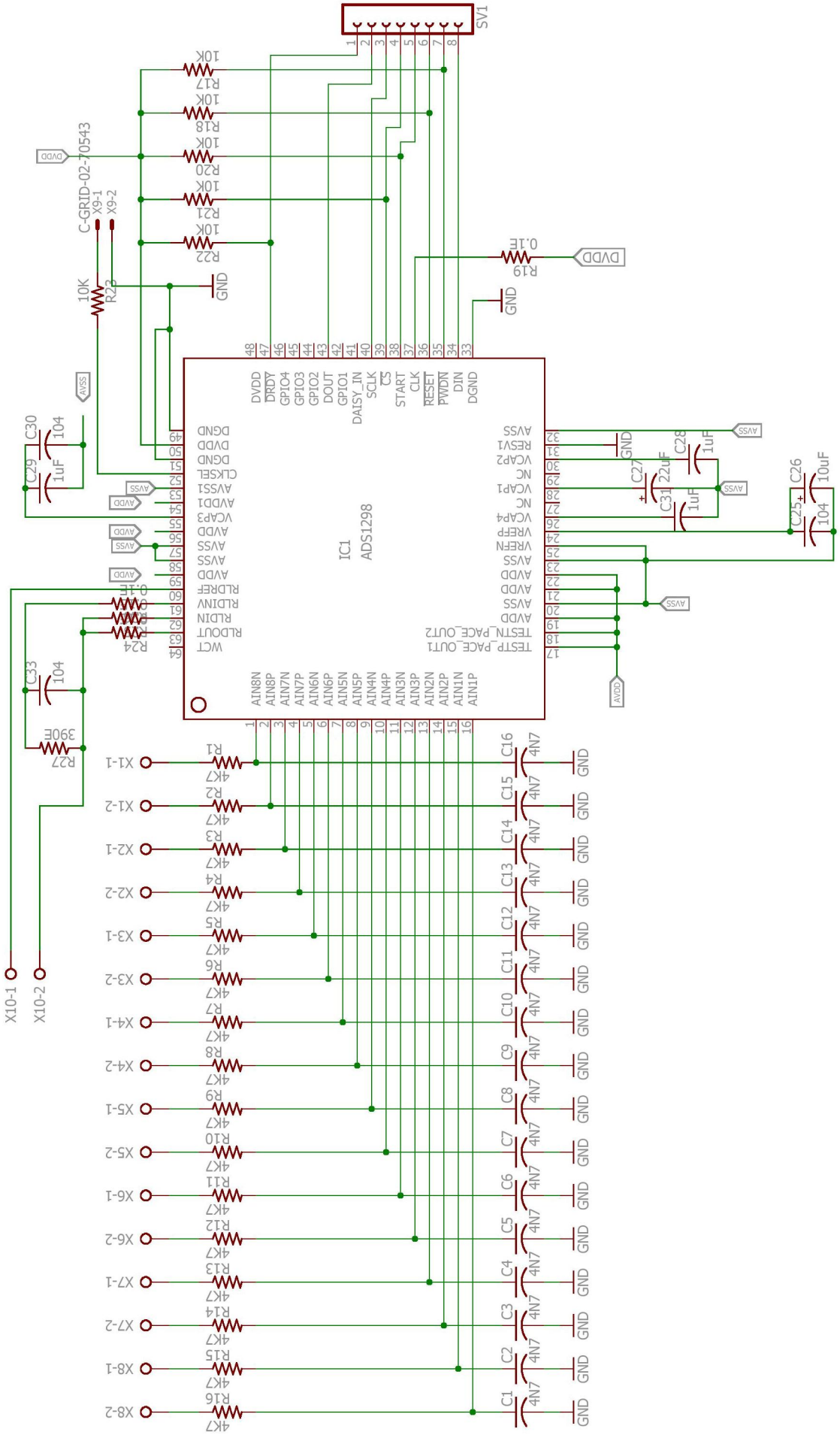

FIGURE 3.8: Schematic of the design

Table 3.2: ADS1298 commands

S.No	Command	Size (Byte)	Code	First Byte	Second byte	Description
1	Start	1	0x08	00001000		Start the conversion
2	Stop	1	0x0A	00001010		Stop the conversion
3	Reset	1	0xO6	00000110		Resets ADS1298
4	Wakeup	1	0x02	00000010		Wakeup ADS1298 from standby mode
5	Standby	1	0x04	00000100		Enter standby mode
6	Read Register	2		001aaaaa	000nnnnn	Read the content of (nnnnn)b registers starting from address (aaaaa)b
7	Write Register	2		010aaaaa	000nnnnn	Write to (nnnnn)b registers starting from address (aaaaa)b
8	Read Data	1	0x12	00001100		
9	Read Data Continuous	1	0x10	00010000		Continuously read data
10	Stop Data Continuous	1	0x11	00010001		Stop the continuous reading of data

3.5.2 Microcontroller

A microcontroller is required for communicating between PC, ADS1298. The present design is built around ATmega2560. It is a low-power CMOS 8-bit microcontroller based on the AVR enhanced RISC architecture. Salient features of ATmega2560 includes 256K bytes of In-System Programmable Flash memory, 4Kbytes EEPROM, 8Kbytes SRAM, 86 general purpose I/O lines, 32 general purpose working registers, 4 USARTs, a 16-channel, 10-bit ADC and a SPI serial port [101]. Fig 3.9 depicts the flowchart of communication of ADS1298 and ATmega2560. Fig 3.10 shows the interconnection of ADS1298 and ATmega2560. SPI is a common protocol used for communication between two devices. It was developed by Motorola to provide a full duplex serial communication between a master (usually a microcontroller) and a slave (a sensor, display, a memory or other microcontroller).In a standard SPI connection, a Master and Slave are connected through the following four lines:

a. **Master Out Slave In (MOSI):** Data is sent from the master to slave's on this line.

b. **Master In Slave Out (MISO):** this line is used by the slaves to transmit data to the master

c. **Chip Select ($\overline{CS}$):** Master uses this line to select a slave to/from which the data is to be transmitted/received.

d. **Serial Clock (SCLK):** This line is the SPI serial clock. This line provides the clock for shifting the data to and fro from master to slave.

3.5.3 Graphical user interface (GUI)

A customize multi tab Graphical User Interface (GUI) was designed in LabVIEW to communicate with ADS1298. The designed GUI was used to send commands to the microcontroller, which further communicate with ADS1298. The acquired SEMG signals are received on the serial bus and displayed on the scope tab. Subsequently, the signals were filtered and stored for further analysis. The front panel of the GUI shown in Fig 3.11 has two main tab: ADC register tab (Fig 3.11 (a)) and scope tab(Fig 3.11 (b)). ADC register tab was used to configure the ADS1298 registers as per requirement. After

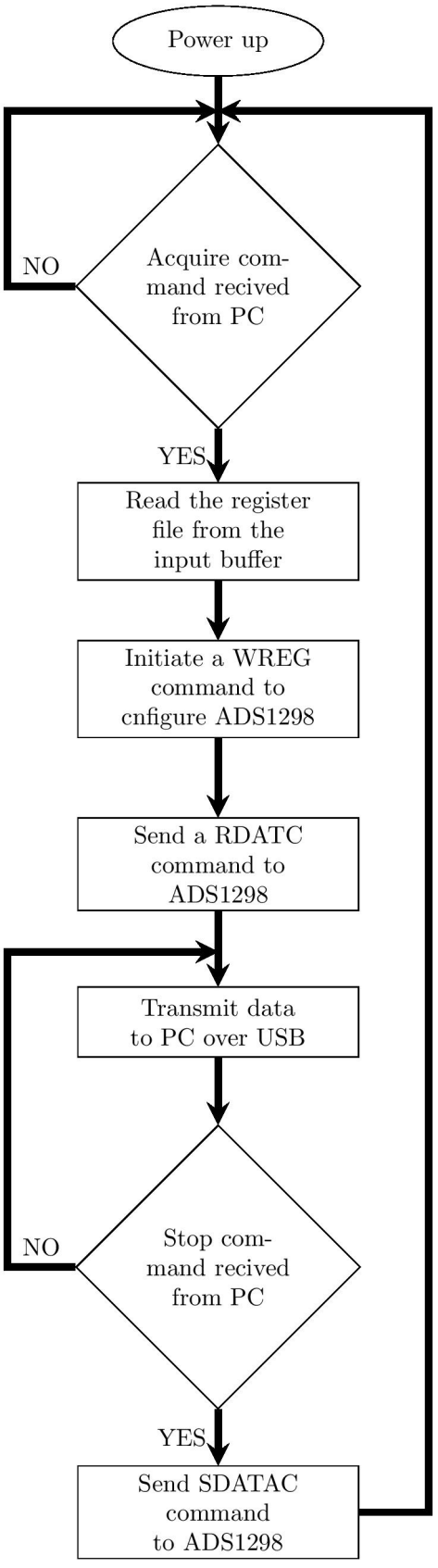

FIGURE 3.9: Flow chart for microcontroller communication with ADS1298 and PC

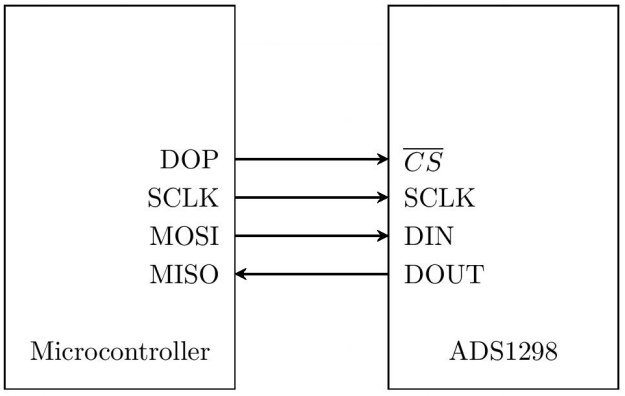

FIGURE 3.10: Interconnection between ADS1298 and ATmega 2560

configuring the registers, SEMG acquisition was initiated by acquire tab. The acquired raw SEMG signal were viewed on the scope tab. The recorded signals were stored using the save control for further analysis.

3.5.4 Testing of the bio instrumentation system

The final developed bio instrumentation system has been tested for internal as well as for external test signal prior to SEMG acquiction. The functioning of Programmable Gain Amplifier (PGA) and ADC were verified by measuring the internally generated test signal (a square wave signal). Fig 3.12(a) indicates the snapshot of the measured internal test signal.

For further testing, an externally generated signal was measured using bioinstrumention system. A sinosoidal signal of 1V peak to peak, 35 Hz was used as an external test signal. The signal was acquired at 1 KSPS, with unity PGA gain. Fig 3.12(b) indicates the snapshot of the measured signal. Fig 3.13 depicts the SEMG recording using the developed bioinstrument system in the lab while performing a standing up / sitting down on a chair activity. Fig 3.14 shows the snapshot of the acquired SEMG signal from vastus lateralis muscle while performing standing up from a chair activity.

3.6 Conclusion

The chapter presents a brief discussion on SEMG signal, its origin, transmission, factors affecting the SEMG signal acquisition and SEMG electrodes, their configuration etc.The

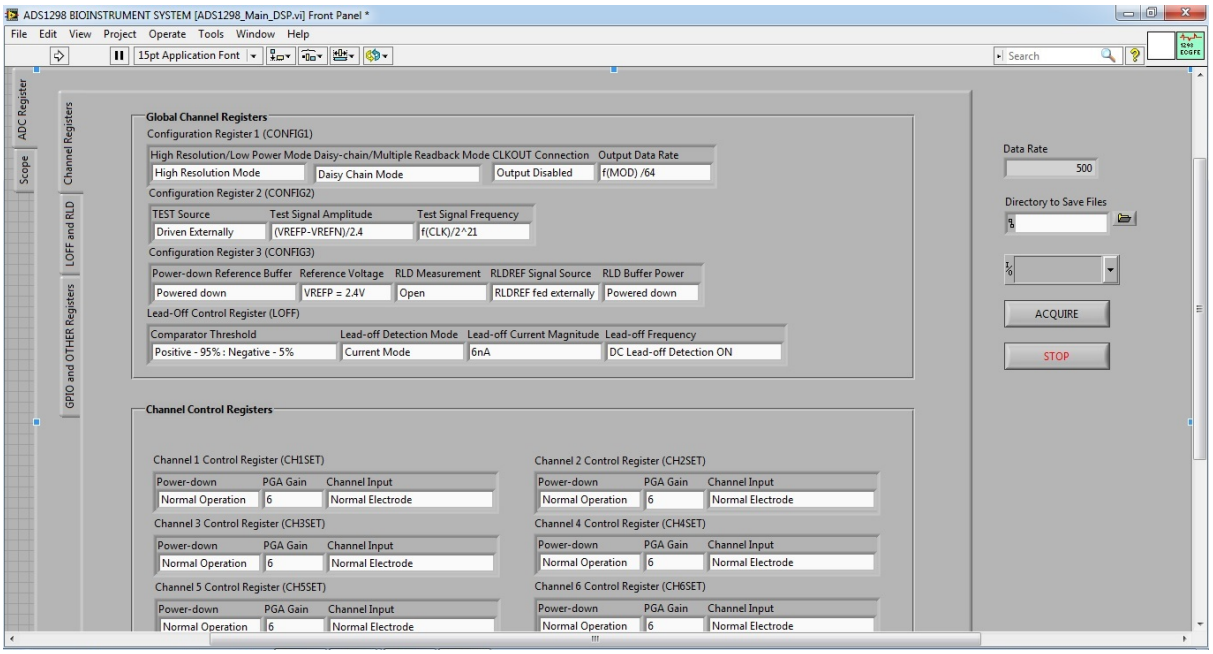

(a) ADC register Tab

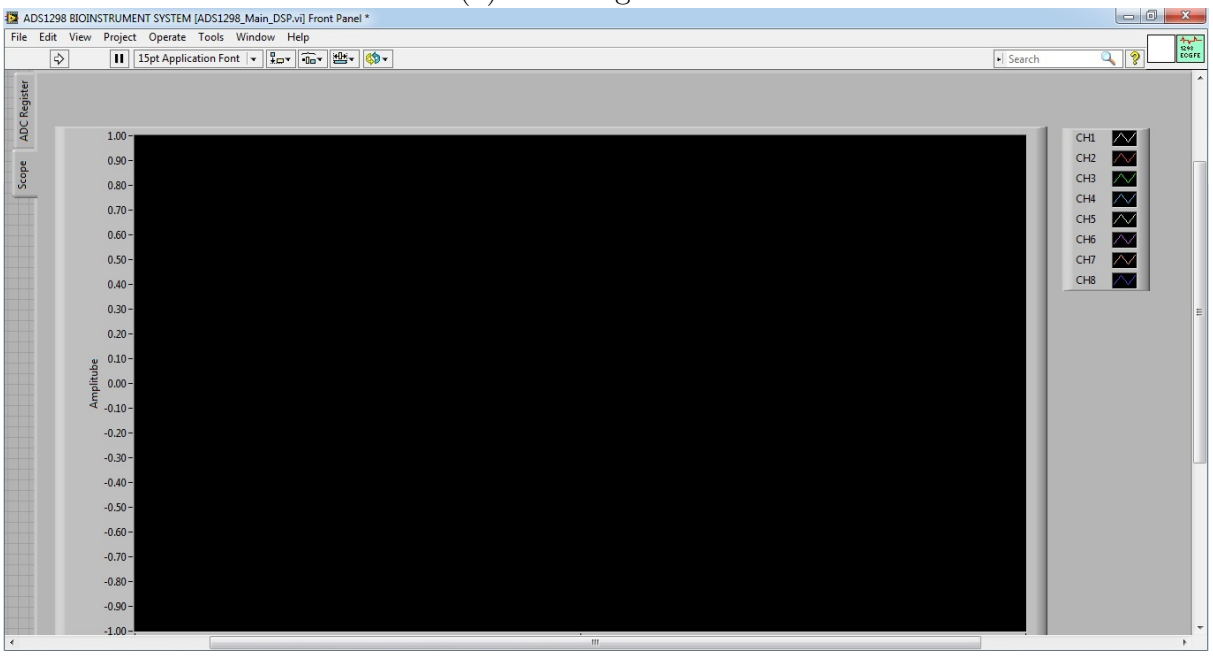

(b) Scope Tab

FIGURE 3.11: Snapshot of GUI

later part of the chapter presents design of multi-channel bioinstrumentation system for recording SEMG signal. The developed system was built around ADS1298, which is a low power eight-channel24-bit analog front end for bio potential measurement. The schematic and board file of the design are presented. Microcontroller (ATmega 2560) was used as an intermediate link between the PC and ADS1298. SPI protocol was used to connect the microcontroller and ADS1298. The GUI of the bio instrument system (developed

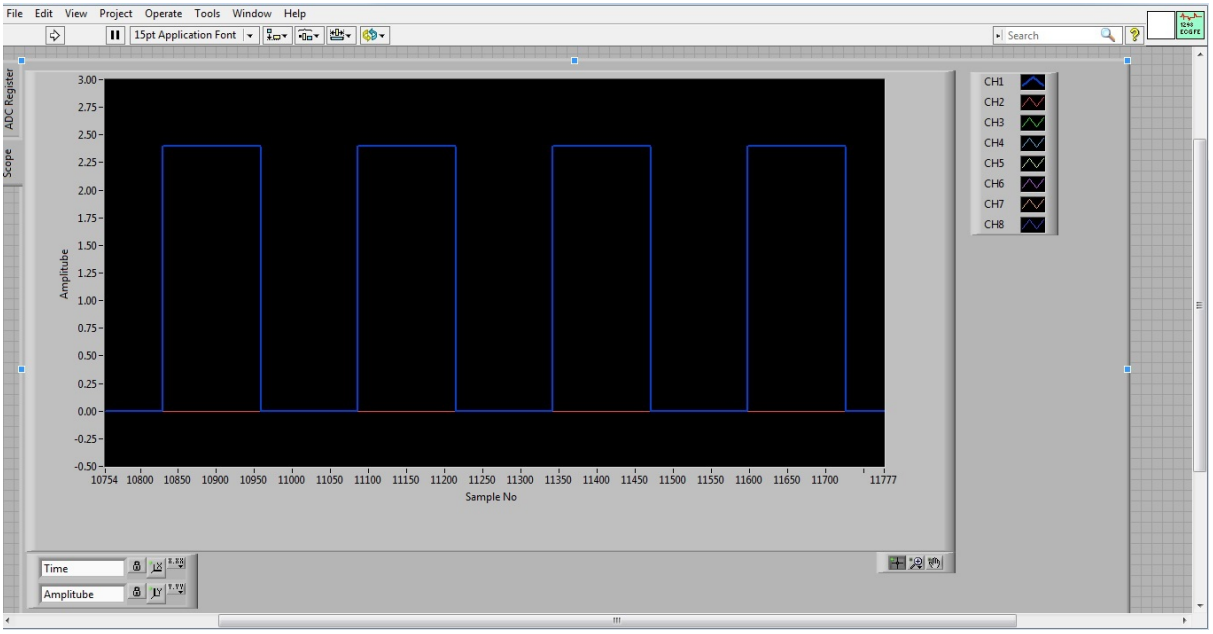

(a) Internal test signal

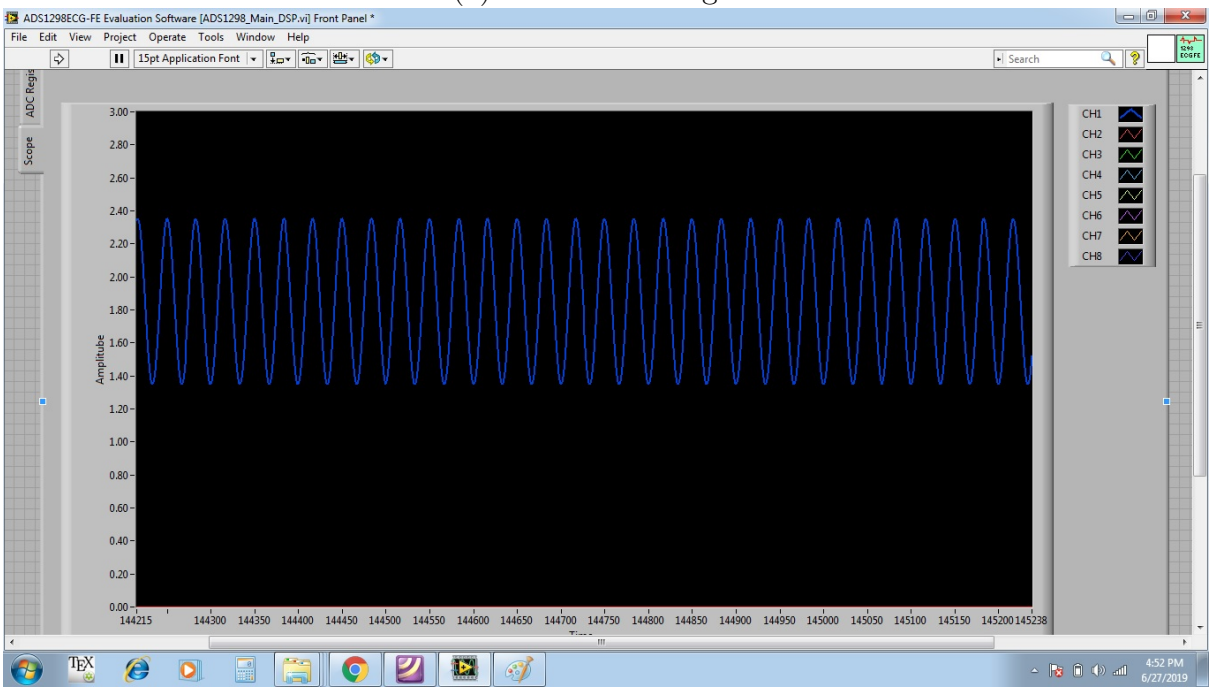

(b) External test signal

FIGURE 3.12: Snapshot of Test Signals

in LabVIEW) enables the user to configure the bioinstrumentation system prior to the SEMG recording. Final developed system was tested for internal as well as externally generated signals.

FIGURE 3.13: Setup for recording SEMG signal during standing up/ sitting down from/on a chair

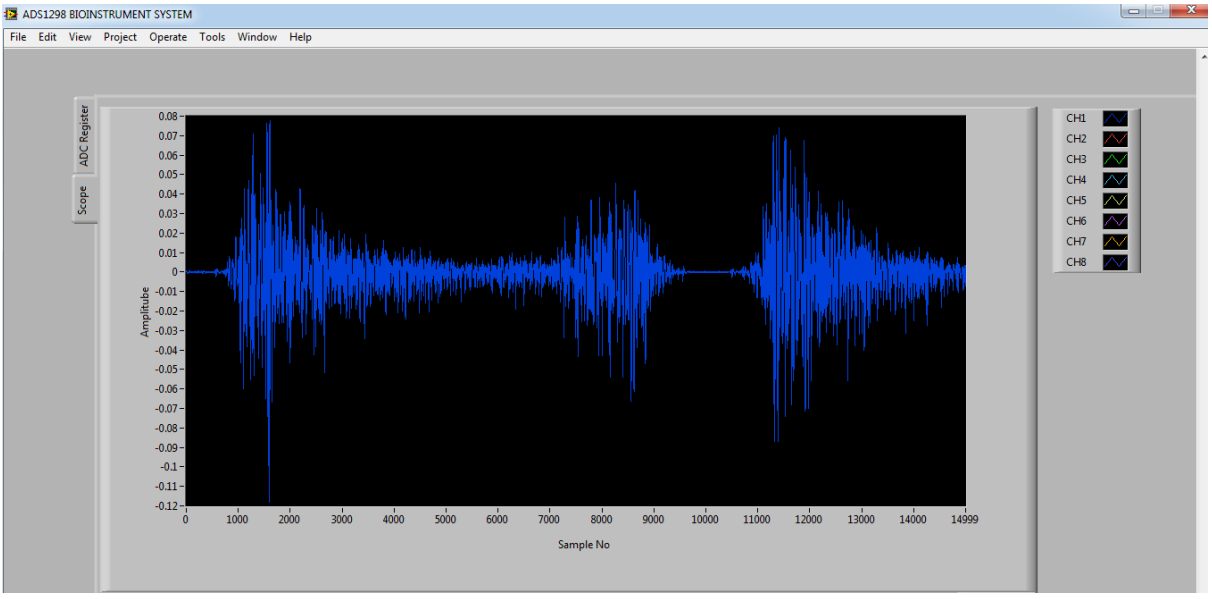

FIGURE 3.14: Snapshot of SEMG signal recorded from VALA muscle during standing up from a chair

Chapter 4

Selection of suitable muscles

The most important consideration of the myoelectric controlled exoskeletons is the selection criteria for muscle recruitment. Biological musculoskeletal model of human is highly redundant in nature. Apart from few exceptions, there exits more muscles than necessary to produce desired joint movement[102]. The human lower limb has more than fifty muscles, but the human motion intent can be predicted by considering only some of these muscles. The scientific research for the muscle recruitment criterion is still going on. None of the EMG based exoskeleton systems mentioned in chapter 2 provides a valid reason for their choice of the set of muscles [1; 14; 17; 38].

The set of questions that comes in mind when building a myoelectric exoskeleton system are: How many muscles will be sufficient to control a myoelectric knee exoskeleton? Which combination of muscles should be used for a two channel, three channels, or four-channel system? The study in this chapter is an attempt to find answers to these questions

4.1 Human knee joint anatomy

It is very crucial to understand the human knee joint anatomy prior to the identification of optimal set of muscles for exoskeleton knee control. Therefore, before discussing the muscle selection a brief anatomical description of the knee joint is presented. The knee is one of the most important joints of human body. It plays an important role in movements related to carrying the body weight in both horizontal (during running and walking) and vertical (during jumps) directions. The knee is part of a chain that includes the pelvis, hip, thigh, shank, ankle and foot. All the parts of the chain work in coordination and rely

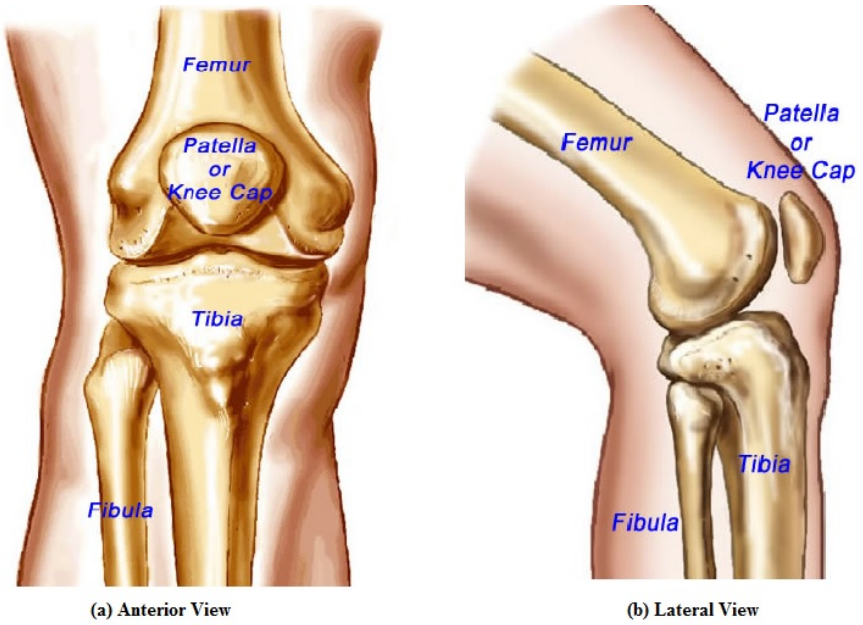

FIGURE 4.1: Knee Joint

upon one another for function and movement. The knee is one of the largest and most complex joints in the body. It is the most susceptible joint as it bears the enormous body weight and pressure loads while providing a flexible movement. During walking, knees support 1.5 times the body weight; climbing stairs is about 3-4 times the body weight and squatting about 8 times [103].

4.1.1 Bones of knee joint

The knee joint is made up of bones, muscles, cartilage, tendons and ligaments. Basic support and rigid structure to the knee joint is provided by their bones, the ligaments offer the stability and muscles helps in the joint movement. There are four bones in human knee joint, namely; femur, tibia, fibula and patella. These bone are also refferd as thigh bone, the shin bone, the smaller bone running alongside the tibia and the kneecap respectively.. Fig 4.1 shows the lateral as well as the anterior view of the knee joint. The two joints of knee, Tibiofemoral (between tibia and femur) and Patellofemoral (between patella and femur), works together and forms a modified joint which allows the knee to flex, extend and rotate slightly (side to side).

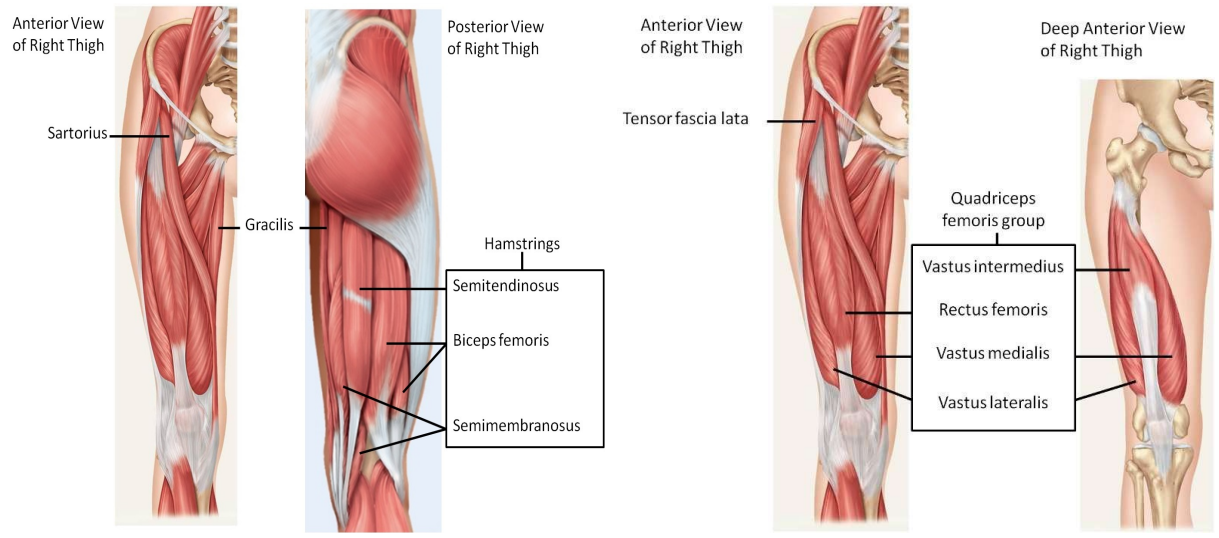

(a) Flexors (b) Extensors

FIGURE 4.2: Knee Muscles

4.1.2 Knee muscles

Muscles are responsible for the movement of a joint. There are two main groups of muscles in the knee joint knee flexors and knee extensors. Knee flexors consist of muscles, which are responsible for knee flexion. The knee flexors shown in Fig 4.2(a), are a group of seven muscles which cross the posterior of the knee joint (except the sartorius muscle). Knee flexors comprise of the hamstrings (biceps femoris, semimembranosus and semitendinosus), the gastrocnemius, the gracilis muscle, the sartorius muscle and the poplites.

The knee extensors are a group of five muscles located towards the anterior thigh. Their contraction induces the extension of the knee joint by pulling the calf and foot back to their anatomical position. During this motion, knee flexors are relaxed returning to their normal position. Knee extensors shown in Fig 4.2(b) comprises of the tensor fasciae latae and the quadriceps (rectus femoris, vastuslateralis, vastusintermedius and vastusmedialis).

4.1.3 Knee movements

The primary movements of knee joint are flexion and extension about the virtual transverse axis in the sagittal plane. When flexed, the knee can be rotated slightly medially

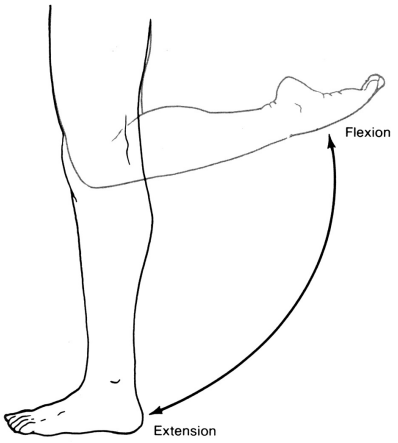

FIGURE 4.3: Knee movement

and laterally. Knee flexion is the movement of the shank towards the thigh thereby decreasing the knee angle. It is achieved by the contraction of the knee flexor muscles. Knee extension is a straightening of knee that is movement of shank away from the back of thigh achieved by contraction of knee extensors and relaxation of knee flexors. Fig 4.3 depicts the knee movements.

4.2 Muscle selection methodology

Anybody Modelling System (AMS) developed at Aalborg University is a general modeling system for making musculoskeletal models. AMS imitates the workings of the CNS by using inverse dynamics analysis. A detailed working of AMS is given in the [104].

The MMHB used in the present study was obtained by modifying the standard template namely "Human" available in the Any Body version 6.0.1. This template is based on an average European male with a height of 1.75 m and a mass of 72 Kg. The model was scaled to match the anthropometric details of the twelve subjects S_1 to S_{12} as reported in Table 4.1 The standard human template had the pelvis segment fixed to the ground reference frame. It was modified by making both the left and right foot fix to the ground reference frame instead of the pelvis. The standard Human template of AMS has fifty-nine muscles in the human lower limb. In the current research, only those muscles that are accountable for knee flexion/extension and hip flexion/extension, were assessed. Table 4.2 lists the muscles considered in this study. Fig 4.4 illustrates the MMHB in Squat (SQ) and Stand (ST) positions. The MMHB was initially set in the ST position by setting the joint angles. A Stand to Squat (ST2SQ) movement was then made by varying the

TABLE 4.1: Anthropometric details of the subjects

Subject	**Age(years)**	**Weight (Kg)**	**Height (cm)**
S_1	35	100	180
S_2	36	85	170
S_3	32	80	170
S_4	33	95	180
S_5	27	90	182
S_6	30	75	162
S_7	29	70	169
S_8	34	72	164
S_9	32	76	165
S_{10}	27	72	170
S_{11}	31	82	175
S_{12}	27	80	177
Average	31.08 ± 3.15	81.42 ± 9.53	172 ± 6.71

TABLE 4.2: Muscles used in inverse dynamic analysis of MMHB

S.No	**Muscle Name**	**Variable**
1	Biceps Femoris	BIFE
2	Gastrocnemius Lateralis	GALA
3	Gastrocnemius Medialis	GAME
4	Gluteus Maximus	GLMA
5	Gluteus Medius	GLME
6	Gluteus Minimus	GLMI
7	Gracilis	GRAC
8	Iliacus	ILIA
9	Poplitues	POPL
10	Quadratus Femoris	QUFE
11	Rectus Femoris	REFE
12	Sartorius	SART
13	Semimembranosus	SEME
14	Semitendinosus	SETE
15	Tensor Fasciae Latae	TFLA
16	Vastus Intermedius	VAIN
17	Vastus Lateralis	VALA
18	Vastus Medialis	VAME

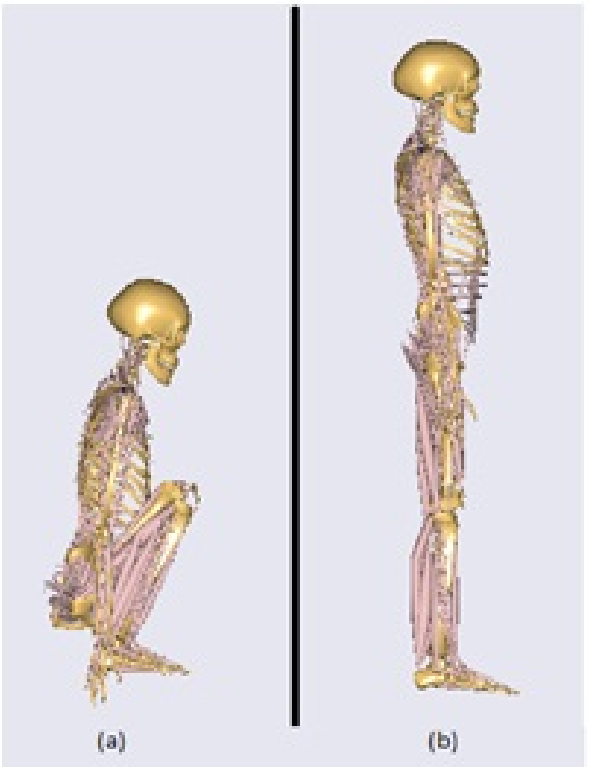

FIGURE 4.4: Musculoskeletal model in (a)Squatting , (b)Standing position

angle of knee flexion and the angle of hip flexion at a constant speed. An Inverse dynamic analysis was performed as the MMHB was made to move in ST2SQ. The Inverse dynamic analysis was performed in 100 steps by varying the knee flexion angle from 0° to 150° and hip flexion angle from 0° to 150°. Force F_i developed in the i^{th} muscles is

$$F_i = [F_{i,1}, F_{i,2}, \cdots, F_{i,j}, \cdots, F_{i,100}]' \tag{4.1}$$

where i represent the muscle number and j represent the step number. Fig 4.5 shows the muscle forces developed in MMHB corresponding to S_1, while performing a ST2SQ.

4.3 Principal component analysis for muscle selection

A principal component analysis was performed on the muscle forces obtained from the ST2SQ movement of MMHB. First the covariance matrix S representing the covariance between the muscle forces was obtained. Each matrix element $S_{(i,j)}$ represents the covariance between the force developed in i^{th} and j^{th} muscle. Mathematically it is represented

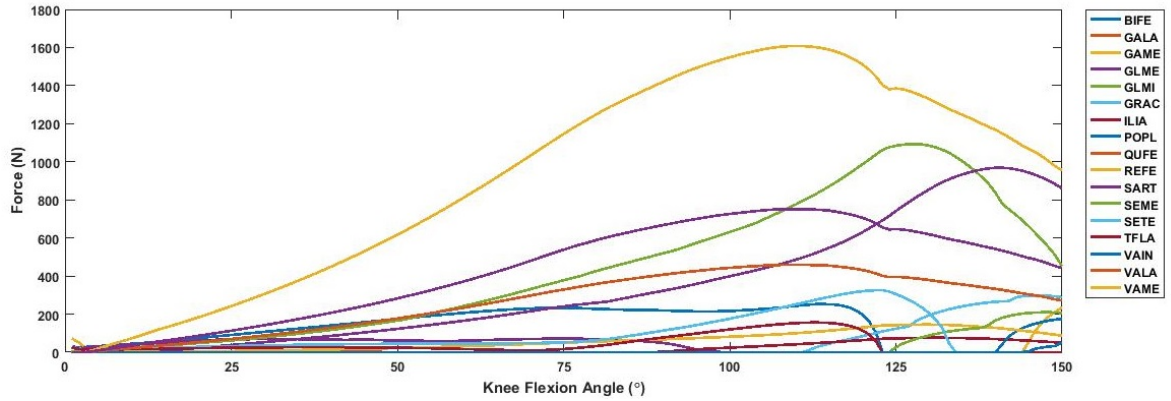

FIGURE 4.5: Muscle force developed in the MMHB corresponding to S_1 while performing a ST2SQ

as

$$S_{i,j} = cov(f_i, f_j) \tag{4.2}$$

A PCA was performed on the covariance matrix S. The PCA linearly transforms a set of initial variables into another set of uncorrelated variables. These uncorrelated variables are called the principal components (PC's). Given the feature vector $\overline{x}$, consisting of M observation of N features, the principal components $\overline{s}$ are given by Eq 4.3.

$$\overline{s} = W \cdot \overline{x} \tag{4.3}$$

where W is the projection matrix consisting of eigenvector of covariance matrix, arranged in decreasing order of corresponding eigenvalue. The PC's are ranked according to their variance, the first component explains the maximum variance followed by the second component and so on. Dimensionality reduction by PCA offers advantages like simplified classifier structure and reduction in response time of classifiers for prediction.

PCA is also an appropriate tool for variable selection. Results obtained by the use of PCA are little changed if some of the variables involved are discarded beforehand [105; 106]. A PCA performed on data of k input variables results in k PCs. p PCs having eigenvalue greater than the average eigenvalue λ_0 are sufficient to summarize the data effectively. The p variables should be retained by rejecting the remaining $(k-p)$ redundant variables [107]. λ_0 is obtained as in Eq 4.4

$$\lambda_0 = \frac{\sum_{i=1}^{k} \lambda_i}{k} \tag{4.4}$$

According to Cadima and Jollife the number of variables to be selected should be p+2.

As, often p+2 input variables contains information matching that of p PCs. So the complexity the system can be reduced by selecting only p+2 variables [108]. A number of techniques for variable selection/rejection are available in the literature, prominent among them are forward selection, backward rejection and method of principal variables.

4.3.1 Variable selection using forward selection and backward rejection

The flowchart for the forward selection method and backward rejection method are depicted in Fig 4.6 and Fig 4.7 respectively. In the method of forward selection, the eigenvector coefficients of the first p components are evaluated and the variable associated with the highest eigenvector coefficient is selected (provided, it has not been selected previously). As the selection proceeds in the forward direction, this method is named Forward Selection Method (referred as B4 in [105]). The backward rejection method derives its name from the direction of progression of rejection. The rejection starts from the last component (having least variance) and proceeds backwards. Eigenvector coefficients of the number of components to be rejected are evaluated. The variable having highest loading is discarded.

4.3.2 Variable selection using principal variable method

A subset of input variables satisfying an optimality criteria is referred as principal variables [109]. The k-vector of variable X can be partitioned as $(X_1^{'},X_2^{'})$ where X_1 is a p-vector of variable retained and X_2 is a $(k-p)$-vector of variable discarded. The covariance matrix S can also be partitioned as

$$cov\,(X) = S = \begin{pmatrix} S_{11} & S_{12} \\ S_{21} & S_{22} \end{pmatrix} \tag{4.5}$$

Where S_{11} is $p \times p$ covariance matrix of X_1, *etc.* Selection of a set of p variables is equivalent to selection of $p \times p$ matrix S_{11} from $\binom{k}{p}$ possible options. Where there are $2^k - 1$ options for all $p = 1, 2, \cdots, k$. To find a subset X_1 of size p, McCabe presented four criteria in [110]. The criteria used in the present study is

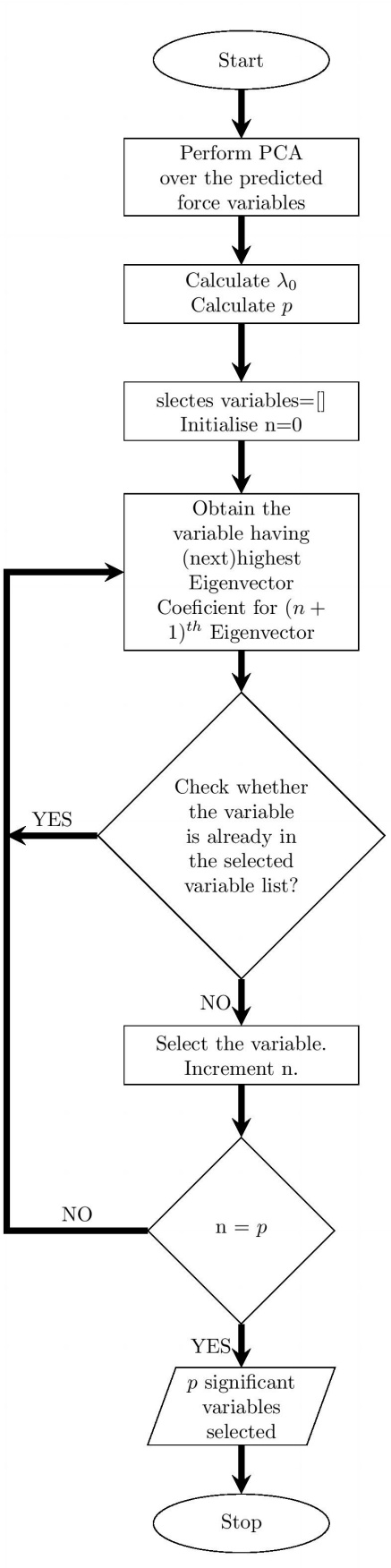

FIGURE 4.6: Flowchart of forward selection method

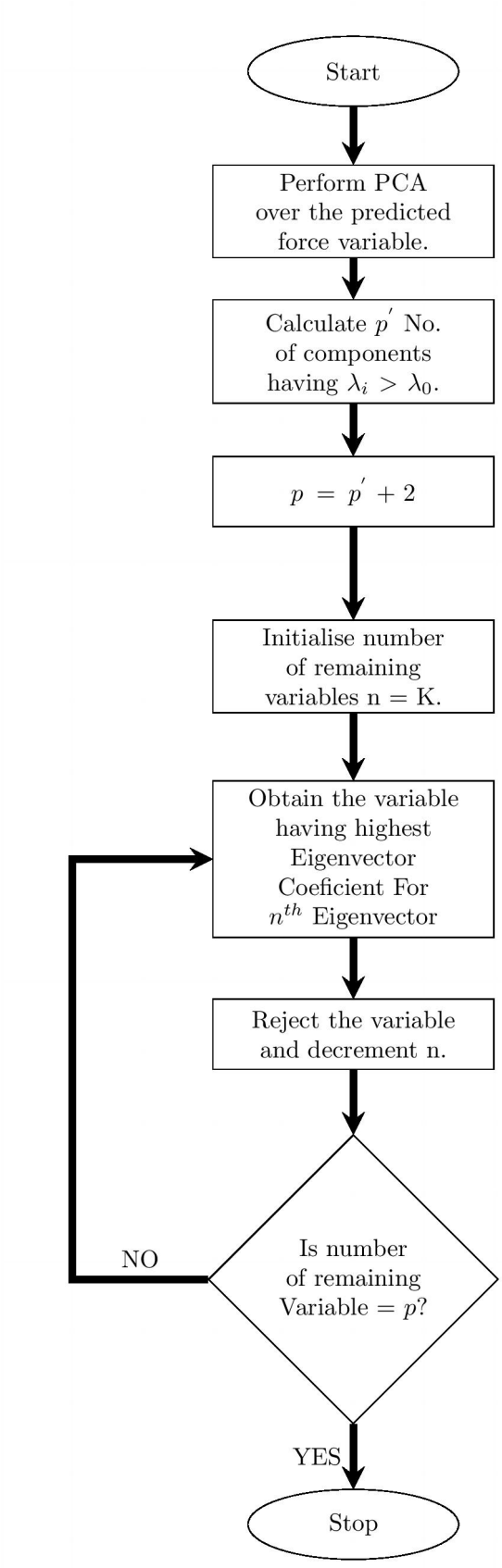

FIGURE 4.7: Flowchart of backward rejection method

$$min \prod_{i=1}^{k-p} \lambda_i^2 = min \left| S_{22.1} \right| \tag{4.6}$$

where $\lambda_i, i = 1, 2, \cdots, (k-p)$ are the eigenvalue of the conditional covariance (or correlation) matrix of $(k-p)$ deleted variables and $S_{22.1}$ is conditional covariance of X_2 given X_1. $S_{22.1}$ is obtained as

$$S_{22.1} = cov(X_2|X_1) = S_{22} - S_{12}S_{11}^{-1}S_{21} \tag{4.7}$$

For partitioned matrix,the covariance S is associated to conditional covariance matrix according to Eq 4.8

$$\left|S\right| = \left|S_{11}\right| \cdot \left|S_{22.1}\right| \tag{4.8}$$

Because S, and hence $\left|S\right|$ is fix for a given random vector X. Minimizing $\left|S_{22.1}\right|$ is equivalent to maximizing $\left|S_{11}\right|$.

Let Y be the principal components then the proportion of variation(PRV) in Y explained by principal variable X_1 is given by

$$PRV = \sum_{i=1}^{k} \lambda_i^* \cdot R_i^2 \tag{4.9}$$

where R_i^2 is the squared multiple correlation coefficient between the i^{th} principal component and i^{th} principal variable and $\lambda_i^* = \lambda_i / \sum \lambda_i$ is the percentage of variance explained by i^{th} principal component. Fig.4.8 shows the flowchart for selection of principal variable. The code was written in MATLAB and was validated by testing it for standard datasets of Fishers Iris available in MATLAB and Jeffer's data on winged aphids obtained from [111]. Results obtained were exactly similar to the results presented in [109; 110].

4.3.3 Muscle force determination from SEMG signal

In order to compare the muscle activity of the MMHB with that of subjects, SEMG signals from the selected muscles were recorded. The sampling frequency was maintained at 2048Hz. SENIAM recommendations were followed for skin preparation and sensor

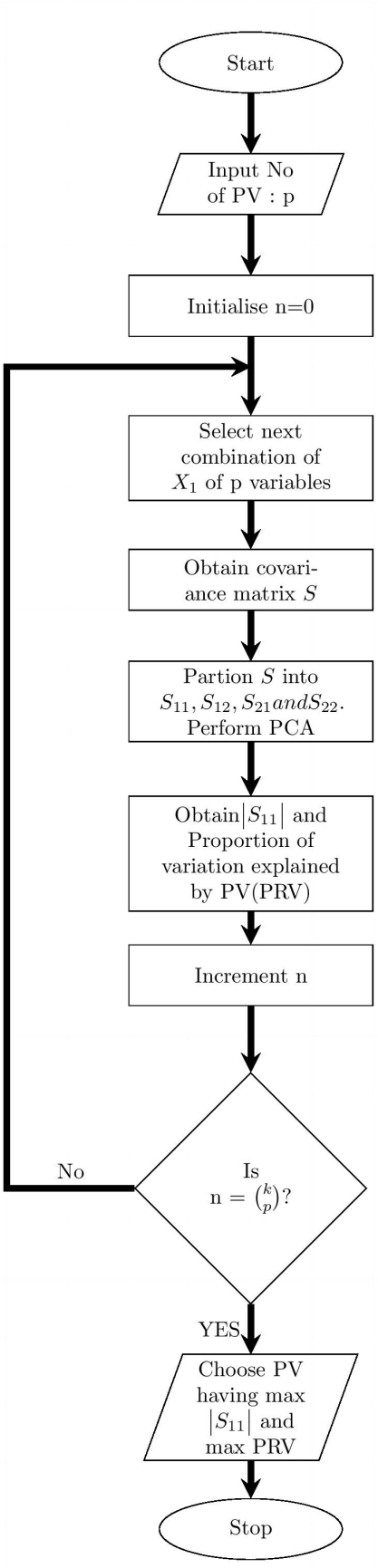

FIGURE 4.8: Flowchart method of principle variable

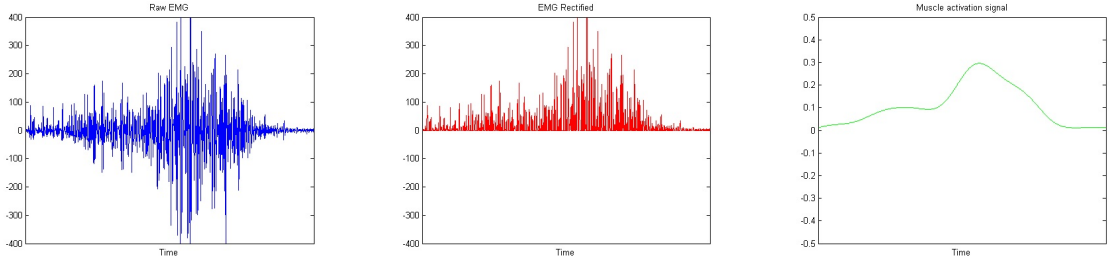

(a) RAW signal (b) Rectified signal (c) Muscle activation signal

FIGURE 4.9: Intermediate signals in obtaining the muscle activation signal

locations [97; 112]. Muscle force was calculated following the same steps as described in literature [48; 113].

Frist of all, DC offset and low frequency noise were removed from raw SEMG signal by using a zero lag 4^{th} order Butterworth band pass filter (10 – 450 Hz). The filtered SEMG signals were then full wave rectified, normalized and envelop was extracted by low pass filtering. Peak value of SEMG signal obtained for all the trial was used to normalize the signal. Frequencies between 1 - 5 Hz have been suggested as optimal for envelop extraction [49; 114; 115]. A 2^{nd} order Butterworth Low Pass filter at 1.5 Hz was used to extract the envelope.

The Intermediate signals in obtaining the muscle activation signal for VALA muscles are shown in Fig 4.9. A muscle fiber activated by a single action potential generates a twitch response, it was modelled as a linear 2^{nd} order critically damped system [113]. For a discrete second order system it can be expressed as

$$u_j(t) = \alpha e_j(t-d) - \beta_1 u_j(t-1) - \beta_2 u_j(t-2) \tag{4.10}$$

where $e_j(t)$ is the high pass filtered, rectified and low pass filtered EMG of muscle j at time t, $u_j(t)$ is the post processed EMG of muscle j at time t, α is gain coefficient of muscle j, β_1 and β_2 are the recursive coefficient of muscle j and d is the electromechanical delay. The transfer function for implementing Eq 4.11 is obtained by z transform of impulse response of Eq 4.10

$$\begin{aligned} H(z) &= \frac{u(z)}{e(z)} \\ &= \frac{\alpha}{1+\beta_1 z^{-1}+\beta_2 z^{-2}} \\ &= \frac{\alpha}{(1+\gamma_1 z^{-1})(1+\gamma_2 z^{-1})} \end{aligned} \tag{4.11}$$

where $\beta_1 = \gamma_1 + \gamma_2$ and $\beta_2 = \gamma_1\gamma_2$. For a stable system with unity gain the parameters β_1,β_2, γ_1 and γ_2 mus follow Eq 4.12 to Eq 4.14.

$$|\gamma_1| \leq 1 \tag{4.12}$$

$$|\gamma_2| \leq 1 \tag{4.13}$$

$$\alpha - \beta_1 - \beta_2 = 1 \tag{4.14}$$

The muscle activation signal for j^{th} muscle as defined in [48; 113] is given by

$$a_j(u) = \frac{e^{Au_j(t)R^{-1}} - 1}{e^A - 1} \tag{4.15}$$

where $u_j\,(t)$ is the post processed SEMG signal of muscle j, R is average of maximum value of u_j for all the trials and A is non-linear shape factor varying between -3(highly exponential) and 0 (linear relationship).

After the muscle activation is obtained, the next step is to determine the muscle force. The Hill type muscle model is used for estimating muscle force. The model consists of two elements. A contractile element which produces active muscle force F_A and a parallel elastic element which produces passive muscle force F_P [50]. Eq 4.16 gives the muscle force as follows

$$F_m = F_A + F_P \tag{4.16}$$

The active muscle force is obtained as

$$F_A = f_A(\tilde{l}^m)F_0^m a(u)\cos(\phi(t)) \tag{4.17}$$

where $a(u)$ is the muscle activation, F_0^m is the maximum isometric force, $f_A(l)$ is the active force-length function obtained by cubic spline interpolation of points on the force-length curve given by [116] and ϕ is the pennation angle. $\tilde{l}^m$ is the normalized fiber length given by

$$\tilde{l}^m = \frac{l_m}{l_0} \tag{4.18}$$

where l_m is the muscle fiber length and l_0 is the optimal fiber length.

The variation in the muscles pennation angle $\phi(t)$ corresponding to the change in muscle fiber length is obtained as follows.

$$\phi(t) = \sin^{-1}\left(\frac{l_0 \sin(\phi_0)}{l(t)}\right) \tag{4.19}$$

The torque contribution of i^{th} muscle is obtained as follows

$$T_i = \left| \vec{I_i} \times \frac{\vec{I_i} - \vec{O_i}}{|\vec{I_i} - \vec{O_i}|} \right| \cdot F_i \tag{4.20}$$

where $\vec{I_i}$ and $\vec{O_i}$ represent the position vector of insertion point and origin point for the i^{th} muscle.

4.4 Results

In the present research work, MMHB was made to move from stand to squat position (ST2SQ). An inverse dynamic analysis was performed in AMS and forces developed within selected muscles were predicted. The predicted force variables were exported to MATLAB. A PCA was conducted on the force variables. Variable selection was then made by using principal variable method. A criterion of minimum conditional covariance of rejected variable was used for selecting variables.

The first step is to determine the number of variables sufficient to summarize the data effectively. Table 4.3 gives the eigenvalues, variance and cumulative variance exhibited by the principal components for S_1 to S_5. For all the subjects only the first two PC_s have eigenvalue grater than the average eigenvalue. So, first two PC_s are sufficient to describe the data effectively. Further, as per Cadima and Jolliffe for two PC_s three or four variable needs to be selected [108]. Principal variable method described in previous section was used to select five best options (from single variable to combination of five variables). Table 4.4 summarizes the results obtained.

The best combination of three variables would be VALA, Rectus Femoris (REFE) and Gluteus Medius (GLME) having $\left|S_{11}\right| = 1.54 \times 10^{14}$ and explaining 99.18 proportion of the variation. The best combination of four variables would be VALA, REFE, Semitendinosus (SETE) and GLME having $\left|S_{11}\right| = 2.82 \times 10^{17}$ and explaining 99.61 proportion of the variation. The best combination of five variables would be VALA, REFE, SETE, Biceps Femoris (BIFE), and GLME having $\left|S_{11}\right| = 2.15 \times 10^{20}$ and explaining 99.75 proportion of the variation.

The forces developed in the subject's muscles while performing a ST2SQ operation were determined from the SEMG signals. SEMG signals were recorded from the VALA, REFE,

TABLE 4.3: Eigenvalue and variance obtained for ST2SQ of MMHB

Subject	PC_s	λ	**% Var**	**Cuml % Var**	λ_0	$\boldsymbol{p}$
S_1	PC_1	531981.82	85.31	85.31	34642.46	2
	PC_2	74077.82	11.88	97.19		
	PC_3	12965.83	2.08	99.27		
	PC_4	2513.50	0.40	99.68		
S_2	PC_1	383731.67	85.51	85.51	24930.73	2
	PC_2	52580.91	11.72	97.23		
	PC_3	9209.88	2.05	99.28		
	PC_4	1789.75	0.40	99.68		
S_3	PC_1	340263.92	85.48	85.48	22115.69	2
	PC_2	46775.43	11.75	97.23		
	PC_3	8174.15	2.05	99.28		
	PC_4	1588.89	0.40	99.68		
S_4	PC_1	480485.76	85.29	85.29	31296.57	2
	PC_2	67032.92	11.90	97.19		
	PC_3	11716.92	2.08	99.27		
	PC_4	2271.66	0.40	99.67		
S_5	PC_1	431973.06	85.21	85.21	28162.94	2
	PC_2	60677.32	11.97	97.18		
	PC_3	10577.98	2.09	99.27		
	PC_4	4050.52	0.40	99.67		

Note:The value of p for the remaining subjects also came 2. So two components are sufficient to effectively summarize the data.

SETE, BIFE and GLME. The recorded SEMG signals were filtered (10-450 Hz) for rejecting the artifact signal, rectified, normalized and low pass filtered (1.5 Hz) to obtain the processed EMG signal $e(t)$. It was then converted to post processed EMG signal $u(t)$ using Eq 4.10. Muscle activation signal a(t) was determined using Eq 4.15. The active component of the muscle force was determined using Eq 4.17. Various constants like F_0, l_m and ϕ_0 for different muscles were taken from literature [117; 118].

Fig 4.10 presents the muscle force determined from the EMG to muscle force transformation and corresponding muscles forces obtained from MMHB. In order to compare whether the muscle forces obtained from EMG and that obtained from inverse dynamic analysis of MMHB are same, a paired t test at 95% confidence interval was performed on the force obtained from inverse dynamic analysis of MMHB and that obtained from SEMG signal for a particular muscle. The result of the paired t test is presented in Table 4.5.

TABLE 4.4: Variable selection by method of principal variables for ST2SQ by MMHB

No of PV's	Principal Variables					$\lvert S_{11} \rvert$	$\sum_i \lambda_i^* R_i^2$
1	VALA					2.80×10^5	81.75
	GLME					1.21×10^5	77.04
	REFE					9.81×10^4	61.16
	VAME					6.16×10^4	81.63
	VAIN					2.28×10^4	81.58
2	VALA	REFE				1.45×10^{10}	96.68
	VALA	GLME				9.02×10^9	94.56
	VAME	REFE				3.23×10^9	96.68
	REFE	GLME				2.38×10^9	84.85
	VALA	GLMI				2.28×10^9	95.81
3	VALA	REFE	GLME			1.54×10^{14}	99.18
	VALA	REFE	SETE			7.05×10^{13}	98.71
	VALA	SETE	GLME			4.26×10^{13}	97.89
	VALA	GLMI	GLME			3.44×10^{13}	99.18
	VAME	REFE	GLME			3.39×10^{13}	99.17
4	VALA	REFE	SETE	GLME		2.82×10^{17}	99.61
	VALA	REFE	SEME	GLME		1.60×10^{17}	99.49
	VALA	REFE	BIFE	GLME		1.19×10^{17}	99.32
	GAME	VALA	REFE	GLME		1.09×10^{17}	99.43
	GAME	VALA	REFE	SETE		7.07×10^{16}	99.30
5	VALA	REFE	SETE	BIFE	GLME	2.15×10^{20}	99.75
	VALA	REFE	SETE	SEME	GLME	1.96×10^{20}	99.75
	GAME	VALA	REFE	SEME	GLME	1.41×10^{20}	99.71
	VALA	REFE	SETE	BIFE	GLME	1.17×10^{20}	99.63
	GAME	VALA	REFE	SETE	GLME	1.08×10^{20}	99.69

The p value for all the five pairs is greater than 0.05, indicating that the muscle force obtained from the SEMG signal is significantly same as that obtained from the inverse dynamic analysis of MMHB at 95%. It justifies the MMHB use for determining set of principal muscle is a valid one.

4.5 Conclusion

One of the main considerations of the myoelectric controlled exoskeleton is the selection of muscles, which can control the exoskeleton system. In the present chapter, a criterion based on internal force developed in the muscle is used as a base for muscle recruitment.

TABLE 4.5: Result of paired t test for comparing the muscle force obtained by inverse dynamic analysis of MMHB with the muscle force evaluated from SEMG signal

Paired Samples Test

Pair		Paired Differences					t	df	Sig. (2-tailed)
		Mean	Std. Deviation	Std. Error Mean	95% Confidence Interval of the Difference				
					Lower	Upper			
1	$VALA_{MMHB}$ $VALA_{SEMG}$	-4.58	140.83	14.013	-32.39	23.21	-.327	100	**0.74**
2	$GLME_{MMHB}$ $GLME_{SEMG}$	-2.95	79.22	7.883	-18.59	12.69	-.375	100	**0.71**
3	$BIFE_{MMHB}$ $BIFE_{SEMG}$	-0.01	80.27	7.987	-15.86	15.84	-.001	100	**1.00**
4	$REFE_{MMHB}$ $REFE_{SEMG}$	0.99	123.61	12.300	-23.41	25.39	.080	100	**0.94**
5	$SETE_{MMHB}$ $SETE_{SETE}$	-3.73	20.74	2.064	-7.82	0.37	-1.806	100	**0.07**

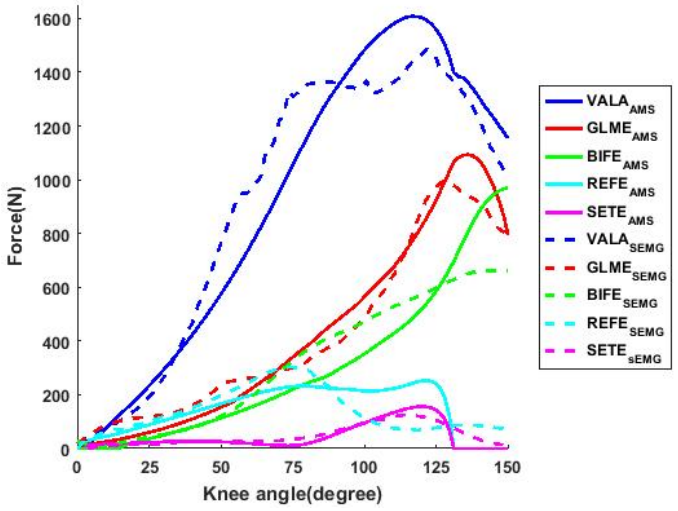

FIGURE 4.10: Comparison of force developed in the muscles during ST2SQ

A MMHB available in the Anybody Modeling system was scaled to match the anthropometric detail of the subject. The force developed in the human lower limb muscles while performing simple tasks like standing up or sitting down were then measured using inverse dynamic analysis. A PCA was performed on the force developed. Significant muscles were determined by principal variable method. For a two-channel system VALA

and REFE are sufficient in describing knee flexion/extension. For a three channel system VALA, REFE and GLME, for a four channel system VALA, REFE, SETE and GLME and for a five channel system VALA, BIFE, REFE, SETE and GLME are sufficient in describing knee flexion/extension. A paired t test at 95% confidence interval was performed on the force obtained from inverse dynamic analysis of MMHB and that obtained from SEMG signal for a particular muscle. The results indicated that the muscle force obtained from the SEMG signals of the five selected muscles is significantly similar to muscle force obtained by inverse dynamic analysis of MMHB.

Chapter 5

Knee angle prediction from SEMG signals

SEMG signals contain vital information regarding human limb movement. In the past three different approaches had been used for myoelectric control [52–65; 119]. In the first approach, SEMG signals had been used to forecast the locomotion mode like level ground walking, ascending/descending stairs and ascending/descending ramps for lower limbs and to anticipate the gestures for upper limb like hand opening/closing, forearm pronation/supination and wrist flexion/extension *etc* [52–60; 119]. The second approach deals with predicting motion variable like joint torque and muscle force from SEMG signals of selected muscles [20; 38; 48; 49]. The muscle activation signals obtain from the SEMG signal of the recruited muscle is fed to a muscle model that estimates the joint forces and/or joint moments. The commonly used muscle models are Hill muscle model [50] and Hammerstains muscle model [51]. This approach has limitation that the muscle models depend on numerous physiological parameters, which vary for different individuals. The third approach uses a regression based system to forecast the exact body postures by predicting the joint positions from SEMG signals [61–65].

Present research work introduces a new approach of predicting the joint angles. The complete range of motion of the knee joint was quantized into levels or classes. The instantaneous level/class of the knee angle was predicted using a classifier with features of the SEMG signals as predictor variables. Two studies were conducted to evaluate the performance of the new approach. In the Study-I the subjects were asked to perform a standing up (sitting down) from (on) a chair and the performance of the classifiers were

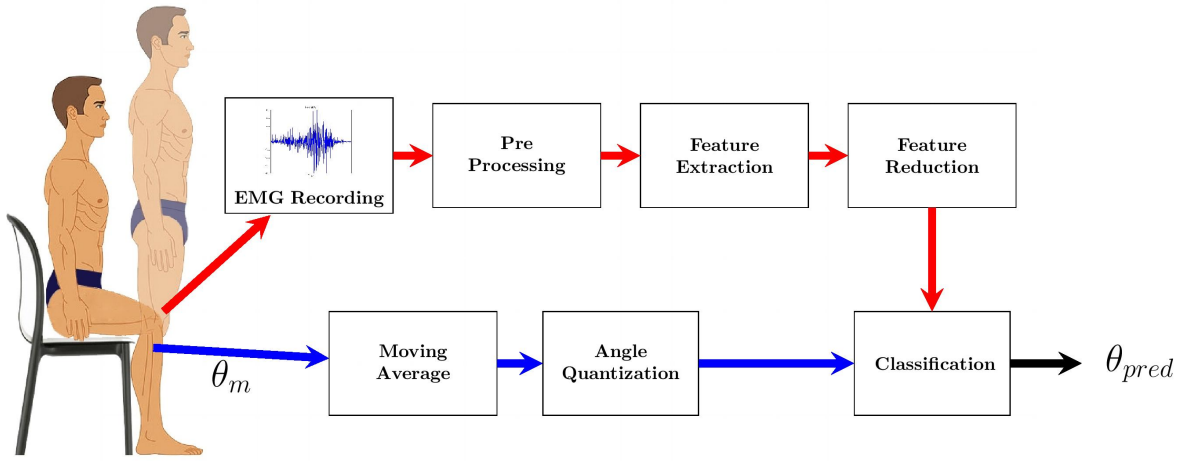

FIGURE 5.1: Block diagram of the system for knee angle prediction

evaluated. Study –II evaluates the performance of the system in predicting knee angle for three different locomotion activity (Stair ascend, plain level walk and stair descend).

5.1 Study-I

Twelve male subjects (S_1 to S_{12}) were engaged in the present research work. Table 4.1 summarizes the anthropometric details of the subjects. They were initially made to sit on a chair and were then asked to perform ten sets of stand-ups from the chair and sit-downs on the chair. Five trials were performed daily with a 15 minutes rest period between successive trials. This was repeated for five days for each subject. Fig 5.1 shows the block-diagram of the classification-based knee angle prediction system.

5.1.1 EMG recording

The SEMG signals from four muscles, including the VALA, BIFE, REFE and SETE from the lower limb, were recorded at 2048 Hz. Bipolar Ag/AgCl electrodes with 20 mm inter-electrode distances were used. SENIAM recommendations for the placement of electrodes were followed [96; 98].

TABLE 5.1: Window sizes evaluated in the present study

Window	Window Size (mS)	Window Increment (mS)
W_1	125	62.50
W_2	250	62.50
W_3	250	125.00
W_4	500	125.00
W_5	500	250.00

5.1.2 Pre-processing

The SEMG signal energy is limited in the frequency range from 0 to 500 Hz. Further, noise due to motion artefacts is dominant in the 0 to 20 Hz frequency range [85]. Accordingly, the EMG signals were bandpass-filtered (20-500 Hz) through a 4^{th} order Butterworth filter. The random nature of the SEMG signal makes its instantaneous value unsuitable for control purposes [120]. Consequently, SEMG signals were segmented using moving windows for data analysis. Two types of windows, including overlapped and disjoint windows, have been proposed in the literature [46]. Overlapped windowing with a suitable window increment fully utilises the computing capacity of the system and provides dense decision streams [46]. Hence, an overlapped windowing scheme was used.

The window size is very critical, it must be short enough to avoid introducing an excessive delay in the system, but must be long enough to form a valid judgement. Further, the response time of the system must lie below 300 ms [66; 121]. In this study, the performances of five window sizes shown in Table 5.1 were evaluated.

5.1.3 Feature extraction

Fifteen features were extracted from the segmented/windowed SEMG signals for each muscle. These included six TD, five Frequency Domain (FD) and four AR coefficients (ARn).

Integrated EMG (IEMG): This is the summation of the absolute values of the EMG signal amplitude. Its value is calculated by Eq 5.1 as follows:

$$IEMG = \sum_{i=1}^{N} |x_i| \tag{5.1}$$

where x_i is the EMG signal of the i^{th} sample and N is the length of the EMG signal.

Simple Square Integral (SSI): This is the summation of the square values of the EMG signal amplitude. It is obtained by Eq 5.2 as follows:

$$SSI = \sum_{i=1}^{N} x_i^2 \tag{5.2}$$

Root Mean Square (RMS): This is one of the most popular features in the analysis of EMG signals. It is modelled as amplitude modulated Gaussian random process and is related to constant force and non-fatiguing contraction. Mathematically, it can be expressed by Eq 5.3 as follows:

$$RMS = \sqrt{\frac{1}{N}\sum_{i=1}^{N} x_i^2} \tag{5.3}$$

Zero Crossing (ZC): This is the number of times the amplitude of the EMG signal crosses a zero level. A threshold must be included in the zero-crossing calculation to reduce the noise induced zero crossings [52]. A suitable value for the threshold parameter is normally chosen between 50 μV and 100 mV [67; 70]. The threshold has been kept at 50 μV. Mathematically, it is calculated by Eq 5.4 as follows:

$$ZC = \sum_{i=1}^{N-1} f_1(-x_i \cdot x_{i+1}) \cdot f_2(|x_i - x_{i+1}|) \tag{5.4}$$

where

$$f_1(x) = \begin{cases} 1 & x \geq 0 \\ 0 & otherwise \end{cases}$$

and

$$f_2(x) = \begin{cases} 1 & x \geq threshold \\ 0 & otherwise \end{cases}$$

Waveform Length (WL): This is the cumulative length of the EMG waveform over the time segment. Mathematically it can be calculated by Eq 5.5 as follows:

$$WL = \sum_{i=1}^{N} |x_{i+1} - x_i| \tag{5.5}$$

Willison Amplitude (WAMP): This is the number of times the difference between the EMG signal amplitude among the two adjoining segments exceeds a predefined threshold [70]. Mathematically it is given by Eq 5.6. The threshold has been kept at 50 μV.

$$WAMP = \sum_{i=1}^{N-1} f(|x_i - x_{i+1}|) \tag{5.6}$$

where

$$f(x) = \begin{cases} 1 & x \geq threshold \\ 0 & otherwise \end{cases}$$

Autoregressive coefficients (ARn): An autoregressive model is a prediction model that describes each sample from the EMG signal as a linear combination of the previous samples [122]. In the classification of the EMG signal, coefficients from the AR model have been used as a feature vector. The model is expressed by Eq 5.7 as follows:

$$x_k = \sum_{i=1}^{N} a_i x_{k-i} + w_k \tag{5.7}$$

where N is the order of the AR model, w_k is the white noise, and a_i is the i^{th} AR coefficient. The 4^{th} order AR is adequate for time series modelling of an EMG signal [67; 122; 123].

Mean Frequency (MNF): This is the mean or average frequency of the signal. It is the ratio of the sum of the product of the EMG power spectrum and the frequency of the total spectrum intensity. It is calculated by Eq 5.8 as follows:

$$MNF = \frac{\sum_{j=1}^{M} f_i Pi}{\sum_{i=1}^{M} P_i} \tag{5.8}$$

where f_j is the frequency of the spectrum at frequency bin j, P_j is the EMG power spectrum at frequency bin j, and M is the length of the frequency bin.

Median Frequency (MDF): This is the frequency that divides the spectrum into two regions with equal amplitude. Mathematically it can be expressed as follows:

$$\sum_{i=1}^{MDF} P_i = \sum_{i=MDF}^{M} P_i = \frac{1}{2}\sum_{i=1}^{M} P_i \tag{5.9}$$

Peak Frequency (PKF): This is the frequency having maximum power in the spectrum. It is given by Eq 5.10 as follows:

$$PKF = max(P_j) \qquad j = 1, 2, \ldots, M \tag{5.10}$$

Mean Power (MNP): This is the average power of the EMG power spectrum. Mathematically, it is obtained from Eq 5.11 as follows:

$$MNP = \frac{\sum_{j=1}^{M} P_j}{M} \tag{5.11}$$

First Spectral Moment (SM1): The spectral moment provides better results for the classification of EMG signals [124]. The first three spectral moments are the most crucial spectral moments [70]. Only the first spectral moment has been evaluated in the present study. Mathematically, it is expressed by Eq 5.12 as follows:

$$SM1 = \sum_{i=1}^{M} P_i f_i \tag{5.12}$$

All the features obtained for a window together constitute a feature vector. The feature vector for the W^{th} window is given by Eq 5.13 as follows:

$$F_w = [f_{1,1}, \ldots, f_{1,15}, f_{i,j}, \ldots, f_{4,1} \ldots, f_{4,15}] \tag{5.13}$$

where i represents the muscle number and j represents the feature number. The min-max normalisation method shown in Eq 5.14 was used to normalise the feature vector.

$$Fnorm_i = \frac{f_i - min_i}{max_i - min_i} \tag{5.14}$$

In Eq 5.14 max_i and min_i are the maximum and minimum values of the i^{th} feature, respectively.

5.1.4 Feature reduction

PCA linearly transforms a set of primary variables into another reduced dimension set of uncorrelated variables. These uncorrelated variables are called the principal components (PCs). Given the feature vector$\bar{X}$ consisting of M observations of N features, the PCs $\bar{S}$ are given by Eq 5.15 as follows:

$$\bar{S} = W \cdot \bar{X} \tag{5.15}$$

where W is the projection matrix consisting of the eigenvector of the covariance matrix arranged in decreasing order from the corresponding eigenvalue. The PCs are ranked in increasing order of their variance; the first component explains the maximum variance followed by the second component and so on. The dimensionality reduction by PCA simplifies the structure of the classifier and reduces the processing time for pattern recognition [71].

5.1.5 Knee angle quantisation

The human knee joint has a typical Range of Motion (ROM) that goes from 0° when fully extended to 140° when maximally flexed. The Knee Angle (KA) was measured using a potentiometer-based goniometer. In the present study, the ROM ranges from KA=0° when in a standing position to KA=115° when sitting on a chair. The voltage signal at the output of the goniometer is digitised using an NI-6009 data acquisition system and the NI LabVIEW 2013 software. The measured KA was low-pass-filtered using a 4^{th} order IIR Butterworth low-pass filter (FC= 2 Hz). Fig 5.2 shows the measured KA along with the SEMG signals for the VALA and REFE muscles during the present study. The KA is quantised into one of the following five classes: 0 (KA $<$ 15°), 30 (15° $<$ KA $\leq$ 45°), 60 (45° $<$ KA $\leq$ 75°), 90 (75° $<$ KA $\leq$ 105°) and 120 (105° $<$KA). The quantised KA is used as a response variable for the classifier.

5.1.6 Classifier

A classifier is a function that takes input values from various features and predicts the class that they belong to [125]. Despite the long tradition of pattern recognition research, there are no definite guidelines for choosing a classifier. Therefore, choosing the right classifier for an application among the several alternatives is a difficult task [126]. The

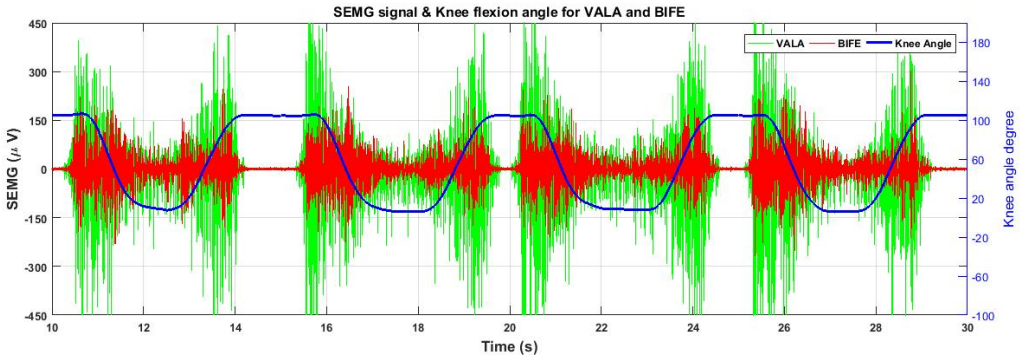

FIGURE 5.2: SEMG signal and knee angle recorded while subject is standing up from a chair and sitting on a chair

present study examines the performance of four classifiers, including LDA, NB, k-NN, and SVM, for predicting the KA from SEMG signals from four lower limb muscles.

The LDA classifier offers high classification performance, is robust for long term use, and has a low computational cost [70]. The LDA classifier is also easy to implement and much faster to train [46]. The NB classifier is based on the Bayes theorem. The NB classifier is often used as a baseline in text classification because of its fast speed and easy implementation [127]. The k-NN classification algorithm predicts a test sample's class according to k training samples, which are the nearest neighbours to the test sample, and classifies the sample to the class that has the most significant probability. The k-NN classifier has been used for the classification of upper limb movements based on SEMG signals [128; 129]. The SVM is a kernel-based approach with a strong theoretical background that has become an increasingly popular tool for machine learning tasks involving classification and regression [130]. It has been successfully applied in several applications ranging from face recognition [131] and image categorisation [76; 132; 133] to SEMG classification [134; 135].

5.2 Study II

The study was conducted on a custom built gait course incorporating three locomotion modes: Stair descend (LM1), Plain Walk (LM2) and Stair ascend (LM3). The trials were conducted at the institute's corridor. Prior to beginning of the trials the subjects were asked to remain stand still and EMG data was recorded for one minute. Subjects then performed LM1 turned 90° towards left, performed LM2, took 180° turn and performed LM2, turned right 90° and performed LM3 and came to rest. Ten trials were recorded for

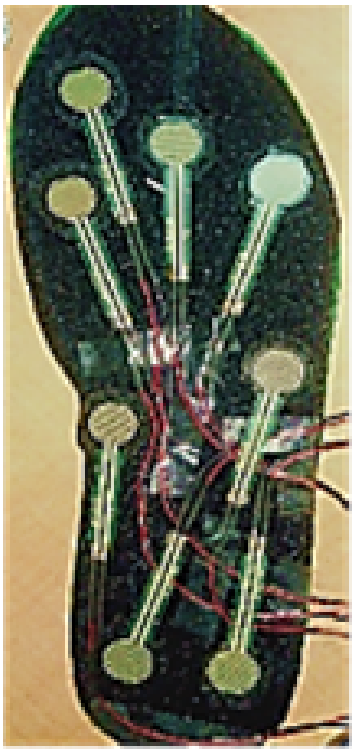

FIGURE 5.3: Shoe sole for detecting heel strike and toe off

each subject daily. The heal strike and toe off event (detected using force sensor resistor placed in the shoe sole shown in Fig 5.3 [136]) were used to sample the data into gate cycles. Only gait cycles with timings in the range ($t_m \pm t_{sd}$) of a particular activities were retained for the analysis. Here t_m represents the mean time of a gait cycle and t_{sd} represents the standard deviation of the time of a gate cycle for particular activity. The data was split into testing and training data to implement ten-fold cross validation. Data of one of the trial was used as testing data and that of the remaining nine trials were used for training.

Fig 5.4 depicts the SEMG signal and KA acquired during the study. For LM1 and LM3 the range of motion of KA varies from 0° to 90°, for LM2 the range of motion for KA is in the range from 0° to 70°. Accordingly, KA was quantized into six different levels: L1 (KA $< 9°$), L2 ($9° < KA \leq 27°$), L3 ($27° < KA \leq 45°$), L4 ($45° < KA \leq 63°$), L5 ($63 < KA < 81°$), and L6 (KA $> 81°$).

5.3 Performance evaluations

Four performance measures including accuracy, sensitivity, specificity, and precision were evaluated using the following parameters:

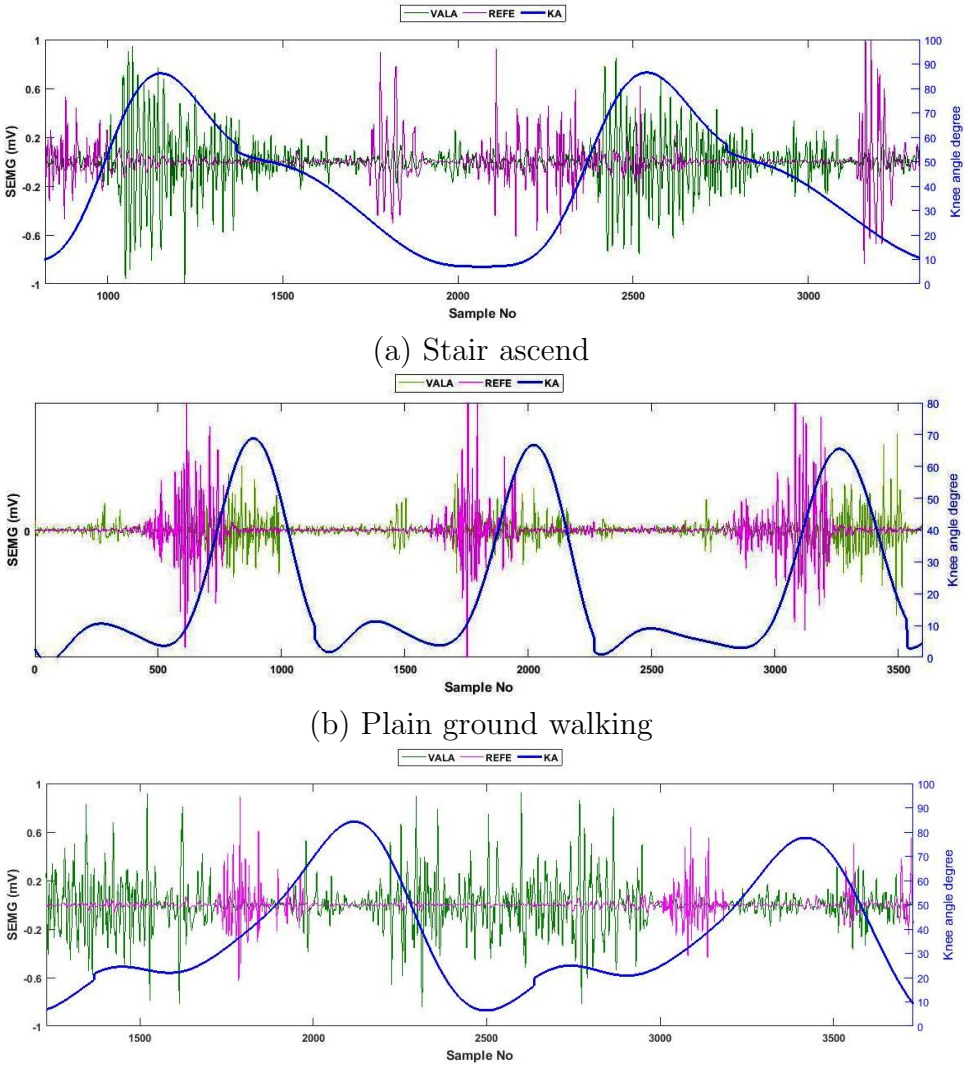

(a) Stair ascend

(b) Plain ground walking

(c) Stair descend

FIGURE 5.4: SEMG signal and KA accquired for different activityduring Study-II

- **True positive (TP)**, for a particular class, the number of correctly classified cases.
- **False positive (FP)**, the number of cases classified into a class that actually belong to another class. It is also called Type-I error.
- **False negative (FN)**, for a particular class, the number of cases that belonged to that class but were wrongly classified into another class. It is also called Type-II error.
- **True negative (TN)**, for a particular class, the number of cases that doesn't belong to a class and were also not classified into that.

Accuracy: This is the percentage of correctly classified cases. Mathematically it is given by Eq 5.16 as follows:

$$ACC = \frac{TP + TN}{TP + FP + FN + TN} \tag{5.16}$$

Sensitivity: This is the percentage of true positives among all the positives. Mathematically it is given by erefeq5017 as follows:

$$SN = \frac{TP}{TP + FN} \tag{5.17}$$

Specificity: This is the percentage of true negatives among all the negatives. Mathematically it is given by Eq 5.18 as follows:

$$SP = \frac{TN}{TN + FP} \tag{5.18}$$

Precision: This is the percentage of the number of correct positive predictions among the total number of accurate predictions. Mathematically it is given by Eq 5.19 as follows:

$$PREC = \frac{TP}{TP + FP} \tag{5.19}$$

A ten-fold cross-validation was performed on each subject to evaluate the performance measures of the different classifiers. The average value of a performance measure was computed from the cross-validation results. Statistically, the performances of the classifiers were compared using anAnalysis of Variance (ANOVA). A post hoc multiple comparison analysis was performed using Tukey's method for significantly different results (p value < 0.05). All statistical computations were performed using the IBM SPSS Statistics 21 software.

5.4 Results

The results obtained form Study-I and Study-II are presented in this section. Studies evaluated the performance of the four classifiers namely LDA, NB, k-NN and SVM in predicting the KA from the SEMG signal.

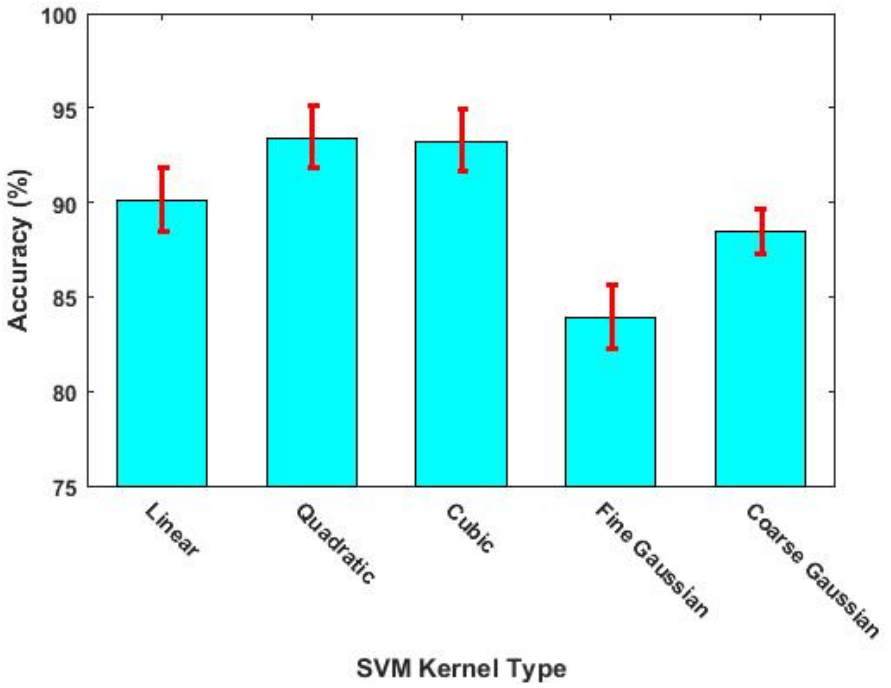

FIGURE 5.5: The classification accuracy obtained for the different SVM kernel functions

5.4.1 Study-I

5.4.1.1 Influence of kernel selection in case of SVM classifier

The selection of the proper kernel is essential for the optimal performance of the SVM classifier. The classification accuracy was evaluated to select the kernel function among linear, quadratic, cubic, fine Gaussian and coarse Gaussian. Fig 5.5 shows the classification accuracy obtained for different kernel functions for Subject-2.

Analysis of variance showed a significant difference in the accuracy for the different kernels with the SVM classifier ($F_{4,45}$= 61.638, p = 0.000). Table 5.2 presents the result from the Tukey's post hoc test for kernel selection. The test revealed that the classification accuracy obtained with the quadratic kernel (93.39 ± 1.64 %) is significantly higher than the linear kernel (90.09 ± 1.67 %, p= 0.0002), fine Gaussian kernel (83.89 ± 1.7 %, p=0.000) and coarse Gaussian kernel (88.45 ± 1.19 %, p=0.000). The classification accuracy obtained from the cubic kernel is 93.24 ± 1.62 %. Although, it is significantly similar to that with the quadratic kernel (p=0.9995). However, the high complexity of cubic kernel compared to quadratic kernel makes the quadratic kernel a preferable choice. Henceforth, the rest of this study considers SVM with the quadratic kernel (SVM with a quadratic kernel (SVMQ)).

TABLE 5.2: Results of post-hoc test for classification accuracy of SVN classifiers for various kernels

Multiple Comparisons

Kernel (I)	**(J) Kernel**	**Mean Difference (I-J)**	**Std. Error**	**Sig.**	**95% Confidence Interval**	
					Lower Bound	**Upper Bound**
Linear	Quadratic	-.03303582*	0.0071	.000	-0.0531	-0.0130
	Cubic	-.03157639*	0.0071	.000	-0.0517	-0.0115
	Gaussian Fine	.06196443*	0.0071	.000	0.0419	0.0820
	Gaussian Coarse	.01637427	0.0071	.159	-0.0037	0.0365
Quadratic	Linear	.03303582*	0.0071	.000	0.0130	0.0531
	Cubic	.00145943	0.0071	1.000	-0.0186	0.0215
	Gaussian Fine	.09500026*	0.0071	.000	0.0749	0.1151
	Gaussian Coarse	.04941009*	0.0071	.000	0.0293	0.0695
Cubic	Linear	.03157639*	0.0071	.000	0.0115	0.0517
	Quadratic	-.00145943	0.0071	1.000	-0.0215	0.0186
	Gaussian Fine	.09354082*	0.0071	.000	0.0735	0.1136
	Gaussian Coarse	.04795066*	0.0071	.000	0.0279	0.0680
Gaussian Fine	Linear	-.06196443*	0.0071	.000	-0.0820	-0.0419
	Quadratic	-.09500026*	0.0071	.000	-0.1151	-0.0749
	Cubic	-.09354082*	0.0071	.000	-0.1136	-0.0735
	Gaussian Coarse	-.04559017*	0.0071	.000	-0.0657	-0.0255
Gaussian Coarse	Linear	-.01637427	0.0071	.159	-0.0365	0.0037
	Quadratic	-.04941009*	0.0071	.000	-0.0695	-0.0293
	Cubic	-.04795066*	0.0071	.000	-0.0680	-0.0279
	Gaussian Fine	.04559017*	0.0071	.000	0.0255	0.0657

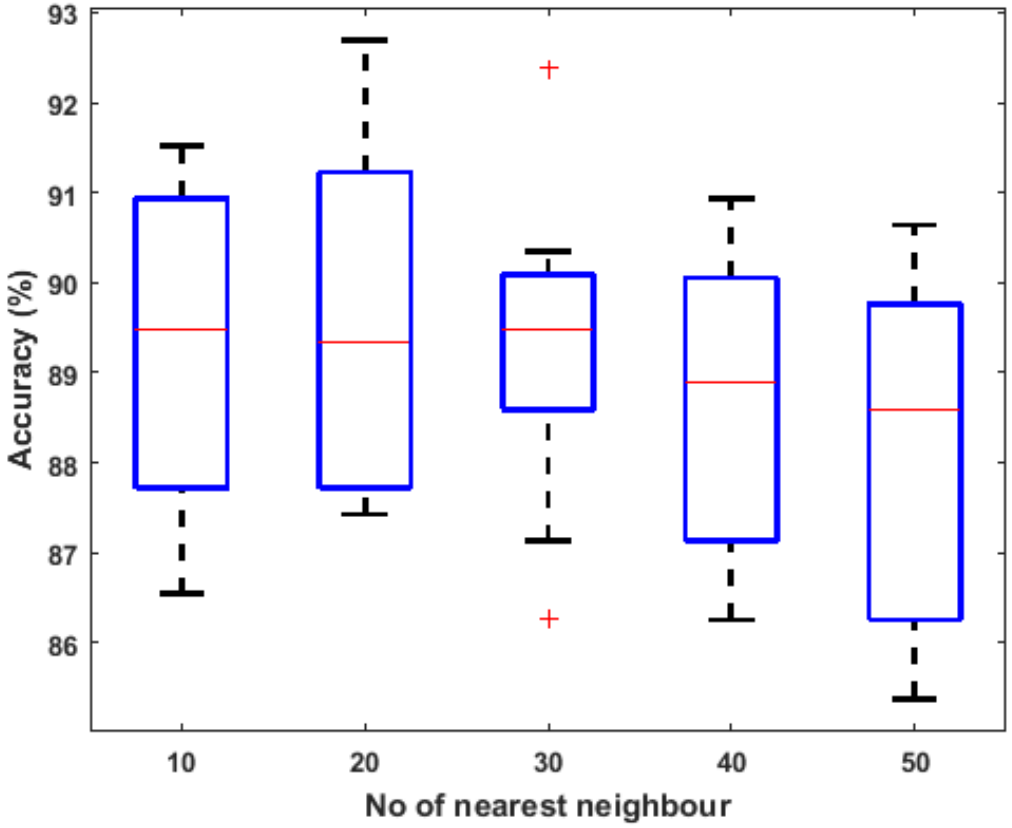

FIGURE 5.6: The classification accuracy obtained for the different values of nearest neighbours

5.4.1.2 The optimal number of nearest neighbours in the case of the k-NN classifier

The classification accuracy was examined to find the optimum value of nearest neighbours (k). Fig 5.6 shows the box plot of the classification accuracy obtained with k values of 10, 20, 30, 40, and 50 for Subject-2. An ANOVA test indicated that the classification accuracy obtained for different values of k is very similar ($F_{4,45}$= 0.715, p=0.586). Table 5.3 presents the ANOVA results. The classification accuracy was at a maximum (89.27 $\pm$ 1.77 %) for k=10. Henceforth, for the rest of this study, the value of k was maintained at 10.

5.4.1.3 Window size selection

Fig 5.7 illustrates the average classification error obtained with the different window sizes for all the classifiers. The results indicate that there is an improvement in the performance of the classifiers as the window size is increased from 125 ms for W1 to 500 ms for W4 and

TABLE 5.3: Result of ANOVA for classification accuracy of k-NN classifier with different k values

	Sum of Squares	**df**	**Mean Square**	**F**	**Sig**
Between Groups	.001	4	.000	.715	.586
Within Groups	.015	45	.000		
Total	.016	49			

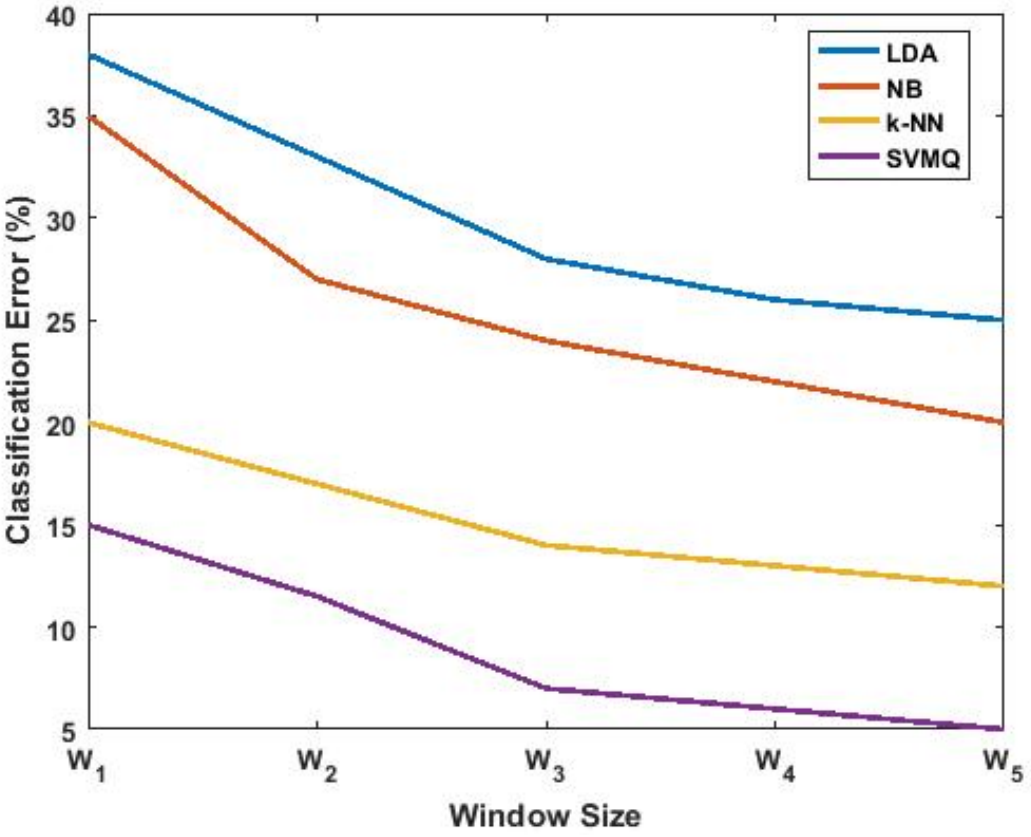

FIGURE 5.7: Classification error obtained with the different window sizes

W5. This increase in the window size provides additional information and reduces the variance among the evaluated features thereby decreasing the classification error. The performance of the classifiers obtained for W3 is significantly similar to that obtained for W4. Furthermore, the system's response time is to be maintained bellow 300 ms [4; 46]. So, both windows W3 and W4 are suitable for feature extraction. Henceforth, W3 with a window size of 250 ms and increment size of 125 ms is used in the present research work.

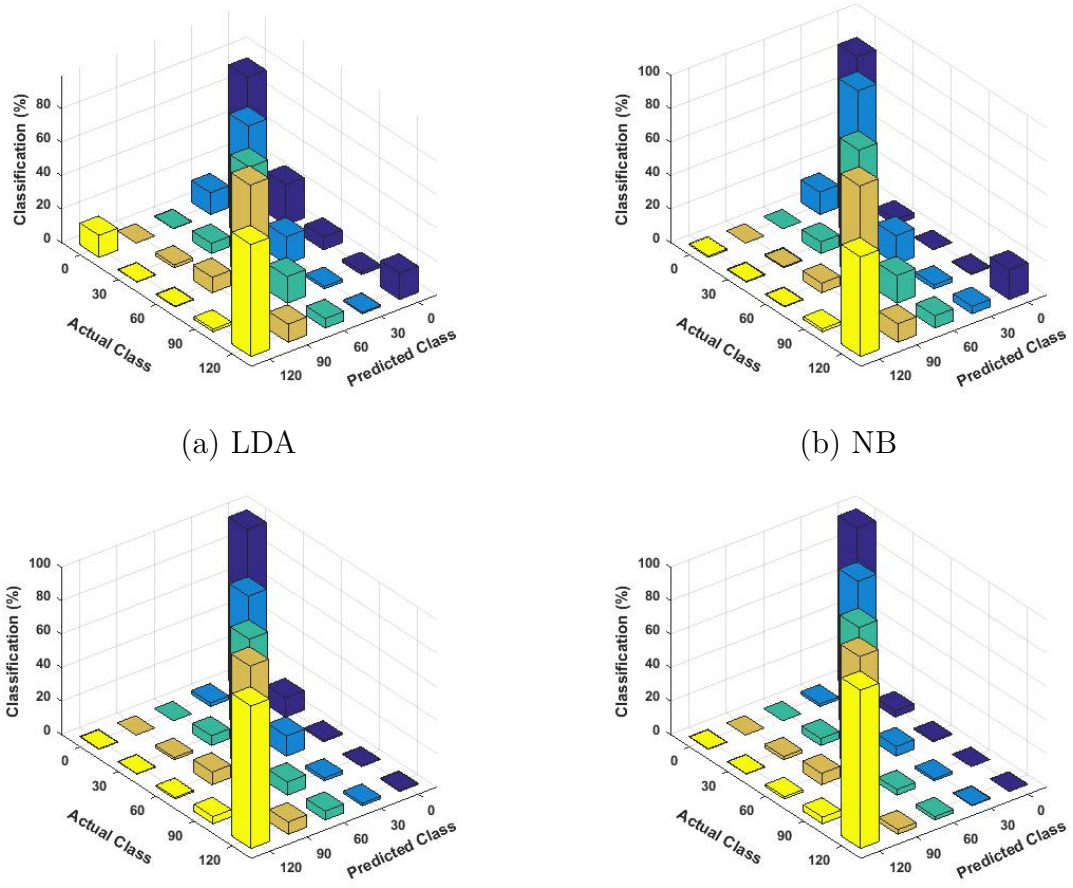

(a) LDA (b) NB

(c) k-NN (d) SVMQ

FIGURE 5.8: Confusion matrix of different classifier for Study-I

5.4.1.4 Comparative performance of classifiers

After finalizing the parameters of the four classifiers and the size and increment of the moving window the study compares the performance of the classifiers. Confusion matrices for the classifiers were evaluated. Fig 5.8 presents the confusion matrices for the classifiers. Eq 5.16 to Eq 5.19 were used to evaluate the accuracy, sensitivity, selectivity and precision of the classifiers.

Table 5.4 presents the classification sensitivity obtained for all the subjects using the different classifiers. Average classification sensitivity of different classifiers obtained is depicted in Fig 5.9. The results of ANOVA presented in Table 5.5 indicates a significant difference in the sensitivity obtained for the different classifiers ($F_{3,476}$= 616.563, p = 0.000). Tukey's post hoc analysis revealed that the sensitivity of the SVMQ classifier (90.19 ± 3.06 %) is significantly higher than that of LDA (69.13 ± 4.54 %, p= 0.000), NB (75.96 ± 4.81 %, p=0.000) and k-NN (84.24 ± 3.63 %, p=0.000) classifiers.

TABLE 5.4: Sensitivity obtained for different classifiers

Subject	LDA	NB	k-NN	SVMQ
S1	72.35 ± 2.75	78.62 ± 2.19	86.59 ± 1.78	91.72 ± 1.77
S2	70.74 ± 1.33	78.93 ± 1.64	85.35 ± 2.51	91.46 ± 2.25
S3	71.65 ± 2.88	78.62 ± 2.09	84.76 ± 2.78	90.50 ± 2.15
S4	60.13 ± 2.88	66.97 ± 3.01	76.19 ± 2.63	82.92 ± 1.91
S5	66.16 ± 1.31	71.56 ± 2.51	83.03 ± 1.64	89.05 ± 1.83
S6	73.44 ± 1.72	81.22 ± 2.30	86.92 ± 1.45	92.11 ± 2.22
S7	70.77 ± 3.95	77.90 ± 2.49	85.13 ± 2.27	91.73 ± 1.71
S8	71.63 ± 1.87	79.78 ± 1.89	87.86 ± 2.07	92.12 ± 1.50
S9	64.77 ± 2.55	71.51 ± 2.97	82.67 ± 2.64	89.31 ± 1.51
S10	65.73 ± 1.74	71.28 ± 1.42	81.95 ± 2.40	88.43 ± 1.85
S11	70.40 ± 3.43	75.99 ± 2.52	84.53 ± 1.62	91.13 ± 1.32
S12	71.80 ± 2.59	79.12 ± 1.16	85.96 ± 2.09	91.74 ± 1.69
Avg	69.13± 4.54	75.96 ± 4.81	84.24 ± 3.64	90.19 ± 3.06

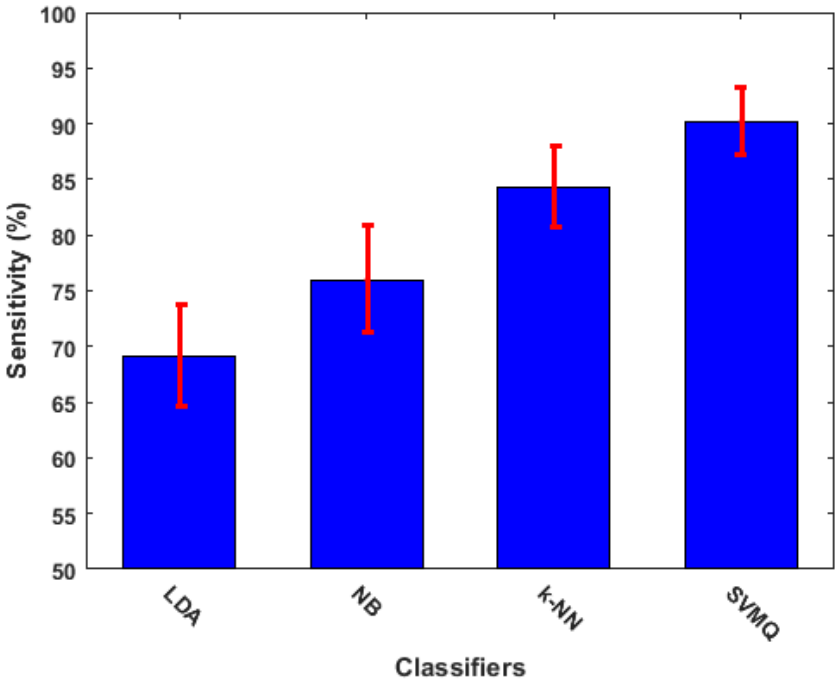

FIGURE 5.9: Sensitivity of different classifiers for Study-I

TABLE 5.5: Result of ANOVA for the classification sensitivity of different classifiers

	Sum of Squares	**df**	**Mean Square**	**F**	**Sig**
Between Groups	3.074	3	1.025	616.563	.000
Within Groups	.791	476	.002		
Total	3.865	479			

TABLE 5.6: Classification accuracy of different classifiers for Study-I

Subject	**LDA**	**NB**	**k-NN**	**SVMQ**
S1	74.70 ± 2.72	76.94 ± 1.90	89.67 ± 1.16	93.07 ± 1.33
S2	72.49 ± 1.82	77.43 ± 1.56	89.27 ± 1.77	93.27 ± 1.47
S3	73.20 ± 2.69	74.75 ± 1.66	88.46 ± 1.91	92.85 ± 1.75
S4	67.09 ± 2.46	70.05 ± 2.33	83.19 ± 1.84	87.72 ± 1.09
S5	68.24 ± 1.37	71.29 ± 2.05	85.71 ± 1.16	90.57 ± 1.57
S6	75.26 ± 0.84	81.03 ± 1.23	89.90 ± 0.99	93.71 ± 1.44
S7	73.11 ± 3.1 0	76.71 ± 1.86	88.95 ± 1.26	93.42 ± 1.36
S8	73.63 ± 1.62	78.17 ± 2.03	90.62 ± 1.19	93.65 ± 1.19
S9	67.38 ± 2.40	72.26 ± 2.38	86.52 ± 2.00	91.55 ± 1.28
S10	68.50 ± 1.99	72.57 ± 1.42	84.70 ± 1.56	90.06 ± 1.28
S11	71.69 ± 2.31	73.70 ± 2.28	88.62 ± 1.30	93.30 ± 1.13
S12	73.33 ± 2.17	76.38 ± 1.78	89.58 ± 1.64	93.83 ± 1.28
Avg	71.55 ± 3.52	75.11 ± 3.59	87.93 ± 2.67	92.25 ± 2.24

Classification accuracy obtained for all the subjects using the different classifiers is presented in Table 5.6 and Fig 5.10. The results of ANOVA test presented in Table 5.7 indicates significant difference in the accuracy obtained with the different classifiers ($F_{3,476}$= 1265.08, p = 0.000). A post hoc multiple comparison analysis was performed using Tukey's method. Table 5.8 presents the results from the Tukey's post hoc test for the classification accuracy. The results revealed that the classification accuracy with the SVMQ classifier (92.2 ± 2.2 %) is significantly higher than with the LDA (71.6 ± 3.5 %, p= 0.000), NB (75.1 ± 3.6 %, p=0.000) and k-NN (87.9 ± 2.7 %, p=0.000) classifiers.

Table 5.9 presents the classification specificity obtained for all the subjects using different classifiers. Table 5.10 summarizes the results of ANOVA, which indicates a significant difference in the specificity obtained for different classifiers ($F_{3,476}$= 1409.106, p = 0.000). Tukey's post hoc analysis revealed that the specificity of the SVMQ classifier (98.11 ± 0.55 %) is significantly higher than that of LDA (92.62 ± 0.96 %, p= 0.000), NB (93.74 ± 1.02 %, p=0.000) and k-NN (97.02 ± 0.66 %, p=0.000) classifiers.

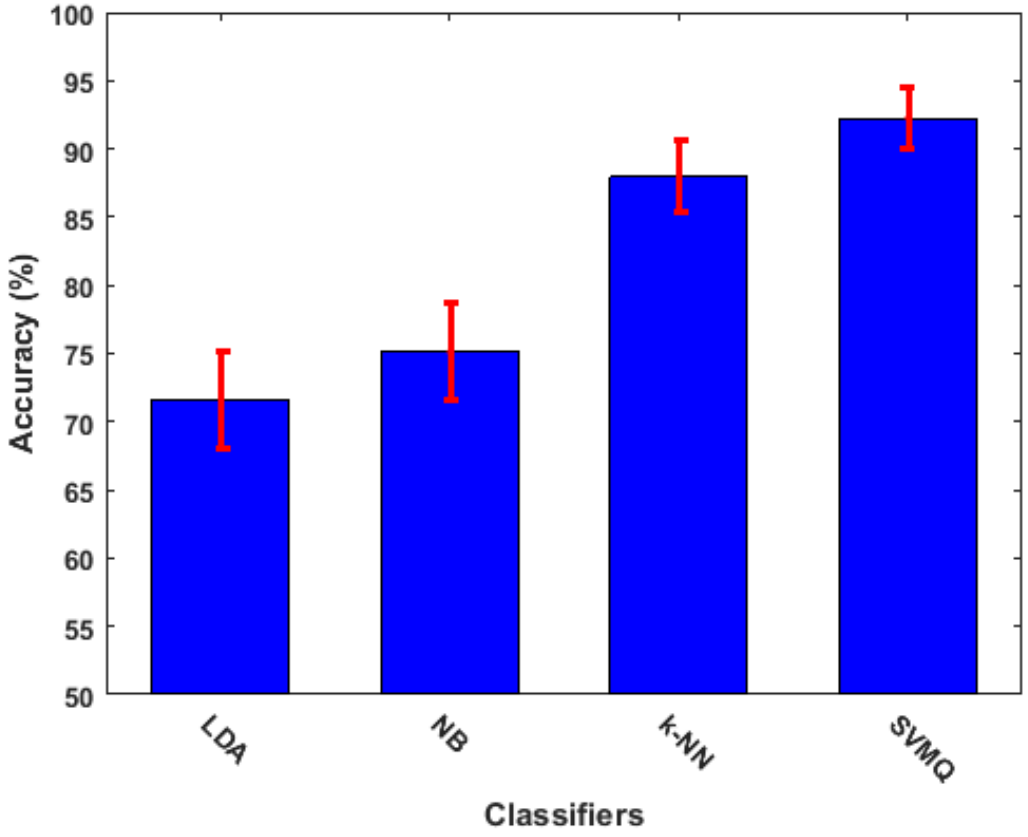

FIGURE 5.10: Classification accuracy of various classifiers for study-I

TABLE 5.7: Result of ANOVA for the classification accuracy of different classifiers for Study-I

	Sum of Squares	**df**	**Mean Square**	**F**	**Sig**
Between Groups	3.560	3	1.187	1265.080	0.000
Within Groups	.446	476	.001		
Total	4.006	479			

Table 5.11 and Fig 5.12 summarises the precision obtained for the different classifiers. Table 5.12 summarizes the results of ANOVA for precision of classifiers. The result indicates a significant difference in the precision obtained for different classifiers ($F_{3,476}$ = 788.867, p = 0.000). Tukey's post hoc test revealed that the precision with the SVMQ classifier (89.38 ± 3.49 %) is significantly higher than that obtained with the LDA (68.63 ± 4.66 %, p= 0.000), NB (73.62 ± 3.98 %, p=0.000) and k-NN (83.77 ± 3.54 %, p=0.000) classifiers.

TABLE 5.8: Test result for Tukey post-hoc test for classification accuracy of different classifiers for Study-I

Classifier	**Classifier**	**Difference**	**Std. Error**	**Sig.**	**95% Confidence Interval**	
(I)	(J)	(I-J)			**Lower Bound**	**Upper Bound**
LDA	NB	-.0355441*	.0039538	.000	-.045737	-.025351
	k-NN	-.1638101*	.0039538	.000	-.174003	-.153617
	SVMQ	-.2069969*	.0039538	.000	-.217190	-.196803
NB	LDA	.0355441*	.0039538	.000	.025351	.045737
	k-NN	-.1282660*	.0039538	.000	-.138459	-.118073
	SVMQ	-.1714528*	.0039538	.000	-.181646	-.161259
k-NN	LDA	.1638101*	.0039538	.000	.153617	.174003
	NB	.1282660*	.0039538	.000	.118073	.138459
	SVMQ	-.0431868*	.0039538	.000	-.053380	-.032993
SVMQ	LDA	.2069969*	.0039538	.000	.196803	.217190
	NB	.1714528*	.0039538	.000	.161259	.181646
	k-NN	.0431868*	.0039538	.000	.032993	.053380

TABLE 5.9: Specificity obtained for different classifiers

Subject	**LDA**	**NB**	**K-NN**	**SVMQ**
S1	93.5 ± 0.7	94.2 ± 0.5	97.5 ± 0.3	98.3 ± 0.3
S2	92.8 ± 0.5	94.2 ± 0.4	97.3 ± 0.4	98.3 ± 0.4
S3	93.1 ± 0.7	93.7 ± 0.4	97.2 ± 0.4	98.3 ± 0.4
S4	91.5 ± 0.7	92.5 ± 0.6	95.8 ± 0.5	96.9 ± 0.3
S5	91.8 ± 0.4	92.9 ± 0.5	96.5 ± 0.3	97.7 ± 0.4
S6	93.5 ± 0.3	95.3 ± 0.3	97.5 ± 0.3	98.5 ± 0.4
S7	92.9 ± 0.8	95.3 ± 0.3	94.1 ± 0.4	98.4 ± 0.3
S8	93.1 ± 0.4	94.4 ± 0.5	97.6 ± 0.3	98.4 ± 0.2
S9	91.7 ± 0.6	93.1 ± 0.6	96.7 ± 0.5	98.0 ± 0.3
S10	91.9 ± 0.5	93.1 ± 0.3	96.3 ± 0.4	97.6 ± 0.3
S11	92.6 ± 0.7	93.4 ± 0.5	97.2 ± 0.3	98.3 ± 2.4
S12	93.1 ± 0.6	94.0 ± 0.5	97.4 ± 0.4	98.5 ± 0.3
Avg	92.6 ± 0.9	93.7 ± 0.9	97.0 ± 0.6	98.1 ± 0.6

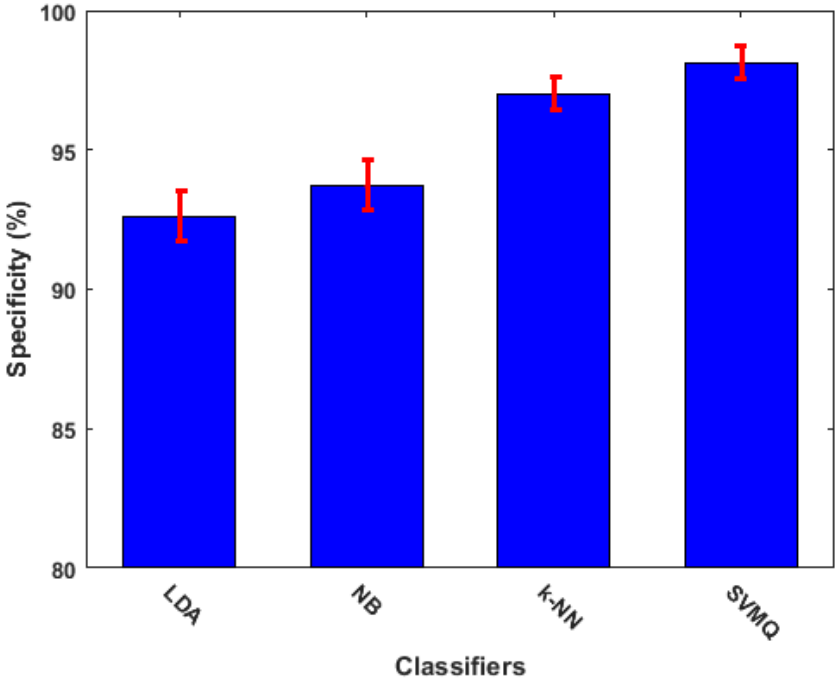

FIGURE 5.11: Classification specificity obtained for different classifiers

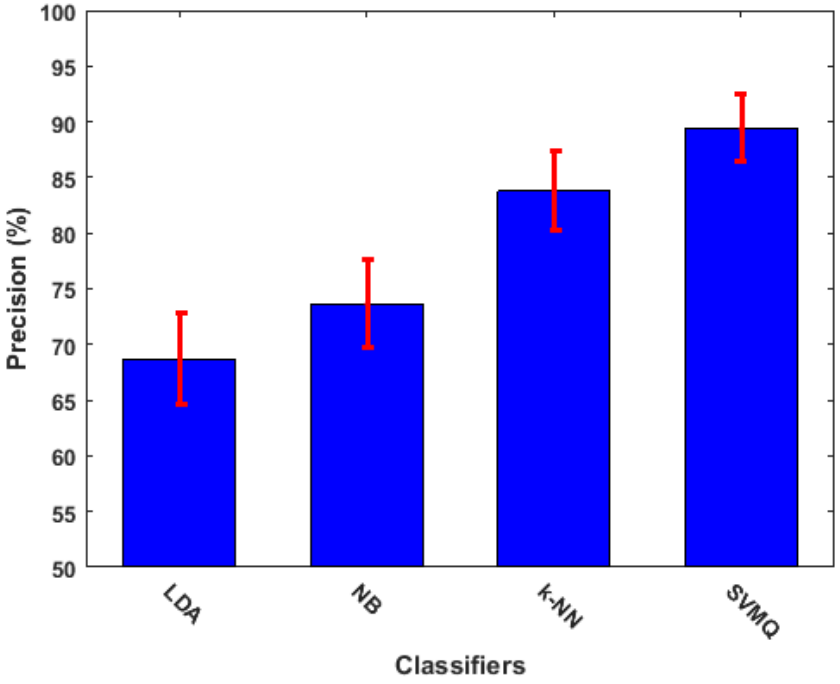

FIGURE 5.12: Classification precision obtained for different classifiers for Study-I

TABLE 5.10: Result of ANOVA obtained for classification specificity for different classifiers

	Sum of Squares	**df**	**Mean Square**	**F**	**Sig**
Between Groups	.245	3	.082	1409.106	.000
Within Groups	.028	476	.000		
Total	.273	479			

TABLE 5.11: Precision obtained for different classifiers

Subject	**LDA**	**NB**	**k-NN**	**SVMQ**
S1	71.9 ± 2.7	76.0 ± 1.7	86.3 ± 1.6	90.9 ± 1.7
S2	70.0 ± 1.8	76.4 ± 1.9	85.0 ± 2.7	90.6 ± 2.0
S3	69.9 ± 2.7	73.8 ± 1.9	84.1 ± 2.8	89.8 ± 2.7
S4	60.8 ± 2.4	65.9 ± 2.5	76.2 ± 2.2	83.1 ± 2.0
S5	66.5 ± 1.2	70.6 ± 2.1	82.4 ± 1.7	88.3 ± 2.2
S6	73.6 ± 1.1	79.1 ± 1.6	86.6 ± 1.3	91.6 ± 1.8
S7	70.4 ± 3.5	75.4 ± 2.4	84.7 ± 1.8	90.9 ± 2.1
S8	71.3 ± 1.6	77.1 ± 1.6	87.4 ± 1.7	91.0 ± 1.6
S9	64.1 ± 2.6	70.3 ± 2.8	82.1 ± 2.6	88.6 ± 1.9
S10	66.2 ± 1.9	71.6 ± 1.5	80.9 ± 2.1	87.2 ± 1.6
S11	68.5 ± 2.5	72.1 ± 2.1	84.0 ± 1.6	90.1 ± 2.0
S12	70.3 ± 2.0	75.2 ± 1.0	85.6 ± 2.0	91.0 ± 2.0
Avg	68.6± 0.4	73.6 ± 4.0	83.7 ± 3.5	89.4 ± 3.0

TABLE 5.12: Result of ANOVA obtained for classification precision for different classifiers

	Sum of Squares	**df**	**Mean Square**	**F**	**Sig**
Between Groups	3.202	3	1.067	788.867	.000
Within Groups	.644	476	.001		
Total	3.846	479			

TABLE 5.13: Classification accuracy obtained for different locomotion modes in Study-II

Subject	LM1		LM2		LM3	
	k-NN	SVMQ	k-NN	SVMQ	k-NN	SVMQ
S1	86.50 ± 1.51	90.28 ± 1.34	85.04 ± 1.70	88.21 ± 1.63	87.05 ± 0.94	90.73 ± 1.44
S2	86.24 ± 1.66	90.28 ± 1.53	85.17 ± 2.06	88.47 ± 1.24	87.10 ± 1.71	91.01± 1.42
S3	85.47 ± 2.30	89.91 ± 1.89	84.26 ± 2.47	88.02 ± 1.75	85.83 ± 2.22	90.97± 1.73
S4	80.47 ± 1.91	84.72 ± 1.08	78.43 ± 2.18	83.17 ± 0.69	80.33 ± 2.37	85.10± 1.72
S5	82.81 ± 1.28	87.37 ± 1.61	80.77 ± 1.62	85.75 ± 1.39	83.31 ± 1.09	88.27 ± 2.08
S6	86.91 ± 0.93	90.89 ± 1.61	85.65 ± 1.22	89.07 ± 1.75	87.56 ± 1.27	90.88 ± 1.48
S7	85.98 ± 1.16	90.26 ± 1.64	85.06 ± 1.50	88.79 ± 1.99	86.99 ± 1.98	91.26 ± 1.17
S8	87.82 ± 1.42	90.55 ± 1.29	86.18 ± 1.31	88.78 ± 1.46	88.30 ± 1.33	91.03 ± 2.04
S9	83.27 ± 2.25	88.54 ± 1.14	81.34 ± 1.99	86.79 ± 1.80	84.25 ± 2.35	89.59 ± 1.26
S10	81.70 ± 1.61	87.15 ± 1.65	80.13 ± 1.84	85.83 ± 1.07	82.42 ± 2.02	88.03 ± 1.81
S11	85.76 ± 1.59	90.16 ± 1.26	84.19 ± 1.91	88.38 ± 1.18	86.13 ± 2.09	90.79 ± 1.10
S12	86.66 ± 1.83	90.93 ± 1.50	84.70 ± 1.72	89.74 ± 1.60	87.13 ± 2.08	91.23 ± 1.73
Avg	84.97 ± 2.73	89.25 ± 2.32	83.41 ± 3.00	87.58 ± 2.30	85.53 ± 2.93	89.91 ± 2.37

5.4.2 Study-II

In this study knee angle prediction from SEMG signals was carried out for three different locomotion activities on a custom built gate course. The performance of LDA and NB classifier was inferior to k-NN and SVMQ classifier in the first study. So, in this study performance of Only k-NN and SVMQ were evaluated. Table 5.13 present the classification accuracy obtained with both the classifiers for different locomotion modes. The results of the ANOVA test on the classification accuracy achieved while performing the three activities indicate that the performance of SVMQ is significantly superior to that of k-NN for all the three activities ($p < 0.05$). The average classification accuracy obtained with SVMQ classifier is 89.25 ± 2.32 % for stair ascend, 87.58 ± 2.30 % for level plain walking and 89.91 ± 2.37 % for stair descend.

5.5 Prototype development

Fig 5.13 shows the SolidWork design of the prototype exoskeleton. The prototype structure consists of thigh segment, shank segment, and an actuator. The design of the prototype is similar to brace used by patients with loco-motor disability. Thigh support and shank support are custom built to match the size of subjects limb. The prototype is

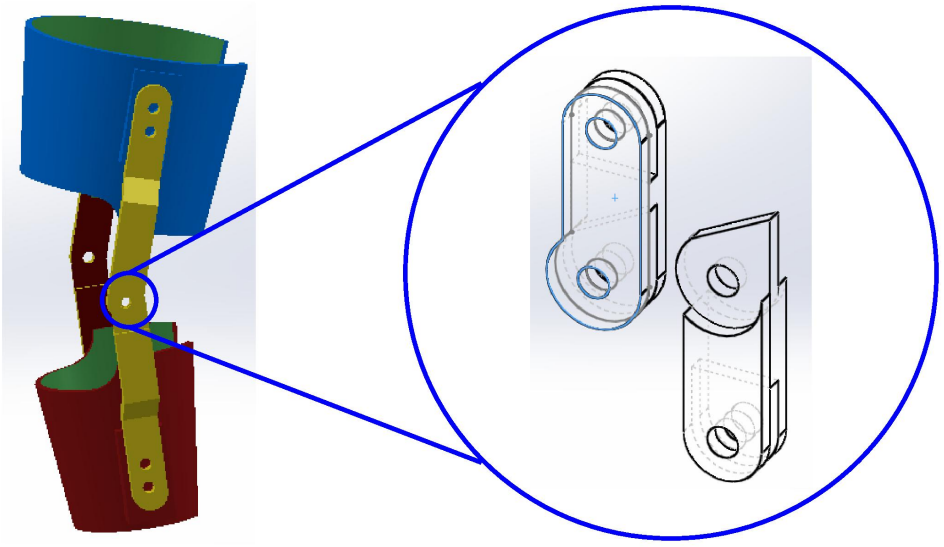

FIGURE 5.13: Solid work design of the exoskeleton prototype

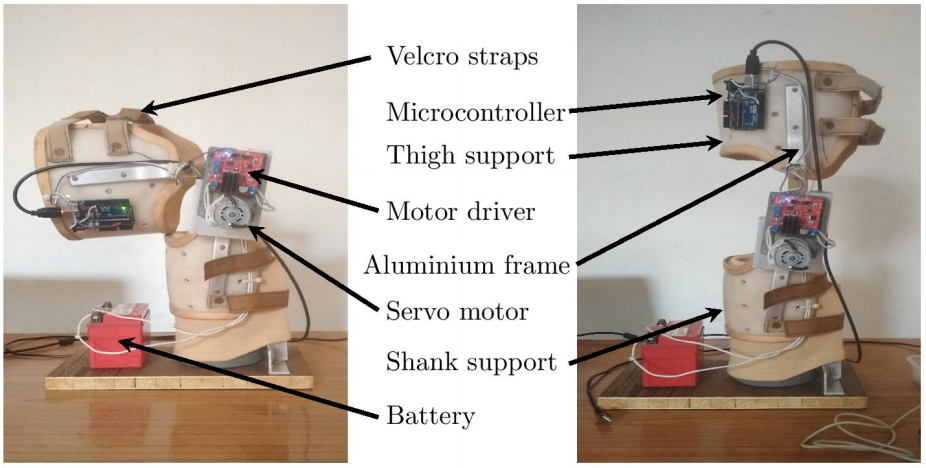

FIGURE 5.14: Design of a prototype exoskeleton knee

fastened to the user using Velcro straps provided on both the thigh and shank support. A high torque servo motor (ASME-02b) is used as an actuator.

Fig 5.14 depicts the exoskeleton prototype in fully erect position (KA = 0°) and corresponding to sitting on chair (KA = 90°). The present design works offline, the value of the knee angle predicted by the classifier (stored as measurement file) is passed to the microcontroller. The microcontroller generates the pulse width modulated control signal corresponding to the instantaneous value of knee angle.

5.6 Conclusion

This chapter proposes a novel approach of predicting the knee angle. The complete range of motion of the knee angle is quantized into a number of level/classes and present class of the knee angle is predicted from the features of SEMG signal using a classifier. The performance of the four common clasifiers LDA, NB, k-NN, and SVM were evaluated for the activity sitting down and standing up from chair. Performance of five different windows with size ranging from 125 ms to 500 ms were analyzed. W3 window with size 250 ms and window increment of 125 ms was selected for subsequent studies. SVM classifier with quadratic kernel performed best with average classification accuracy of 92.25 ± 2.24 %, sensitivity of 90.19 ± 3.06 %, speficity of 98.11 ± 0.55 % and 89.38 ± 2.96 % precision for standing up and sitting down on chair.

A second study was conducted to evaluate the performance of the top two classifiers (k-NN and SVMQ) of the first study for three different locomotion modes: stair assend, walking on level ground, and stair descend. SVMQ classifier performed significantly better than k-NN classifier with classification accuracy of 89.25 ± 2.32 % for stair ascend, for 87.58 ± 2.30 % level plain walking and 89.91 ± 2.37 % for stair descend. The chapter ends with a design proposal of a prototype exoskeleton knee with single degree of freedom in sagital plane .

Chapter 6

Conclusions and future scope

Exoskeleton is anthropomorphic in nature and is worn by a user. It works in parallel with the users limb movement and enhance their muscular strength artificially. Its major applications are in the field of military, manufacturing industry, disaster management, medical/rehabilitation of population having neuromotor disorder or aged population. Control strategies of exoskeleton includes mechanical sensor based control and biosensor based control. Biosensor based control strategies of exoskeleton enhances its efficacy and performance multifold. In this strategy, user limb movement intention is predicted well before the actual limb movement so the exoskeleton works in synergy with the user. SEMG signal is evolving as an effective tool to extract the user limb movement intention. The presented work is an attempted to develop a myoelectric control for exoskeleton knee capable of predicting joint angle while performing basic daily life activities like; standing up, sitting down, walking on plain ground, stair ascend/descend *etc.*

SEMG signal can be acquired non invasively from the surface of the individual muscle. It is stochastic in nature have low amplitude and major information in the frequency range of 50 – 150 Hz. Acquiring SEMG signal in laboratory environment is itself a challenge as its more prone to noise contamination. Here, an eight channel bio instrumentation system along with its user front end was developed to acquire SEMG signal in laboratory environment. The developed system utilized ADS1298 along with microcontroller and LabVIEW platform. ADS1298 has eight low power, multichannel, simultaneously sampling, 24-bit delta sigma ADCs with integrated PGAs. Microcontroller was used to configure ADS1298 and also to interlink it with the front end GUI (developed in LabVIEW). The GUI facilitates the user to configure the bioinstrumentation system, to start and stop the signal recoding task also to visualize the acquired signal in real time. The

developed system was tested for internally generated test signal, externally applied test signal and lower limb muscle SEMG signal.

The human lower limb has more than fifty muscles however; the motion intent can be predicted by considering some of these muscles. Preliminary requirement for a myoelectric controlled system is the optimal selection of muscles. This research work presents a novel technique of muscle selection. The force developed in the muscle was used as a basis for muscle recruitment. A MMHB of human body developed in AMS was scaled to match the anthropometric detail of subjects. It was made to perform a stand to squat movement and the forces developed in eighteen lower limb muscles were obtained by inverse dynamic analysis. Method of principal variable was applied to obtain the optimum set of muscles capable of controlling the knee movement. The best set of five muscles came out as VALA, BIFE, REFE, SETE and GLME. SEMG signal from the selected muscles were acquired while performing the stand to squat movement. Force developed in muscles was estimated using Hill's model. The estimated forces were compared with the force obtained by the inverse dynamic analysis using MMHB.

A novel technique of predicting the human knee angle from SEMG signal was developed. The complete range of motion of knee joint was quantized in to pre-defined levels/classes. Instantaneous level of the knee angle was predicted using a classifier. Performance of four classifiers (LDA, NB, k-NN and SVM) for predicting the class of knee angle while performing basic activities like; sitting down/standing up from a chair, walking on a plain ground, stair ascend and stair descend were evaluated. The SVM classifier with quadratic kernel outperformed other classifiers with average classification accuracy of 92.25 $\pm$ 2.24 % for sitting down/standing up from a chair, 87.58$\pm$ 2.30 % for walking of plain ground, 89.25 $\pm$ 2.32 % for ascending stairs and 89.91 $\pm$ 2.37 % for descending stairs.

A prototype of the knee exoskeleton was designed in SolidWorks. It has a shank support segment, a thigh support segment and an actuator. The segment were designed to prevent accidental hyper flexion. The mechanical design was made an aluminum frame and ASME02B high torque servo motor as an actuator. The SEMG signal from the selected lower limb muscles were used to predict the knee angle and the predicted knee angle was used to control the prototype offline. This work presents a successful development of a myoelectric knee angle prediction capable of controlling exoskeleton.

For the future development of myoelectric controlled exoskeleton, following suggestions are made:

- The hardware based machine learning system composed of electronic representation of the output of classifier in online mode can be designed for the motion recognition. It should be like a system on chip platform implementation to decrease the detection delay.
- Deep learning and muscle synergy are evolving techniques. There use can further enhance the performance of the system.
- Recent advancement in 2-D High Density EMG (HDEMG) electrodes can overcome the shortcomings of the conventional SEMG acquisition and achieve better motion classification performance beneficial for exoskeleton myoelectric control.
- To remove the motion artifacts from wired electrode systems, wireless SEMG acquisition system is likely to produce better results.
- The mechanical structure of prototype can be made more effective by incorporating various dynamic structural analysis which will in turn make the exoskeleton more efficient.

Bibliography

[1] J. Rosen, M. Brand, M. B. Fuchs, and M. Arcan. A myosignal-based powered exoskeleton system. *Systems, Man and Cybernetics, Part A: Systems and Humans, IEEE Transactions on*, 31(3):210–222, 2001.

[2] Renee L Attwells, Stewart A Birrell, Robin H Hooper, and Neil J Mansfield. Influence of carrying heavy loads on soldiers' posture, movements and gait. *Ergonomics*, 49(14):1527–1537, 2006.

[3] A.B. Zoss, H. Kazerooni, and A. Chu. Biomechanical design of the berkeley lower extremity exoskeleton (BLEEX). *Mechatronics, IEEE/ASME Transactions on*, 11 (2):128–138, April 2006. ISSN 1083-4435. doi: 10.1109/TMECH.2006.871087.

[4] Andrew Chu, Hami Kazerooni, and Adam Zoss. On the biomimetic design of the berkeley lower extremity exoskeleton (bleex). In *Robotics and Automation, 2005. ICRA 2005. Proceedings of the 2005 IEEE International Conference on*, pages 4345–4352. IEEE, 2005.

[5] Stephen C Jacobsen, M Olivier, FM Smith, David F Knutti, R Todd Johnson, GE Colvin, and WB Scroggin. Research robots for applications in artificial intelligence, teleoperation and entertainment. *The International Journal of Robotics Research*, 23(4-5):319–330, 2004.

[6] Carmen Constantinescu, Daniela Popescu, Paul-Cristian Muresan, and Sebastian-Ioan Stana. Exoskeleton-centered process optimization in advanced factory environments. *Procedia CIRP*, 41:740–745, 2016.

[7] Michiel P De Looze, Tim Bosch, Frank Krause, Konrad S Stadler, and Leonard W O'Sullivan. Exoskeletons for industrial application and their potential effects on physical work load. *Ergonomics*, 59(5):671–681, 2016.

[8] Magdo Bortole, Anusha Venkatakrishnan, Fangshi Zhu, Juan C Moreno, Gerard E Francisco, Jose L Pons, and Jose L Contreras-Vidal. The h2 robotic exoskeleton for gait rehabilitation after stroke: early findings from a clinical study. *Journal of neuroengineering and rehabilitation*, 12(1):54, 2015.

[9] Dennis R Louie and Janice J Eng. Powered robotic exoskeletons in post-stroke rehabilitation of gait: a scoping review. *Journal of neuroengineering and rehabilitation*, 13(1):53, 2016.

[10] Sai K Banala, Suni K Agrawal, and John P Scholz. Active leg exoskeleton (alex) for gait rehabilitation of motor-impaired patients. In *2007 IEEE 10th International Conference on Rehabilitation Robotics*, pages 401–407. IEEE, 2007.

[11] Jan F Veneman, Rik Kruidhof, Edsko EG Hekman, Ralf Ekkelenkamp, Edwin HF Van Asseldonk, and Herman Van Der Kooij. Design and evaluation of the lopes exoskeleton robot for interactive gait rehabilitation. *IEEE Transactions on Neural Systems and Rehabilitation Engineering*, 15(3):379–386, 2007.

[12] Zachary F Lerner, Diane L Damiano, Hyung-Soon Park, Andrew J Gravunder, and Thomas C Bulea. A robotic exoskeleton for treatment of crouch gait in children with cerebral palsy: Design and initial application. *IEEE Transactions on Neural Systems and Rehabilitation Engineering*, 25(6):650–659, 2017.

[13] Cheng-Hua Wu, Hui-Fen Mao, Jwu-Sheng Hu, Ting-Yun Wang, Yi-Jeng Tsai, and Wei-Li Hsu. The effects of gait training using powered lower limb exoskeleton robot on individuals with complete spinal cord injury. *Journal of neuroengineering and rehabilitation*, 15(1):14, 2018.

[14] K. Yamamoto, K. Hyodo, and T. Ishii, M.and Matsuo. Development of power assisting suit for assisting nurse labor. *JSME International Journal Series C*, 45 (3):703–711, 2002.

[15] Kyoungchul Kong and Doyoung Jeon. Design and control of an exoskeleton for the elderly and patients. *IEEE/ASME Transactions on mechatronics*, 11(4):428–432, 2006.

[16] Samuel Galle, Wim Derave, F Bossuyt, Patrick Calders, Philippe Malcolm, and Dirk De Clercq. Exoskeleton plantarflexion assistance for elderly. *Gait & posture*, 52:183–188, 2017.

[17] S. Lee and Y. Sankai. Power assist control for walking aid with hal-3 based on emg and impedance adjustment around knee joint. In *Intelligent Robots and Systems, 2002. IEEE/RSJ International Conference on*, volume 2, pages 1499–1504. IEEE, 2002.

[18] Allan C Gelber, Marc C Hochberg, Lucy A Mead, Nae-Yuh Wang, Fredrick M Wigley, and Michael J Klag. Body mass index in young men and the risk of subsequent knee and hip osteoarthritis. *The American journal of medicine*, 107(6): 542–548, 1999.

[19] Christian Fleischer and Günter Hommel. Torque control of an exoskeletal knee with emg signals. *Vdi Berichte*, 1956:79, 2006.

[20] Ettore E Cavallaro, Jacob Rosen, Joel C Perry, and Stephen Burns. Real-time myoprocessors for a neural controlled powered exoskeleton arm. *IEEE Transactions on Biomedical Engineering*, 53(11):2387–2396, 2006.

[21] Mervin Chandrapal, XiaoQi Chen, Wenhui Wang, Benjamin Stanke, and Nicolas Le Pape. Preliminary evaluation of intelligent intention estimation algorithms for an actuated lower-limb exoskeleton. *International Journal of Advanced Robotic Systems*, 10(2):147, 2013.

[22] Massimo Cenciarini and Aaron M Dollar. Biomechanical considerations in the design of lower limb exoskeletons. In *2011 IEEE International Conference on Rehabilitation Robotics*, pages 1–6. IEEE, 2011.

[23] Ana Cecilia Villa-Parra, Denis Delisle-Rodriguez, Thomaz Botelho, John Jairo Villarejo Mayor, Alberto López Delis, Ricardo Carelli, Anselmo Frizera Neto, and Teodiano Freire Bastos. Control of a robotic knee exoskeleton for assistance and rehabilitation based on motion intention from semg. *Research on Biomedical Engineering*, (AHEAD), 2018.

[24] B Giroux and M Lamontagne. Comparisons between surface electrodes and intramuscular wire electrodes in isometric and dynamic conditions. *Electromyography and clinical neurophysiology*, 30(7):397–405, 1990.

[25] Hugh Herr. Exoskeletons and orthoses: classification, design challenges and future directions. *Journal of neuroengineering and rehabilitation*, 6(1):21, 2009.

[26] N. Yagn. Apparatus for facilitating walking, running and jumping, January 28 1890. URL https://www.google.com/patents/US420179. US Patent 420,179.

[27] Aaron M Dollar and Hugh Herr. Lower extremity exoskeletons and active orthoses: challenges and state-of-the-art. *IEEE Transactions on robotics*, 24(1):144–158, 2008.

[28] B.R. Fick and J.B. Markinson. "Final Report On HARDIMAN I Protoype For Machine Augmentation Of Human Strength And Endurance ". Technical report, General Electric Company, Schenectady, New York 12345, 1971.

[29] J.A. Moore and Los Alamos National Laboratory. *PITMAN, a Powered Exoskeletal Suit for the Infantryman*. Los Alamos National Laboratory, 1986. URL http://books.google.co.in/books?id=stisGwAACAAJ.

[30] Homayoon Kazerooni. Human-robot interaction via the transfer of power and information signals. *IEEE Transactions on systems, Man, and Cybernetics*, 20(2): 450–463, 1990.

[31] H Kazerooni and Jenhwa Guo. Human extenders. *Journal of Dynamic Systems, Measurement, and Control*, 115(2B):281–290, 1993.

[32] C.J. Walsh, D. Paluska, K. Pasch, W. Grand, A. Valiente, and H. Herr. Development of a lightweight, underactuated exoskeleton for load-carrying augmentation. In *Robotics and Automation, 2006. ICRA 2006. Proceedings 2006 IEEE International Conference on*, pages 3485–3491. IEEE, 2006.

[33] C.J. Walsh, K. Endo, and H. Herr. A quasi-passive leg exoskeleton for load-carrying augmentation. *International Journal of Humanoid Robotics*, 4(03):487–506, 2007.

[34] E. Guizzo and H. Goldstein. The rise of the body bots [robotic exoskeletons]. *Spectrum, IEEE*, 42(10):50–56, 2005.

[35] H Kazerooni and R Steger. The berkeley lower extremity exoskeleton. *Journal of dynamic systems, measurement, and control*, 128(1):14–25, 2006.

[36] H Kazerooni. Exoskeletons for human power augmentation. In *Intelligent Robots and Systems, 2005.(IROS 2005). 2005 IEEE/RSJ International Conference on*, pages 3459–3464. IEEE, 2005.

[37] Christian Fleischer, Christian Reinicke, and Günter Hommel. Predicting the intended motion with emg signals for an exoskeleton orthosis controller. In *2005 IEEE/RSJ International Conference on Intelligent Robots and Systems*, pages 2029–2034. IEEE, 2005.

[38] C. Fleischer and G. Hommel. A human–exoskeleton interface utilizing electromyography. *Robotics, IEEE Transactions on*, 24(4):872–882, 2008.

[39] Tommaso Lenzi, Stefano Marco Maria De Rossi, Nicola Vitiello, and Maria Chiara Carrozza. Intention-based emg control for powered exoskeletons. *IEEE transactions on biomedical engineering*, 59(8):2180–2190, 2012.

[40] Tommaso Lenzi, Nicola Vitiello, Stefano Marco Maria De Rossi, Stefano Roccella, Fabrizio Vecchi, and Maria Chiara Carrozza. Neuroexos: A variable impedance powered elbow exoskeleton. In *2011 IEEE International Conference on Robotics and Automation*, pages 1419–1426. IEEE, 2011.

[41] Nicola Vitiello, Tommaso Lenzi, Stefano Roccella, Stefano Marco Maria De Rossi, Emanuele Cattin, Francesco Giovacchini, Fabrizio Vecchi, and Maria Chiara Carrozza. Neuroexos: A powered elbow exoskeleton for physical rehabilitation. *IEEE Transactions on Robotics*, 29(1):220–235, 2013.

[42] Howard A Baldwin. Realizable models of muscle function. In *Biomechanics*, pages 139–147. Springer, 1969.

[43] Mervin Chandrapal, XiaoQi Chen, Wenhui Wang, and Chris Hann. Nonparametric control algorithms for a pneumatic artificial muscle. *Expert Systems with Applications*, 39(10):8636–8644, 2012.

[44] Mervin Chandrapal, XiaoQi Chen, WenHui Wang, Benjamin Stanke, and Nicolas Le Pape. Investigating improvements to neural network based emg to joint torque estimation. *Paladyn, Journal of Behavioral Robotics*, 2(4):185–192, 2011.

[45] Kevin Englehart, Bernard Hudgins, Philip A Parker, and Maryhelen Stevenson. Classification of the myoelectric signal using time-frequency based representations. *Medical engineering & physics*, 21(6-7):431–438, 1999.

[46] Kevin Englehart and Bernard Hudgins. A robust, real-time control scheme for multifunction myoelectric control. *IEEE transactions on biomedical engineering*, 50(7):848–854, 2003.

[47] P Lawrence, P Herberts, and R Kadefors. Experiences with a multifunctional hand prosthesis controlled by myoelectric patterns. *Advances in External Control of Human Extremities*, pages 47–65, 1973.

[48] David G Lloyd and Thor F Besier. An emg-driven musculoskeletal model to estimate muscle forces and knee joint moments in vivo. *Journal of biomechanics*, 36(6):765–776, 2003.

[49] Lin Wang and Thomas S Buchanan. Prediction of joint moments using a neural network model of muscle activations from emg signals. *Neural Systems and Rehabilitation Engineering, IEEE Transactions on*, 10(1):30–37, 2002.

[50] Felix E Zajac. Muscle and tendon: properties, models, scaling, and application to biomechanics and motor control. *Critical reviews in biomedical engineering*, 17(4): 359–411, 1989.

[51] Kenneth J Hunt, Marko Munih, ND Donaldson, and Fiona MD Barr. Investigation of the hammerstein hypothesis in the modeling of electrically stimulated muscle. *IEEE Transactions on Biomedical Engineering*, 45(8):998–1009, 1998.

[52] Bernard Hudgins, Philip Parker, and Robert N Scott. A new strategy for multifunction myoelectric control. *IEEE Transactions on Biomedical Engineering*, 40(1): 82–94, 1993.

[53] G Chang, W Kang, J Luh, and C Cheng. Principal component for classification of preshaping movement. In *IEEE, 17th Ann. Conf*, pages 1019–25, 1994.

[54] Mahyar Zardoshti-Kermani, Bruce C Wheeler, Kambiz Badie, and Reza M Hashemi. Emg feature evaluation for movement control of upper extremity prostheses. *IEEE Transactions on Rehabilitation Engineering*, 3(4):324–333, 1995.

[55] He Huang, Todd A Kuiken, Robert D Lipschutz, et al. A strategy for identifying locomotion modes using surface electromyography. *IEEE Transactions on Biomedical Engineering*, 56(1):65–73, 2009.

[56] He Huang, Fan Zhang, Levi J Hargrove, Zhi Dou, Daniel R Rogers, and Kevin B Englehart. Continuous locomotion-mode identification for prosthetic legs based on neuromuscular–mechanical fusion. *IEEE Transactions on Biomedical Engineering*, 58(10):2867–2875, 2011.

[57] AJ Young, TA Kuiken, and LJ Hargrove. Analysis of using emg and mechanical sensors to enhance intent recognition in powered lower limb prostheses. *Journal of neural engineering*, 11(5):056021, 2014.

[58] Rohit Gupta and Ravinder Agarwal. Continuous human locomotion identification for lower limb prosthesis control. *CSI Transactions on ICT*, pages 1–15, 2017.

[59] Rohit Gupta and Ravinder Agarwal. Electromyographic signal-driven continuous locomotion mode identification module design for lower limb prosthesis control. *Arabian Journal for Science and Engineering*, 43(12):7817–7835, 2018.

[60] Aaron J Young, Ann M Simon, and Levi J Hargrove. A training method for locomotion mode prediction using powered lower limb prostheses. *IEEE Transactions on Neural Systems and Rehabilitation Engineering*, 22(3):671–677, 2013.

[61] Feiyun Xiao, Yong Wang, Yongsheng Gao, Yanhe Zhu, and Jie Zhao. Continuous estimation of joint angle from electromyography using multiple time-delayed features and random forests. *Biomedical Signal Processing and Control*, 39:303–311, 2018.

[62] Zhang Lei. An upper limb movement estimation from electromyography by using bp neural network. *Biomedical Signal Processing and Control*, 49:434–439, 2019.

[63] Alberto L Delis, Joao LA Carvalho, Adson F Da Rocha, Renan U Ferreira, Suélia S Rodrigues, and Geovany A Borges. Estimation of the knee joint angle from surface electromyographic signals for active control of leg prostheses. *Physiological measurement*, 30(9):931, 2009.

[64] Feng Zhang, Pengfeng Li, Zeng-Guang Hou, Zhen Lu, Yixiong Chen, Qingling Li, and Min Tan. semg-based continuous estimation of joint angles of human legs by using bp neural network. *Neurocomputing*, 78(1):139–148, 2012.

[65] Jiangcheng Chen, Xiaodong Zhang, Yu Cheng, and Ning Xi. Surface emg based continuous estimation of human lower limb joint angles by using deep belief networks. *Biomedical Signal Processing and Control*, 40:335–342, 2018.

[66] Kevin Englehart, Bernard Hudgins, Philip A Parker, et al. A wavelet-based continuous classification scheme for multifunction myoelectric control. *IEEE Transactions on Biomedical Engineering*, 48(3):302–311, 2001.

[67] Reza Boostani and Mohammad Hassan Moradi. Evaluation of the forearm emg signal features for the control of a prosthetic hand. *Physiological measurement*, 24 (2):309–319, 2003.

[68] Levi Hargrove, Kevin Englehart, and Bernard Hudgins. A training strategy to reduce classification degradation due to electrode displacements in pattern recognition based myoelectric control. *Biomedical signal processing and control*, 3(2): 175–180, 2008.

[69] Yi-Chun Du, Chia-Hung Lin, Liang-Yu Shyu, and Tainsong Chen. Portable hand motion classifier for multi-channel surface electromyography recognition using grey relational analysis. *Expert Systems with Applications*, 37(6):4283–4291, 2010.

[70] Angkoon Phinyomark, Pornchai Phukpattaranont, and Chusak Limsakul. Feature reduction and selection for emg signal classification. *Expert Systems with Applications*, 39(8):7420–7431, 2012.

[71] J-U Chu, Inhyuk Moon, and M-S Mun. A real-time emg pattern recognition system based on linear-nonlinear feature projection for a multifunction myoelectric hand. *IEEE Transactions on biomedical engineering*, 53(11):2232–2239, 2006.

[72] Jun-Uk Chu, Inhyuk Moon, Yun-Jung Lee, Shin-Ki Kim, and Mu-Seong Mun. A supervised feature-projection-based real-time emg pattern recognition for multifunction myoelectric hand control. *IEEE/ASME Transactions on Mechatronics*, 12 (3):282–290, 2007.

[73] Hardeep S Ryait, AS Arora, and Ravinder Agarwal. Semg signal analysis at acupressure points for elbow movement. *Journal of electromyography and Kinesiology*, 21(5):868–876, 2011.

[74] Hardeep S Ryait, AS Arora, and Ravinder Agarwal. Interpretations of wrist/grip operations from semg signals at different locations on arm. *IEEE transactions on biomedical circuits and systems*, 4(2):101–111, 2010.

[75] Hardeep S Ryait, AS Arora, and Ravinder Agarwal. Realisation of semg-based multifunctional prototype elbow prosthesis. *International Journal of Biomedical Engineering and Technology*, 9(1):72–87, 2012.

[76] Sanjeev Kumar, Arindam Chatterjee, and Amod Kumar. Design of a below elbow myoelectric arm with proportional grip force. *Journal of Scientific and Industrial Research*, 71:262–265, 2012.

[77] Sanjeev Verma, Arindam Chatterjee, Harpreet Pal Singh, Amod Kumar, Kanta Garg, and Kashidas Chattopadhyay. A design approach for myoelectric arm with hand and wrist motions using single actuator. *The International Journal of Advanced Manufacturing Technology*, 67(5-8):1899–1907, 2013.

[78] Yee Mon Aung and Adel Al-Jumaily. Estimation of upper limb joint angle using surface emg signal. *International Journal of Advanced Robotic Systems*, 10(10):369, 2013.

[79] Jianda Han, Qichuan Ding, Anbin Xiong, and Xingang Zhao. A state-space emg model for the estimation of continuous joint movements. *IEEE Transactions on Industrial Electronics*, 62(7):4267–4275, 2015.

[80] Karan Veer and Renu Vig. Analysis and recognition of operations using semg from upper arm muscles. *Expert Systems*, 34(6):e12221, 2017. doi: https://doi.org/10.1111/exsy.12221.

[81] Karan Veer and Renu Vig. Identification and classification of upper limb motions using pca. *Biomedical Engineering/Biomedizinische Technik*, 63(2):191–196, 2018.

[82] Michael R Tucker, Jeremy Olivier, Anna Pagel, Hannes Bleuler, Mohamed Bouri, Olivier Lambercy, José del R Millán, Robert Riener, Heike Vallery, and Roger Gassert. Control strategies for active lower extremity prosthetics and orthotics: a review. *Journal of neuroengineering and rehabilitation*, 12(1):1, 2015.

[83] Muhammad Zahak Jamal. Signal acquisition using surface emg and circuit design considerations for robotic prosthesis. In *Computational Intelligence in Electromyography Analysis-A Perspective on Current Applications and Future Challenges*. IntechOpen, 2012.

[84] Edward A Clancy, Evelyn L Morin, and Roberto Merletti. Sampling, noise-reduction and amplitude estimation issues in surface electromyography. *Journal of electromyography and kinesiology*, 12(1):1–16, 2002.

[85] Carlo J De Luca. Surface electromyography: Detection and recording. *DelSys Incorporated*, 10(2):1–10, 2002.

[86] Hakw Tam and John G Webster. Minimizing electrode motion artifact by skin abrasion. *IEEE Transactions on Biomedical Engineering*, (2):134–139, 1977.

[87] Daniel P Burbank and John G Webster. Reducing skin potential motion artefact by skin abrasion. *Medical and Biological Engineering and Computing*, 16(1):31–38, 1978.

[88] Rubana Chowdhury, Mamun Reaz, Mohd Ali, Ashrif Bakar, Kalaivani Chellappan, and Tae Chang. Surface electromyography signal processing and classification techniques. *Sensors*, 13(9):12431–12466, 2013.

[89] Silvia Conforto, Tommaso D'Alessio, and Stefano Pignatelli. Optimal rejection of movement artefacts from myoelectric signals by means of a wavelet filtering procedure. *Journal of Electromyography and Kinesiology*, 9(1):47–57, 1999.

[90] Angkoon Phinyomark, Pornchai Phukpattaranont, and Chusak Limsakul. Wavelet-based denoising algorithm for robust emg pattern recognition. *Fluctuation and Noise Letters*, 10(02):157–167, 2011.

[91] Scott Day. Important factors in surface emg measurement. *Bortec Biomedical Ltd publishers*, pages 1–17, 2002.

[92] Björn Gerdle, Stefan Karlsson, Scott Day, and Mats Djupsjöbacka. Acquisition, processing and analysis of the surface electromyogram. In *Modern techniques in neuroscience research*, pages 705–755. Springer, 1999.

[93] Silvestro Micera, Jacopo Carpaneto, and Stanisa Raspopovic. Control of hand prostheses using peripheral information. *IEEE reviews in biomedical engineering*, 3:48–68, 2010.

[94] Peter Konrad. The abc of emg. *A practical introduction to kinesiological electromyography*, 1, 2005.

[95] Carlo J De Luca. The use of surface electromyography in biomechanics. *Journal of applied biomechanics*, 13(2):135–163, 1997.

[96] B Frericks. The recommendations for sensors and sensor placement procedures for surface electromyography. *SENIAM deliverable 8, European Recommendations for Surface Electromyography*, pages 15–53, 1999.

[97] D Stegeman and H Hermens. Standards for surface electromyography: The european project surface emg for non-invasive assessment of muscles (seniam). *Línea). Disponible en: http://www. med. uni-jena. de/motorik/pdf/stegeman. pdf [Consultado en agosto de 2008]*, 2007.

[98] Hermie J Hermens, Bart Freriks, Roberto Merletti, Dick Stegeman, Joleen Blok, Günter Rau, Cathy Disselhorst-Klug, and Göran Hägg. European recommendations for surface electromyography. *Roessingh research and development*, 8(2):13–54, 1999.

[99] Hermie J Hermens, Bart Freriks, Catherine Disselhorst-Klug, and Günter Rau. Development of recommendations for semg sensors and sensor placement procedures. *Journal of electromyography and Kinesiology*, 10(5):361–374, 2000.

[100] Texas Instruments. Low-power, 8-channel, 24-bit analog front-end for biopotential measurements. *ADS1298 datasheet*, 2012.

[101] ATmega2560 Datasheet Anonim. pdf1. alldatasheet. com/datasheet pdf/view/78532/atmel. *ATMega. html*.

[102] Kurt Manal, Roger V Gonzalez, David G Lloyd, and Thomas S Buchanan. A real-time emg-driven virtual arm. *Computers in biology and medicine*, 32(1):25–36, 2002.

[103] Andor WJM Glaudemans, Rudi AJO Dierckx, Jan LMA Gielen, and Johannes Hans Zwerver. *Nuclear medicine and radiologic imaging in sports injuries*. Springer, 2015.

[104] M. Damsgaard, J. Rasmussen, S.T. Christensen, E. Surma, and M. de Zee. Analysis of musculoskeletal systems in the anybody modeling system. *Simulation Modelling Practice and Theory*, 14(8):1100–1111, 2006.

[105] I.T. Jolliffe. Discarding variables in a principal component analysis. I: Artificial data. *Applied statistics*, pages 160–173, 1972.

[106] I.T. Jolliffe. Discarding variables in a principal component analysis. II: Real data. *Applied Statistics*, pages 21–31, 1973.

[107] Alvin C Rencher and William F Christensen. *Methods of multivariate analysis*, volume 709. John Wiley & Sons, New Jersey, 2012.

[108] J. FCL Cadima and I. T. Jolliffe. Variable selection and the interpretation of principal subspaces. *Journal of agricultural, biological, and environmental statistics*, 6(1):62–79, 2001.

[109] Ian Jolliffe. *Principal component analysis*. Wiley Online Library, 2005.

[110] P. McCabe, George. Principal variables. *Technometrics*, 26(2):137–144, 1984.

[111] W.J. Krzanowski. Selection of variables to preserve multivariate data structure, using principal components. *Applied Statistics*, pages 22–33, 1987.

[112] SENIAM group. Recommendations for sensor locations on individual muscles. http://seniam.org/sensor_location.htm, 2013.

[113] Thomas S Buchanan, David G Lloyd, Kurt Manal, and Thor F Besier. Neuromusculoskeletal modeling: estimation of muscle forces and joint moments and movements from measurements of neural command. *Journal of applied biomechanics*, 20(4): 367–395, 2004.

[114] Sandra J Olney and David A Winter. Predictions of knee and ankle moments of force in walking from emg and kinematic data. *Journal of biomechanics*, 18(1): 9–20, 1985.

[115] JR Potvin and SHM Brown. Less is more: high pass filtering, to remove up to 99% of the surface emg signal power, improves emg-based biceps brachii muscle force estimates. *Journal of Electromyography and Kinesiology*, 14(3):389–399, 2004.

[116] AM Gordon, Andrew F Huxley, and FJ Julian. The variation in isometric tension with sarcomere length in vertebrate muscle fibres. *The Journal of physiology*, 184 (1):170–192, 1966.

[117] Edith M Arnold, Samuel R Ward, Richard L Lieber, and Scott L Delp. A model of the lower limb for analysis of human movement. *Annals of biomedical engineering*, 38(2):269–279, 2010.

[118] GT Yamaguchi, AGU Sawa, DW Moran, MJ Fessler, and JM Winters. A survey of human musculotendon actuator parameters. *Multiple muscle systems: Biomechanics and movement organization*, pages 717–773, 1990.

[119] Ganesh R Naik, Dinesh Kant Kumar, et al. Twin svm for gesture classification using the surface electromyogram. *IEEE Transactions on Information Technology in Biomedicine*, 14(2):301–308, 2009.

[120] Levi J Hargrove, Guanglin Li, Kevin B Englehart, and Bernard S Hudgins. Principal components analysis preprocessing for improved classification accuracies in pattern-recognition-based myoelectric control. *IEEE Transactions on Biomedical Engineering*, 56(5):1407–1414, 2009.

[121] Yonghong Huang, Kevin B Englehart, Bernard Hudgins, and Adrian DC Chan. A gaussian mixture model based classification scheme for myoelectric control of powered upper limb prostheses. *IEEE Transactions on Biomedical Engineering*, 52 (11):1801–1811, 2005.

[122] Daniel Graupe, Javad Salahi, and Kate H Kohn. Multifunctional prosthesis and orthosis control via microcomputer identification of temporal pattern differences in single-site myoelectric signals. *Journal of Biomedical Engineering*, 4(1):17–22, 1982.

[123] Han-Pang Huang, Yi-Hung Liu, Li-Wei Liu, and Chin-Shin Wong. Emg classification for prehensile postures using cascaded architecture of neural networks with self-organizing maps. In *Robotics and Automation, 2003. Proceedings. ICRA'03. IEEE International Conference on*, volume 1, pages 1497–1502. IEEE, 2003.

[124] Sijiang Du and Marko Vuskovic. Temporal vs. spectral approach to feature extraction from prehensile emg signals. In *Information Reuse and Integration, 2004. IRI 2004. Proceedings of the 2004 IEEE International Conference on*, pages 344–350. IEEE, 2004.

[125] Francisco Pereira, Tom Mitchell, and Matthew Botvinick. Machine learning classifiers and fmri: a tutorial overview. *Neuroimage*, 45(1):S199–S209, 2009.

[126] Diego Raphael Amancio, Cesar Henrique Comin, Dalcimar Casanova, Gonzalo Travieso, Odemir Martinez Bruno, Francisco Aparecido Rodrigues, and Luciano da Fontoura Costa. A systematic comparison of supervised classifiers. *PloS one*, 9 (4):e94137, 2014.

[127] Jason D Rennie, Lawrence Shih, Jaime Teevan, and David R Karger. Tackling the poor assumptions of naive bayes text classifiers. In *Proceedings of the 20th international conference on machine learning (ICML-03)*, pages 616–623, 2003.

[128] Xun Chen and Z Jane Wang. Pattern recognition of number gestures based on a wireless surface emg system. *Biomedical Signal Processing and Control*, 8(2): 184–192, 2013.

[129] Kang Soo Kim, Heung Ho Choi, Chang Soo Moon, and Chi Woong Mun. Comparison of k-nearest neighbor, quadratic discriminant and linear discriminant analysis in classification of electromyogram signals based on the wrist-motion directions. *Current applied physics*, 11(3):740–745, 2011.

[130] Mohammadreza Asghari Oskoei and Huosheng Hu. Support vector machine-based classification scheme for myoelectric control applied to upper limb. *IEEE transactions on biomedical engineering*, 55(8):1956–1965, 2008.

[131] Yongmin Li, Shaogang Gong, Jamie Sherrah, and Heather Liddell. Support vector machine based multi-view face detection and recognition. *Image and Vision Computing*, 22(5):413–427, 2004.

[132] Jitendra Virmani, Vinod Kumar, Naveen Kalra, and Niranjan Khandelwal. Svm-based characterization of liver ultrasound images using wavelet packet texture descriptors. *Journal of digital imaging*, 26(3):530–543, 2013.

[133] Jitendra Virmani, Ravinder Agarwal, et al. Effect of despeckle filtering on classification of breast tumors using ultrasound images. *Biocybernetics and Biomedical Engineering*, 39(2):536–560, 2019.

[134] Zeeshan O Khokhar, Zhen G Xiao, and Carlo Menon. Surface emg pattern recognition for real-time control of a wrist exoskeleton. *Biomedical engineering online*, 9 (1):41, 2010.

[135] Marie-Françoise Lucas, Adrien Gaufriau, Sylvain Pascual, Christian Doncarli, and Dario Farina. Multi-channel surface emg classification using support vector machines and signal-based wavelet optimization. *Biomedical Signal Processing and Control*, 3(2):169–174, 2008.

[136] Abhinandan Aggarwal, Rohit Gupta, and Ravinder Agarwal. Design and development of integrated insole system for gait analysis. In *2018 Eleventh International Conference on Contemporary Computing (IC3)*, pages 1–5. IEEE, 2018.

Publications

Referred Journals

[1] **Inderjeet Singh Dhindsa**, Hardeep Singh Ryait and Ravinder Agarwal, Performance evaluation of various classifiers for predicting knee angle from electromyography signals, *Expert Systems*, vol. 36, no. 3, e12381, 2019 . **DOI** https://doi:10.1111/exsy.12381.

[2] **Inderjeet Singh Dhindsa**, Hardeep Singh Ryait and Ravinder Agarwal, Principal component analysis-based muscle identification for myoelectric controlled exoskeleton knee, *Journal of Applied Statistics, Taylor & Francis*,vol. 44, no. 10, 1707-1720, 2017. **DOI** https://doi: 10.1080/02664763.2016.1221907.

[3] Rohit Gupta, **Inderjeet Singh Dhindsa** and Ravinder Agarwal, Continuous angular position estimation of human ankle during unconstrained locomotion, *Biomedical Signal Processing and Control*,vol. 60, 101968, 2020. **DOI** https://doi.org/10.1016/j.bspc.2020.101968.

Papers published in National and International Conferences

[1] **Inderjeet Singh Dhindsa**, Hardeep Singh Ryait and Ravinder Agarwal, Muscle Force Measurement from SEMG Signals for Exoskeleton Devices, *9th International Conference on Advances in Metrology [AdMet 2016]*,February 23-26, 2016, National Physical Laboratory, New Delhi

[2] **Inderjeet Singh Dhindsa**, Hardeep Singh Ryait and Ravinder Agarwal, A novel algorithm to predict knee angle from EMG signals for controlling a lower limb exoskeleton, *Information Technologies and Nanotechnologies (ITNT-2016)*, May 17-19, 2016, Samara State Aerospace University, Samara, Russia

[3] **Inderjeet Singh Dhindsa**, Hardeep Singh Ryait and Ravinder Agarwal, EMG feature evaluation of knee movements along with daily life activities,*3rd National Conference onAdvances in Metrology[AdMet 2014]*, February 19-21, 2014, Thapar University, Patiala.

[4] **Inderjeet Singh Dhindsa**, Hardeep Singh Ryait and Ravinder Agarwal, Identification of muscles for controlling a myoelectric lower limb exoskeleton, *First International Conference on Large Area Flexible Microelectronics (ILAFM 2014) Materials, Devices, Systems and Applications*, December 18-20, 2014, R V College of Engineering, Bangalore